THE UNIVERSITY OF MICHIGAN

INDUSTRY PROGRAM OF THE COLLEGE OF ENGINEERING

VOID FRACTION MEASUREMENTS IN A CAVITATING VENTURI

Willy Smith
Gerald L. Atkinson
Frederick G. Hammitt

September, 1962

IP-581

PREFACE

This work was performed as a term project in partial fulfillment of the requirements for the Master's Degree in the Nuclear Engineering Department of the University of Michigan by Mr. G. L. Atkinson, under the general supervision of Professor F. G. Hammitt.

Direct supervision of the work was furnished by Mr. W. Smith, Research Assistant in the Nuclear Engineering Department. The cavitation facility itself was operated by Mr. M. J. Robinson, also Research Assistant in the Nuclear Engineering Department.

Financial support for the overall cavitation research project is provided under a grant from the NASA. Most of the electronic instrumentation for this particular experiment was kindly furnished by the Nuclear Engineering Department and the Phoenix Project of the University of Michigan.

TABLE OF CONTENTS

APPENDICES

LIST OF FIGURES

APPENDICES

LIST OF FIGURES CONT'D

I. INTRODUCTION

A. Motivation for Investigation

The present research investigation on cavitation-erosion damage in flowing systems has been concentrated on the examination of the phenomenon in geometrically similar venturi test sections. However, if the results are to be applied to other situations, it is necessary that detailed information on the two phase flow regimes in the venturi be obtained under different combinations of the applicable flow parameters. While this appears fairly straight-forward under the considerations of classical cavitation theory, in practice it has been found that there are substantial variations from such ideal theory [1,2,3,4]. Thus it has been necessary to employ various special techniques to determine as far as possible the details of the flow pattern. So far these have included, in addition to measurements of static pressure, local velocity measurements [2,3], high-speed motion pictures of the flow [2,5], and local density (or void fraction) determination using gamma-ray densitometer techniques [2,3,6,8].

The initial investigations using a gamma-ray densitometer were partially in the nature of feasibility investigations to discover whether or not useful information could be obtained. It was determined that it could, and, in fact useful preliminary data[2] was obtained with water as the test fluid. However, it was apparent that greater precision in the technique would be most desirable. In addition it was desired to take measurements in mercury to compare with the initial water measurements as well as with future more precise water measurements. Thus it was

necessary to develop a precision densitometer for immediate use in mercury (or in other heavy fluids as molten lead), but with the possibility of later conversion, with a minimum of modification, to water.

The development of such an instrument, and a discussion of the data obtained with mercury as the test fluid is the subject of the present report.

B. Review of Previous Work

Previous work under this research investigation [2,3,6,7,8], indicates the feasibility of the determination of the void fraction, or local density, occuring in a cavitating venturi by using a gamma-ray densitometer. However, after a critical evaluation of the technique used, it became evident that several errors had been introduced, and that a more refined procedure was not only possible but desirable. At the same time, the need of a computer program to reduce the experimental data to a more tractable form became obvious.

The experimental equipment is essentially that used by Adyanthaya,[8] who made preliminary void fraction measurements in cavitating mercury.* The main difference between the present and Adyanthaya's investigation[8] consists in a very careful calibration of the electronic equipment, in such a fashion that only the 1.17 Mev gammas of a Co^{60} source were counted. Background and statistical errors were reduced to a minimum within the practical limitations imposed by the need of restricting the counting times in order to keep the overall time required for the experiment to a feasible limit.

*His work differed from that of Pérez[6] in that mercury rather than water was used. Also, a much better collimation and precision in the location of the measurement was obtained.

Another source of error in the previous experiments (particularly Pérez's work[6]) was the lack of a proper location of the collimated gamma-ray beam with respect to the geometry of the cavitating venturi. Some effort was devoted to avoid this difficulty, but as explained later in this report, the determination of the center-line of the venturi with reference to the collimated beam is of such importance that the accuracy obtained in the present experiment is still not entirely adequate. It is clear that the technique should be further improved in this direction.

The design of the gamma ray densitometer using a collimated gamma-ray beam is discussed in Reference 7. The detector efficiency was determined to be between 18.5% and 63% depending upon the discriminator setting. This efficiency was computed on the basis of an average 1.25 Mev gamma energy from Co^{60} and a 2" by 2" NaI(Tl) scintillation crystal. The use of C_o^{60} was demanded by the strong attenuation of gammas in mercury. The above calculations showed that a 20 millicurie Co^{60} source would be required to obtain statistically reliable observations of small void fractions in a reasonable counting time. It was shown that the standard deviation for a one minute counting time with the fluid cavitating sufficiently to cause a 2% void is much smaller than the difference between the non-cavitating condition count rate and cavitating condition count rate from which the void fraction is calculated. Therefore the 20 mc source gives sufficient strength to determine reliably 2% void fractions with this densitometer using a one minute counting time.

Reference 8 sets forth the general experimental and calculation procedures used in this report. The significant portions are summarized in the Appendices.

II. DESCRIPTION OF EQUIPMENT

A. General

The cavitation facility previously described [2,3], consists of a closed loop circuit powered by a centrifugal pump and including a cavitating venturi test section (Figure 1). Figure 2 shows the plexiglas venturi used to produce the cavitation field. The diffuser angle is approximately 6 degrees and the throat diameter is about 0.5 inches. In the same figure, the cavitation termination points for the different cavitation conditions mentioned in this report are indicated.

During the experiment, the stainless steel holders which are normally used to insert the metal test specimens were removed, and plexiglas fillers were inserted in their place to give continuity to the material density.

B. Densitometer

Reference 8 gives the details of the design of the collimator. However, the significant portions are summarized here for convenience. Figure 3 is a schematic diagram of the gamma-ray collimator and detector which respectively define a gamma beam and measure its attenuation upon passing through the venturi. Figure 4 shows two photographs of the densitometer.

The collimators have rectangular apertures, 0.030" by 0.200", accurately aligned. The longer aperture dimension is such that it is parallel to the direction of fluid flow within the venturi. The change in flow conditions in the axial direction over the length of the aperture

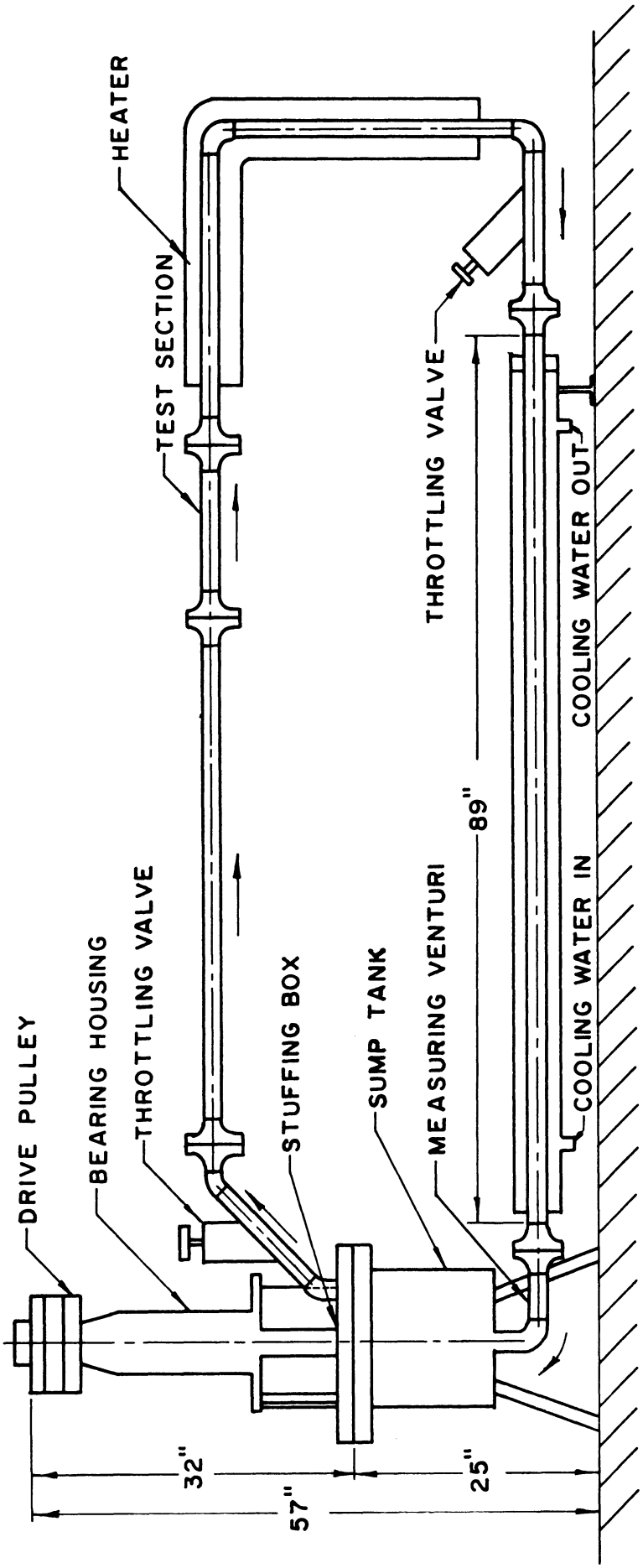

Figure 1. Overall Loop Schematic.

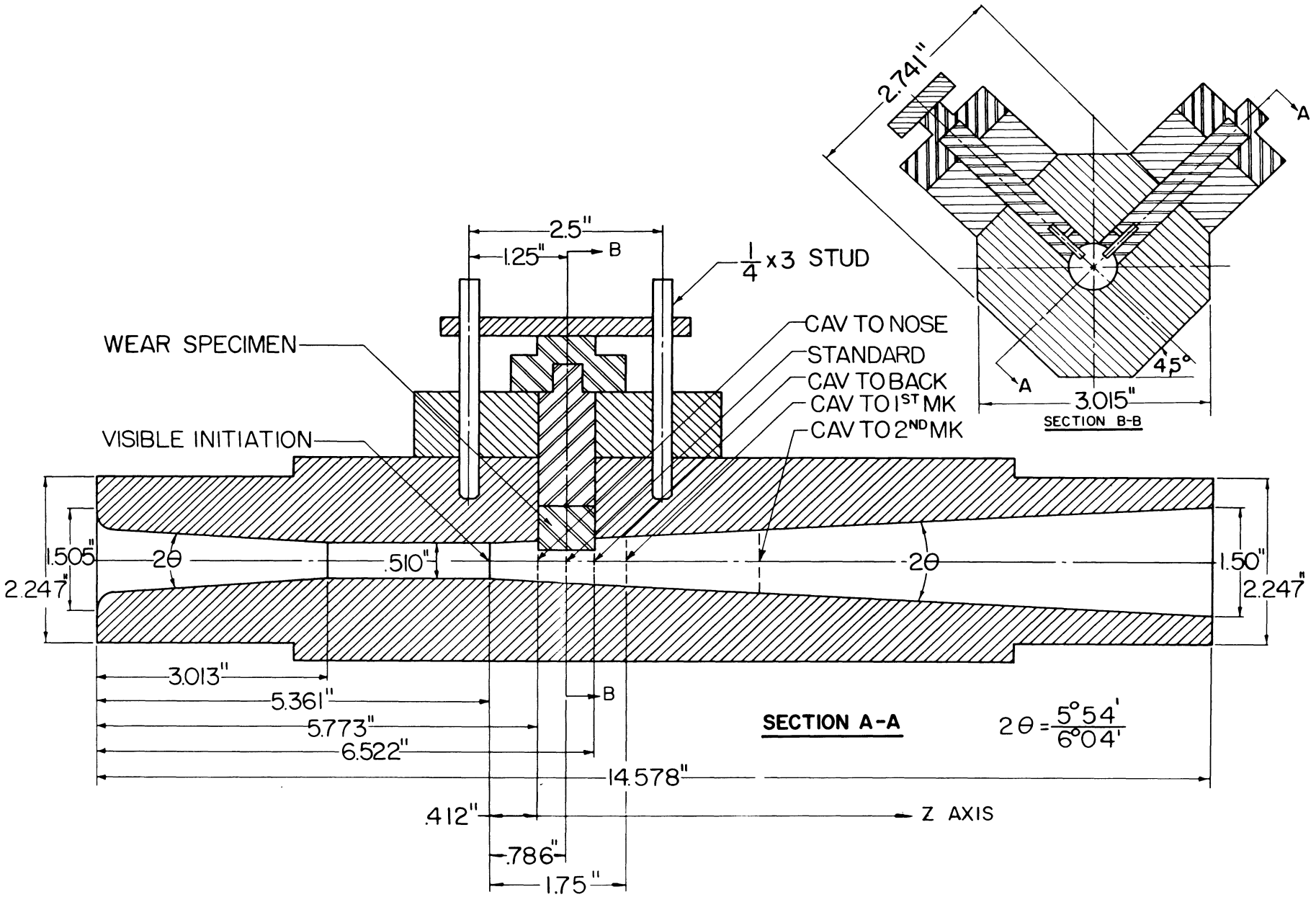

Figure 2. Cavitating Venturi Test Section.

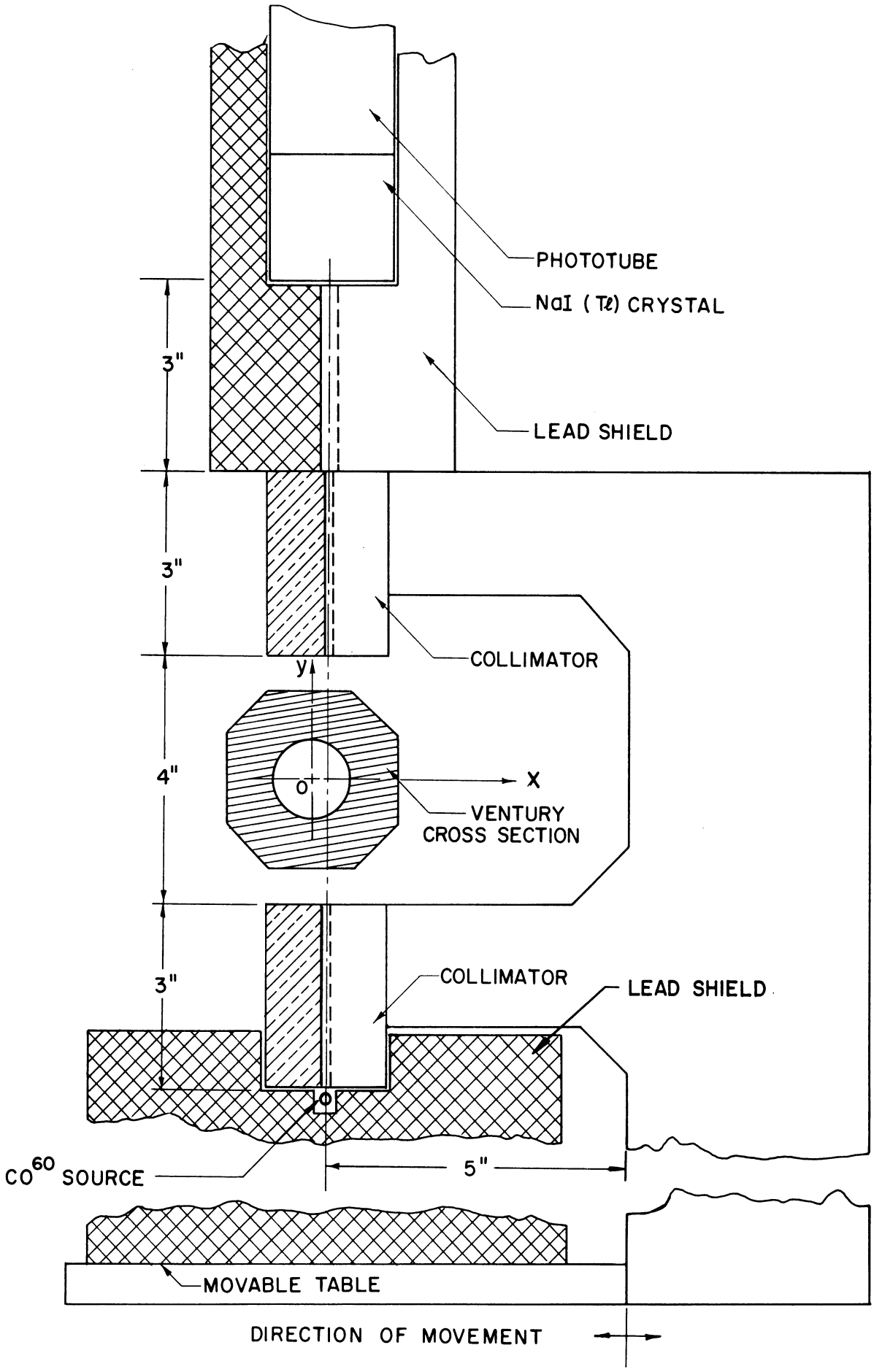

Figure 3. Schematic of Densitometer.

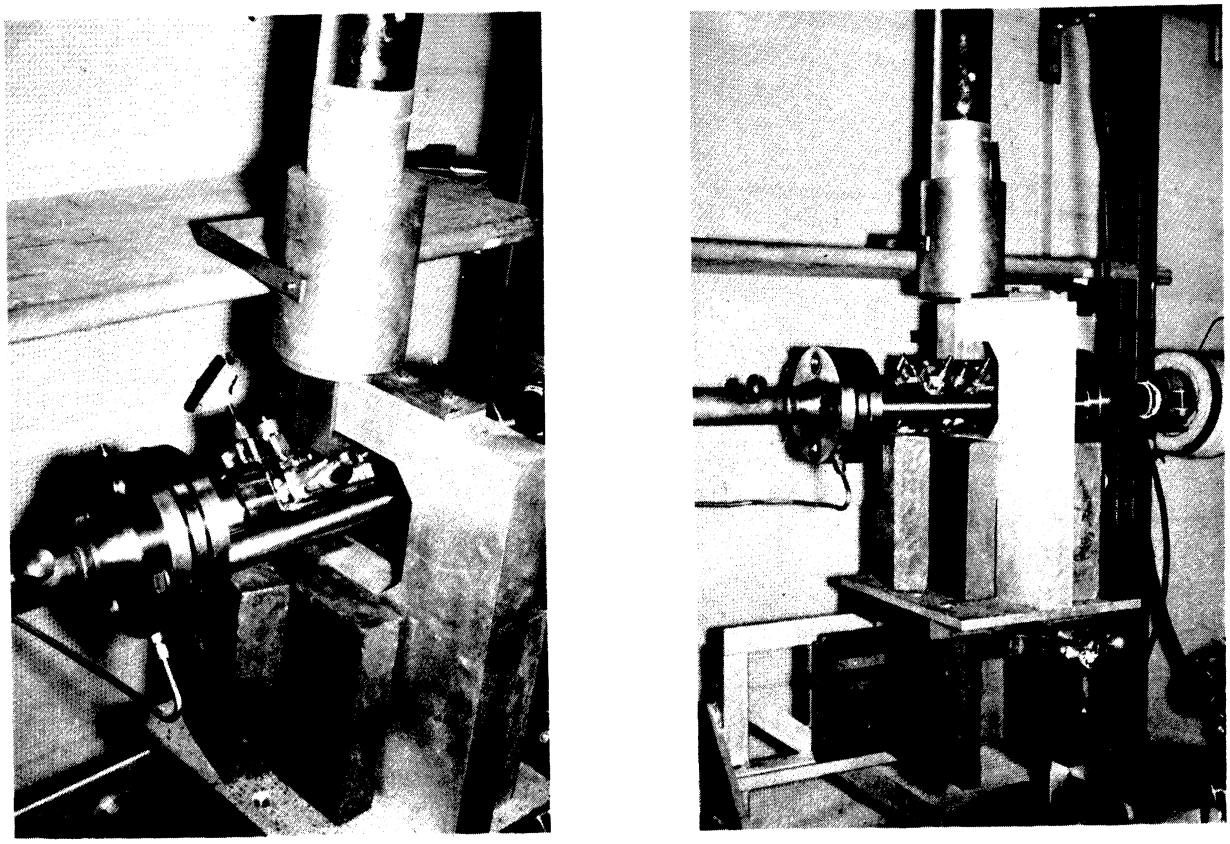

Figure 4. Photographs of Densitometer.

is not very rapid compared to the radial variations, and the 0.030" aperture is small enough to detect these variations as well as allow the passage of enough gammas to give statistical accuracy of about 1% with the 20 mc Co^{60} source which was used.

The whole assembly is mounted on a cross-compound index table so that the horizontal movement of the vertical gamma-ray beam in the radial and axial directions is possible to 0.001" accuracy. The detector and source were heavily shielded with lead bricks for personnel protection.

The source consisted of a 0.040" diameter piece of natural cobalt wire (100% Co^{59}), 0.252" long, encapsulated in a small aluminum holder 5/16" diameter by 2 inches long, sealing it permanently. It was irradiated in the Ford Nuclear Reactor at the University of Michigan. The aluminum holder also serves as means for attaching the source to the collimator assembly.

C. Electronic Equipment

The electronic equipment consisted of a sodium iodide thallium-activated scintillation crystal detector, photomultiplier tube, high-voltage power supply, pre-amplifier, non-overloading amplifier, single channel differential analyzer, count-rate meter, scaler and cathode-ray oscilloscope. Figure 5 shows a block diagram of the units used, which are listed with manufacturers and serial numbers in Appendix A.

The amplifier, although supposedly non-overloading, was easily overdriven during the calibration, and at times, upon moving the phototube. This, of course, would give spurious count rates which would

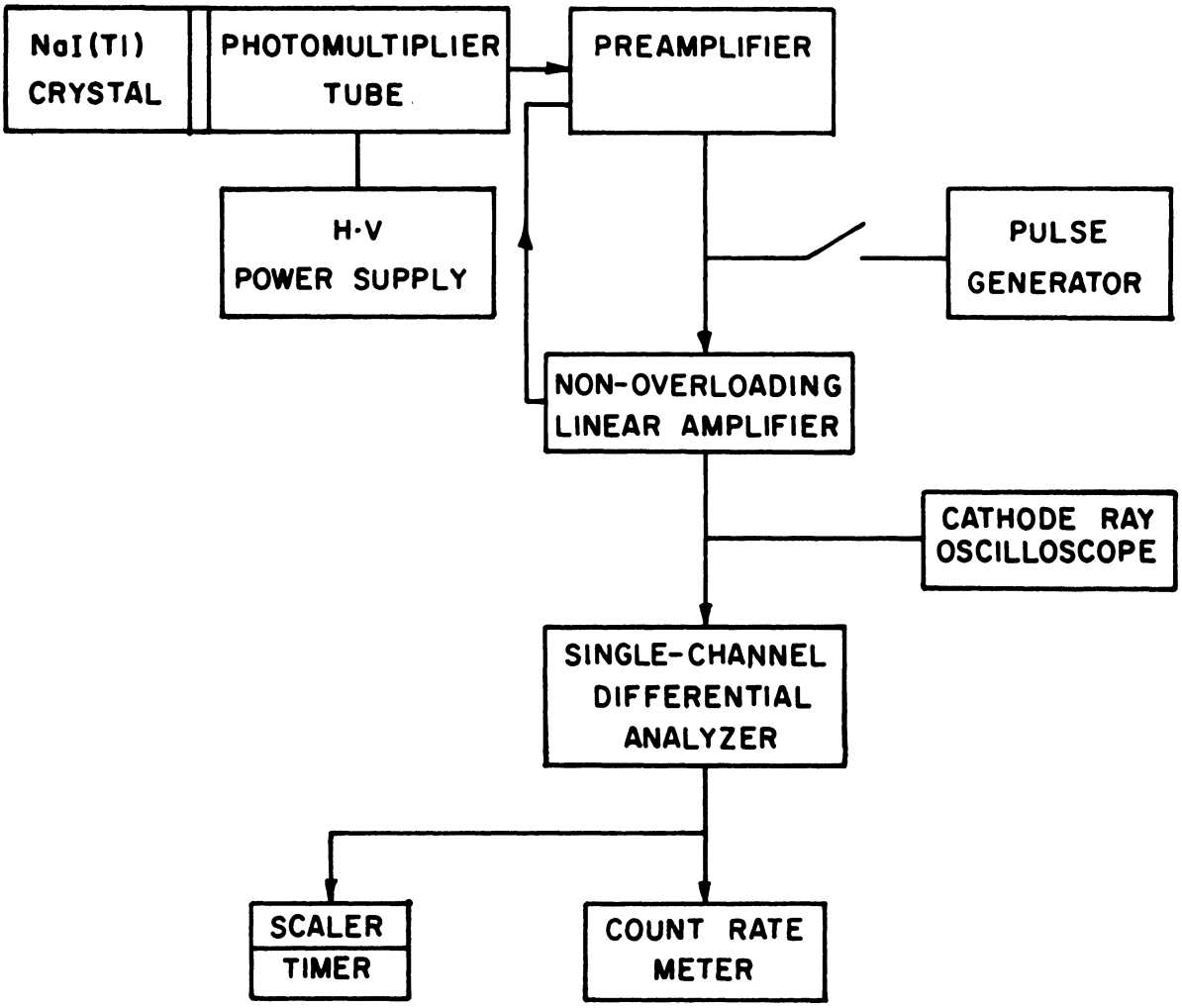

Figure 5. Block Diagram of Electronic Equipment.

adversely affect the data taken. Continuous observation of the pulses on an oscilloscope eliminated such errors.

The technique of observing only the 1.17-Mev gammas of Co^{60} in this experiment required an extensive calibration of the electronic equipment, especially the single channel analyzer. Details of the calibration procedure are given in Appendix A.

III. EXPERIMENTAL PROCEDURE

The table that holds the collimator, Figure 3, was placed in an arbitrary position beneath the venturi in the mercury loop. Axial alignment was attempted by shining a light through the collimator apertures and observing the position of the beam as the micrometer was actuated to move the densitometer in a transverse direction. The table was then adjusted by hand until this light beam traced a path parallel to the sharp outer edge of the venturi test section. By repeating the procedure at the opposite edge, the center line of the venturi, at that particular axial position of the table, was determined. Moving the table axially, the position of the center line was completely fixed, and reference zeros were recorded on the micrometer densitometer positioners, both in the axial and transverse directions. A log was then kept of each micrometer adjustment which was necessary to keep track of the position of the collimator aperture relative to the venturi throughout the experiment. A constant and perplexing source of error was eliminated by this procedure.

It must be noted that the arbitrary assignment of the zero positions relative to the venturi were "best guess" approximation by eyesight and that the actual venturi centerline was accurately determined by symmetry consideration once the data had been collected. The axial zero was placed as near as possible to the throat exit also by using a beam of light.

Some time after completion of the experiment it was verified that this procedure of alignment using a light beam may lead to very

large errors due to the diffraction in the plexiglas, unless the beam is perfectly perpendicular to the upper surface of the venturi and opposite faces of the venturi are exactly parallel. For future experiments, provisions should be made for bolting or securing the table to the floor in some manner so that the axial alignment, once accurately determined, can be maintained and to ensure that the vibration of the cavitating system doesn't move the table during the test, which is a distinct possibility.

Background counts were taken at the start of each day's runs and two or three times during the day. These counts were taken for ten minutes with the source in position on the shielded test table and the scintillation detector removed to a remote site from the test apparatus. This procedure was mandatory, since the removal of the Co^{60} from the collimator could not be accomplished without a considerable dose exposure for the operators.

Provision was made to shield the source in all directions to eliminate scattered radiation. Background corrections were made to the data in accordance with the closest time of background determination and test run. Table IX shows that generally these counts did not vary appreciably. Where there was considerable deviation, an average was taken, and applied to the data taken between the two background determinations.

Test runs at a constant flow rate were made for different cavitation conditions and axial (z) positions from the throat as specified in Table X. Each axial position required a "no cavitation" run for comparison to the cavitation runs from which void fractions were calculated. The "no cavitation" runs could not be made with the fluid completely

stagnant because bubbles of gas collected at various positions in the test section. Hence, the pump was used to circulate the mercury at a low rate which eliminated the bubbles, but which could be considered definitely "non-cavitating".

The experimental data were taken by advancing the table in the transverse (x) direction by increments of the aperature width, 0.030", in regions of relatively gradual change, and by 0.010" increments where the counts from point to point showed rapid change. Unfortunately, however, this was not done in the first experimental runs, and, as became apparent when reducing the data, introduced a rather large uncertainty in the region of the curves close to the walls.

All possible loop parameters such as flow rate, room temperature, mercury temperature, cavitation conditions, pressures, as well as the settings of the electronic equipment and background count data were recorded, although they are not reproduced here. Of special interest is the electronic equipment warming time. It was found that erratic results were obtained if this was less than about one hour. Consequently, the equipment was left on at all times, even overnight, with the exception of the voltage to the detector tube.

The experimental count rates, c, after background correction, b, are plotted in Figures 6 through 31. Each plot is for a certain cavitation condition at a particular axial distance z from the throat. Count rate was plotted versus x, the transverse distance with reference to the arbitrarily chosen zero (i.e., approximate venturi centerline). The curve was constructed and the assumed axial symmetry of the flow used to locate

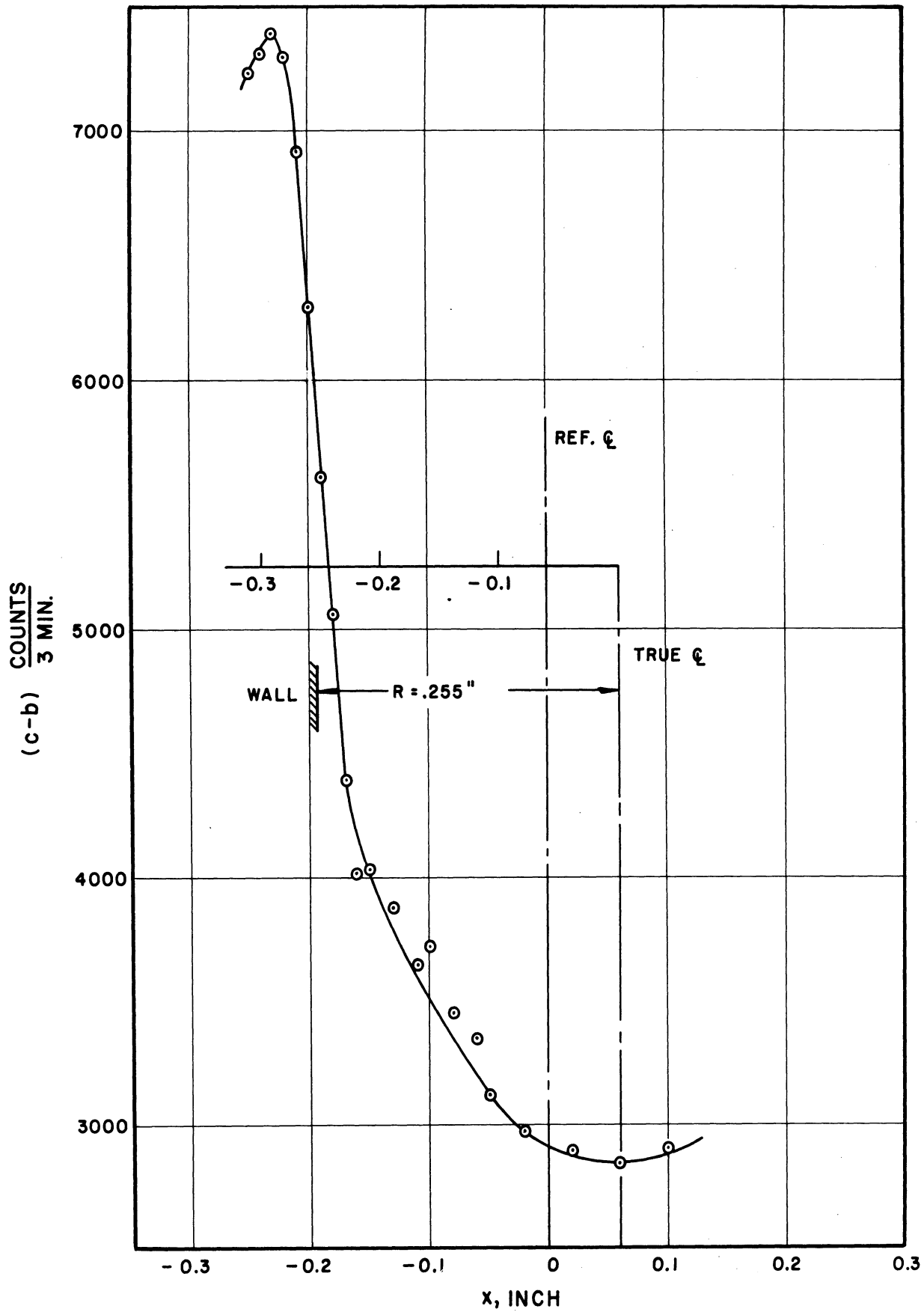

Figure 6. Run N°23, Zero Cavitation. Z = -0.25, R = 0.255, D = 1.0.

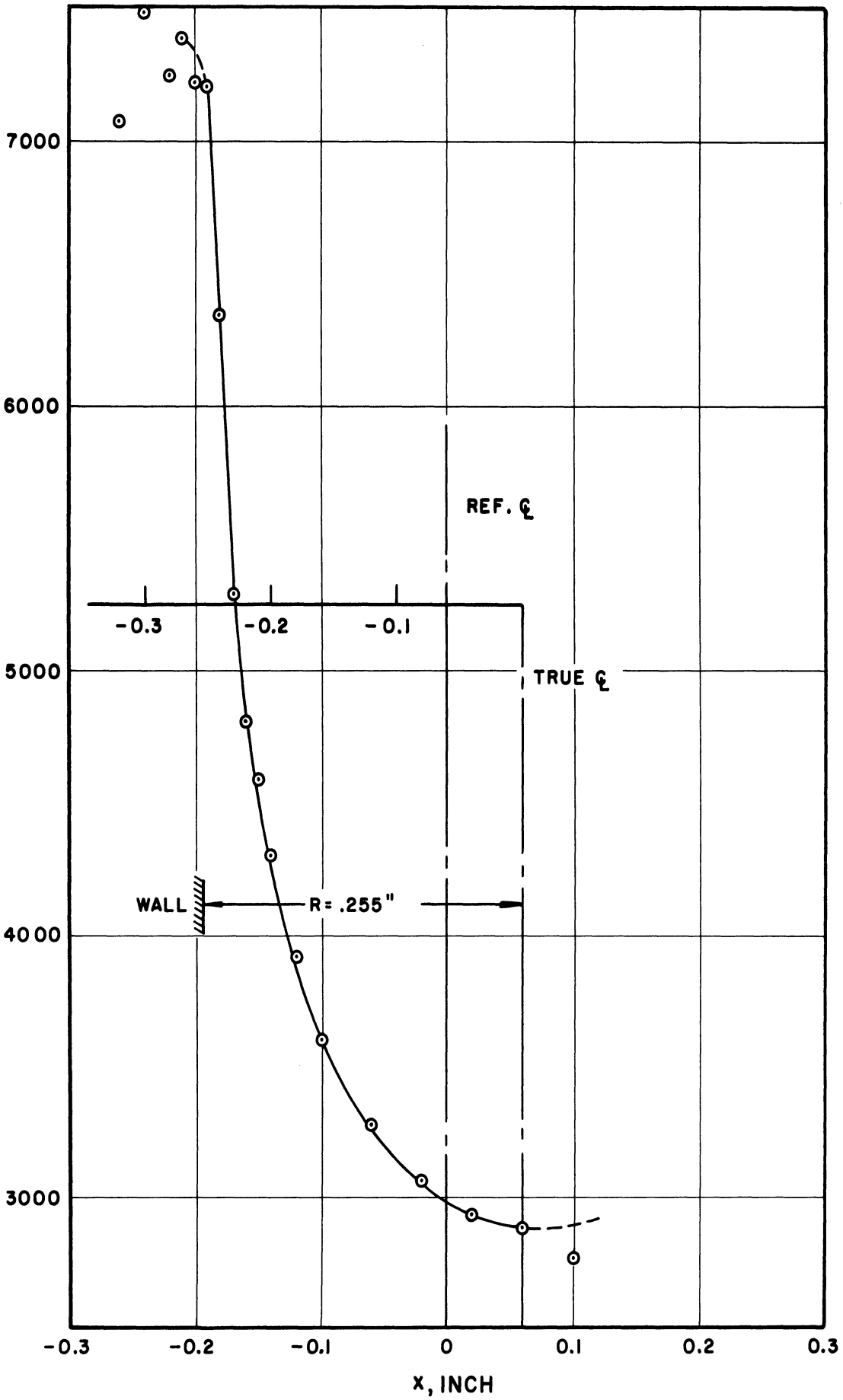

Figure 7. Run N°22, Visible Initiation Cavitation. Z = -0.25, R = 0.255, D = 2.5.

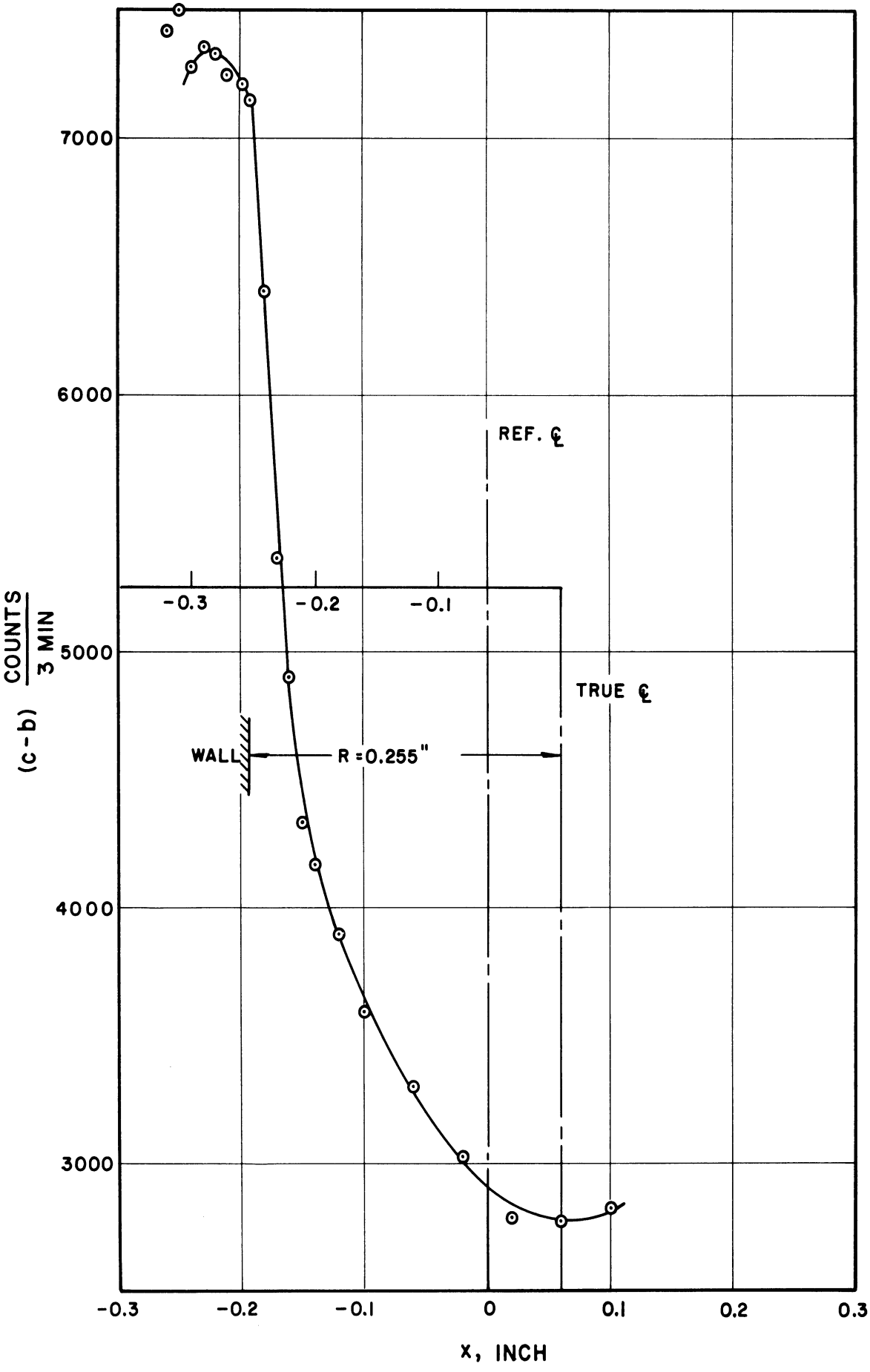

Figure 8. Run N°21, First Mark Cavitation. Z = -0.25, R = 0.255, D = 2.5.

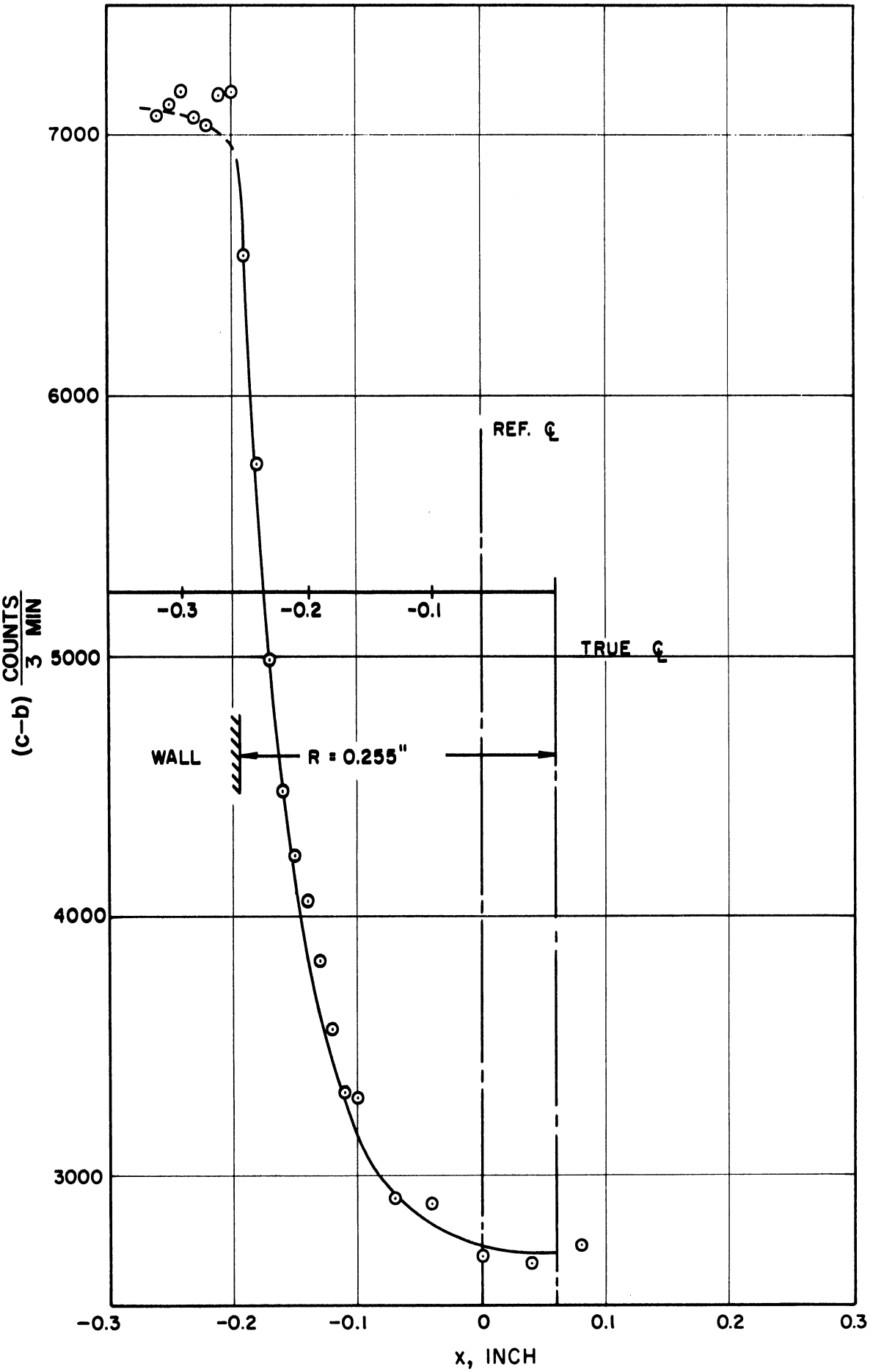

Figure 9. Run N°19, Zero Cavitation. Z = 0.00, R = 0.255, D = 1.0.

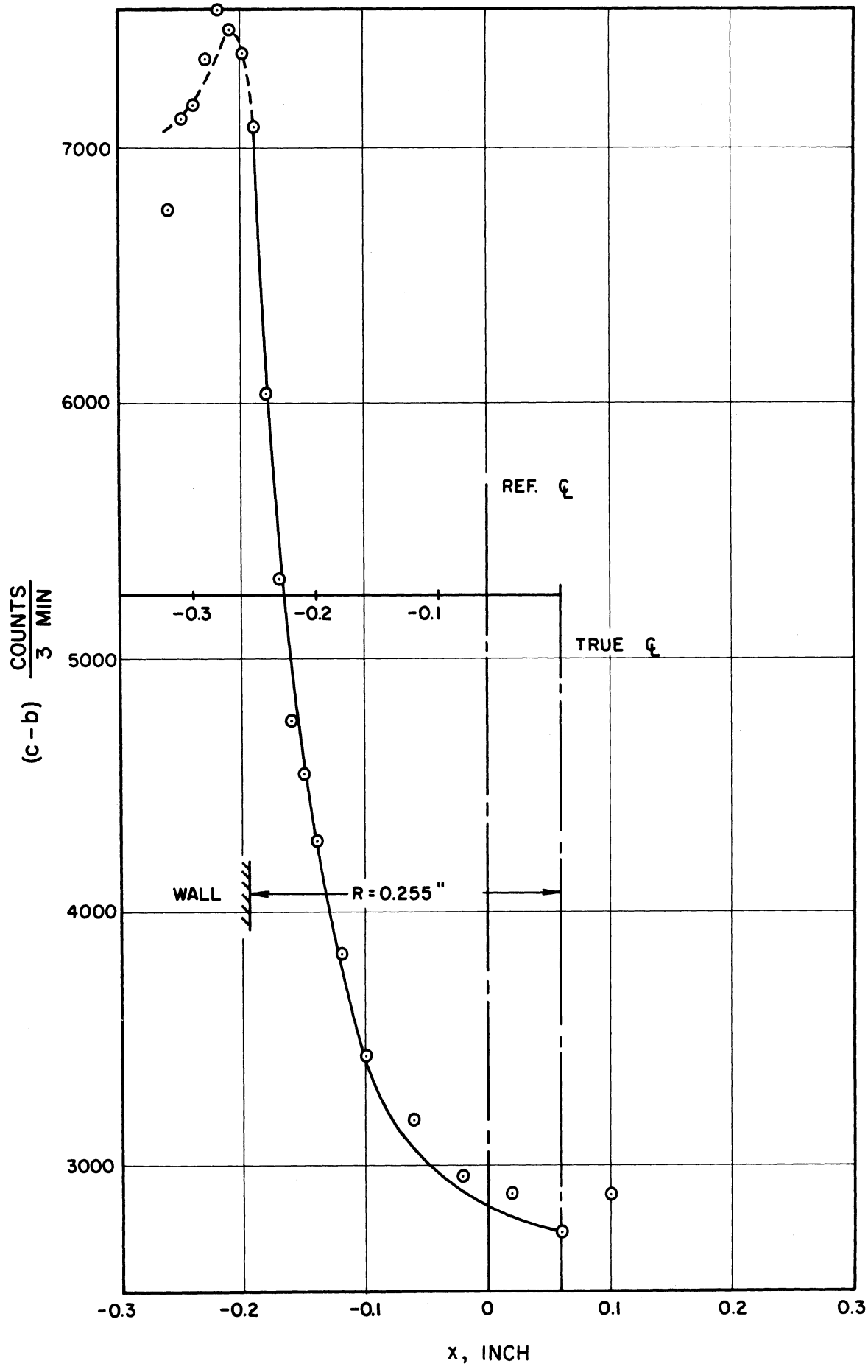

Figure 10. Run N°17, Visible Initiation Cavitation. Z = 0.00, R = 0.255, D = 2.5.

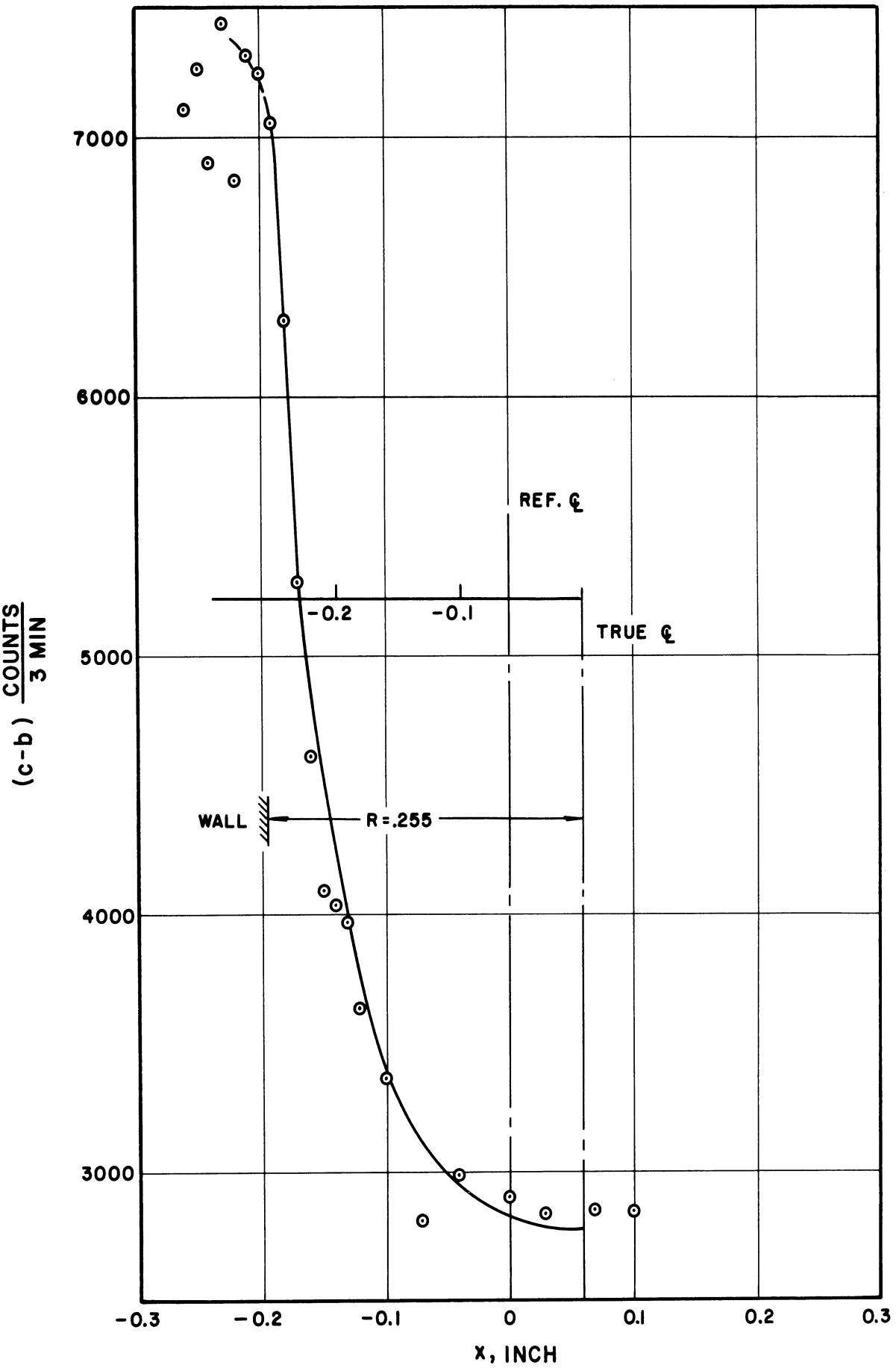

Figure 11. Run N°18, Standard Cavitation. Z = 0.00, R = 0.255, D = 2.5.

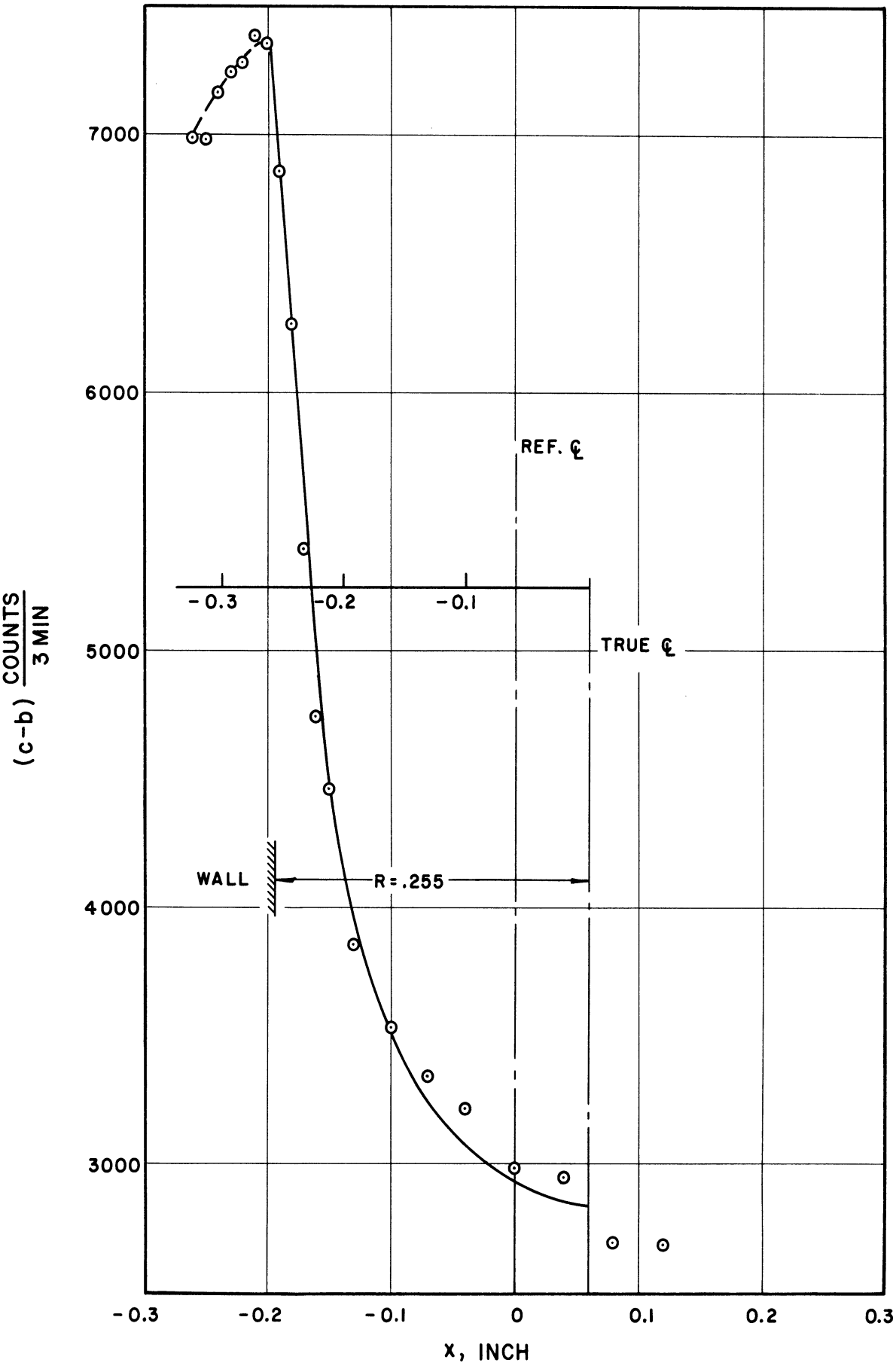

Figure 12. Run N°20, First Mark Cavitation. Z = 0.00, R = 0.255, D = 2.5.

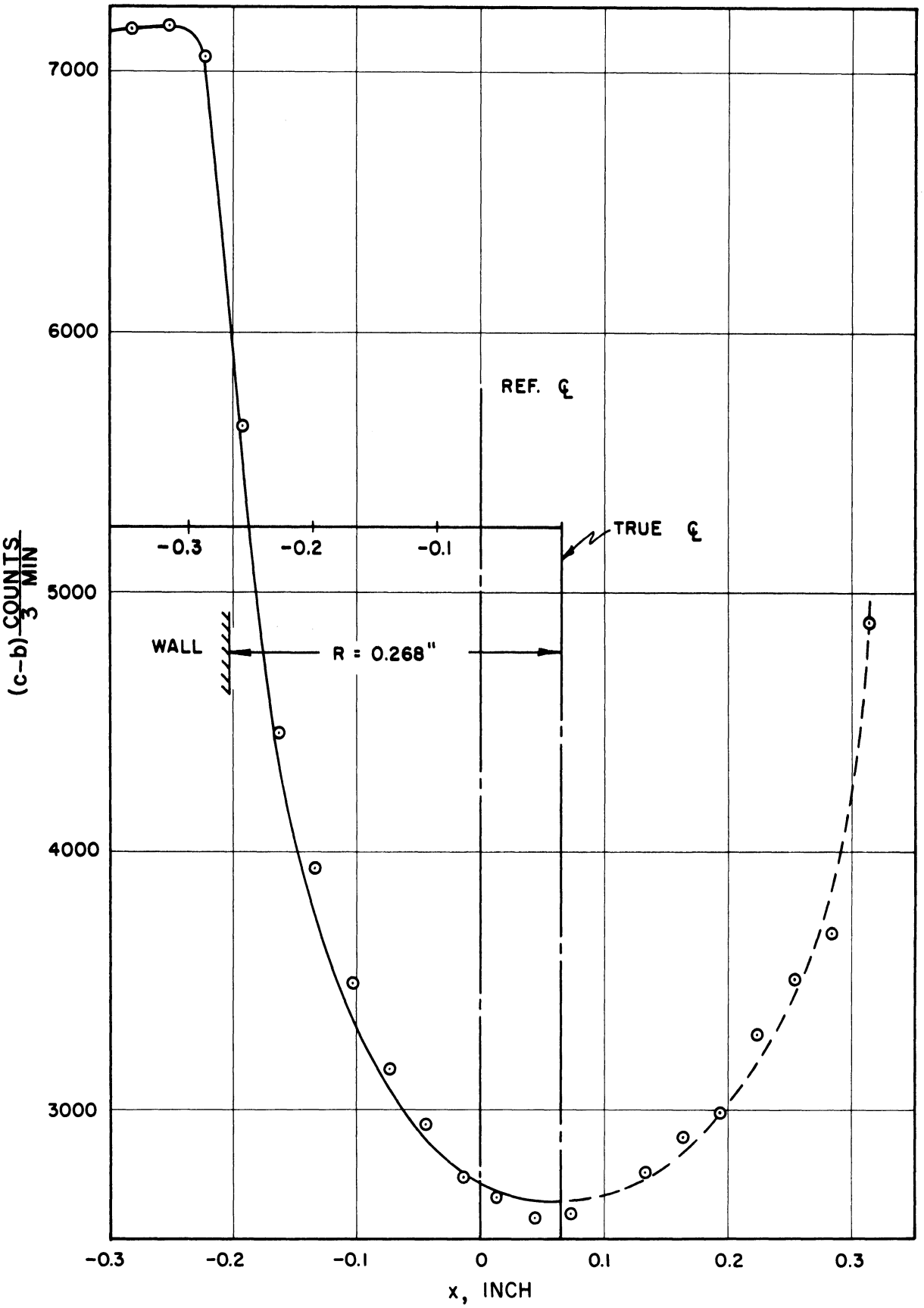

Figure 13. Run N°2, Zero Cavitation. Z = 0.25, R = 0.268, D = 2.0.

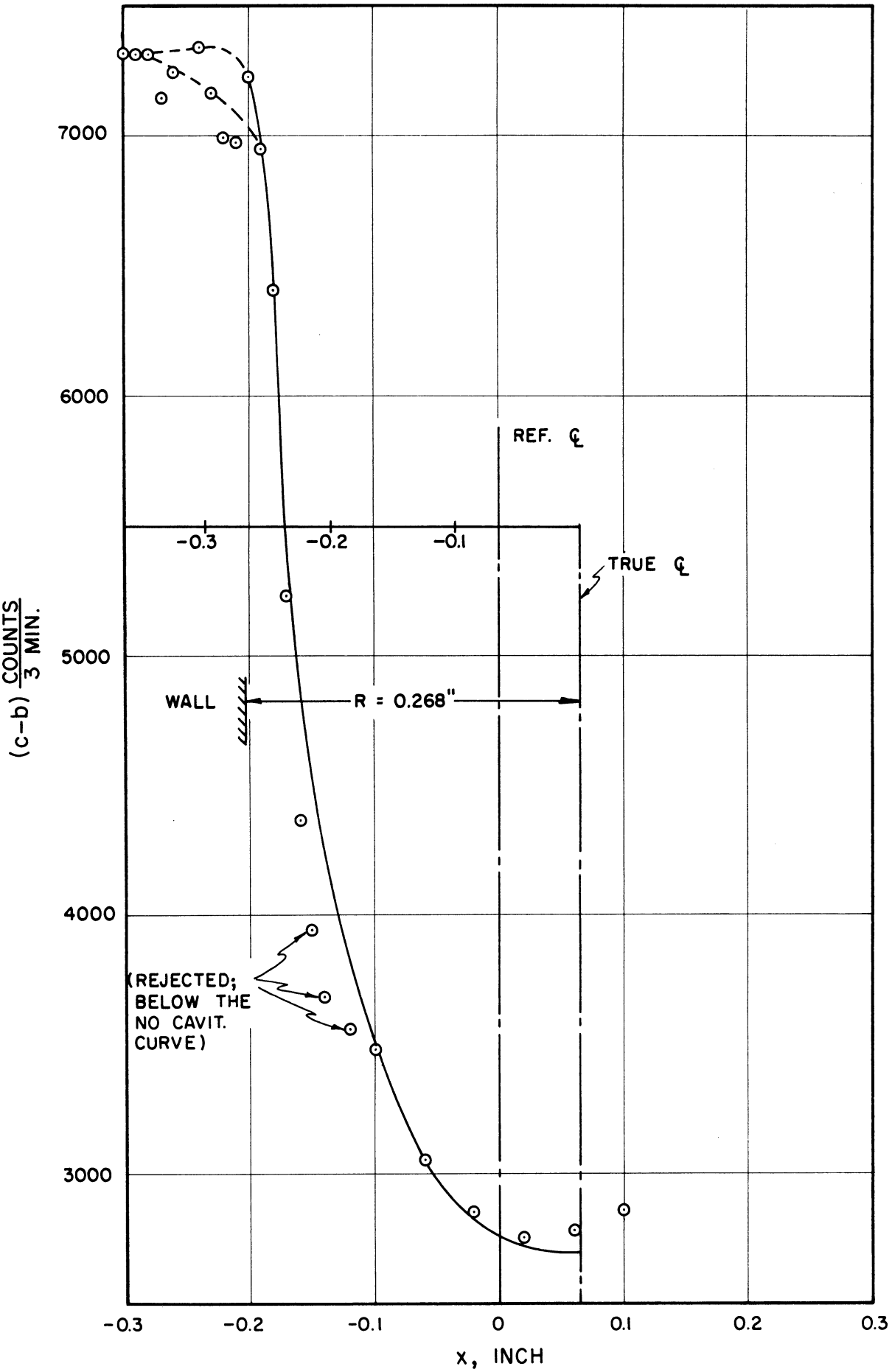

Figure 14. Run N°15, Standard Cavitation. Z = 0.25, R = 0.268, D = 2.5.

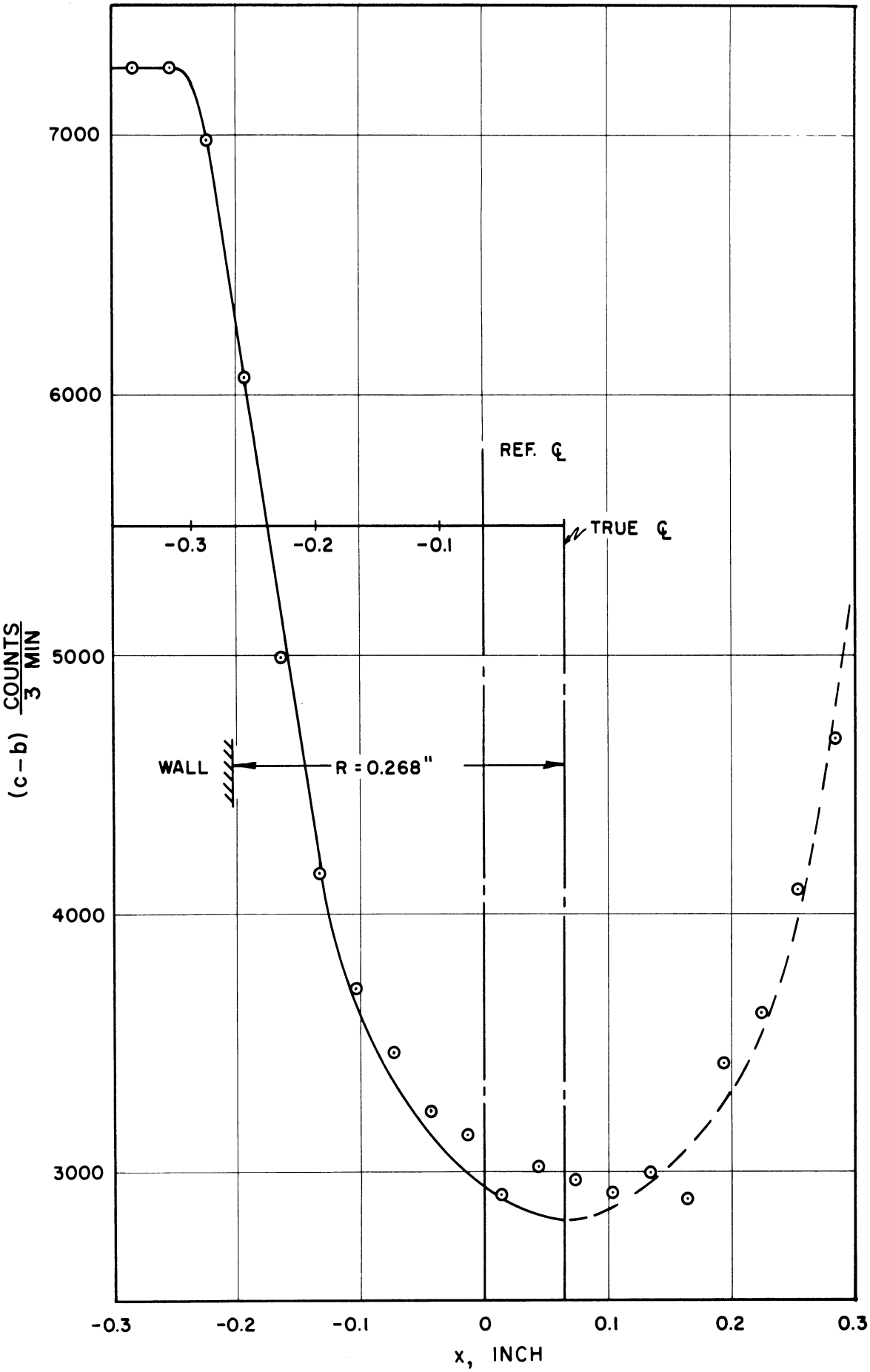

Figure 15. Run N°1, Cavitation to Nose. Z = 0.25, R = 0.268, D = 2.5.

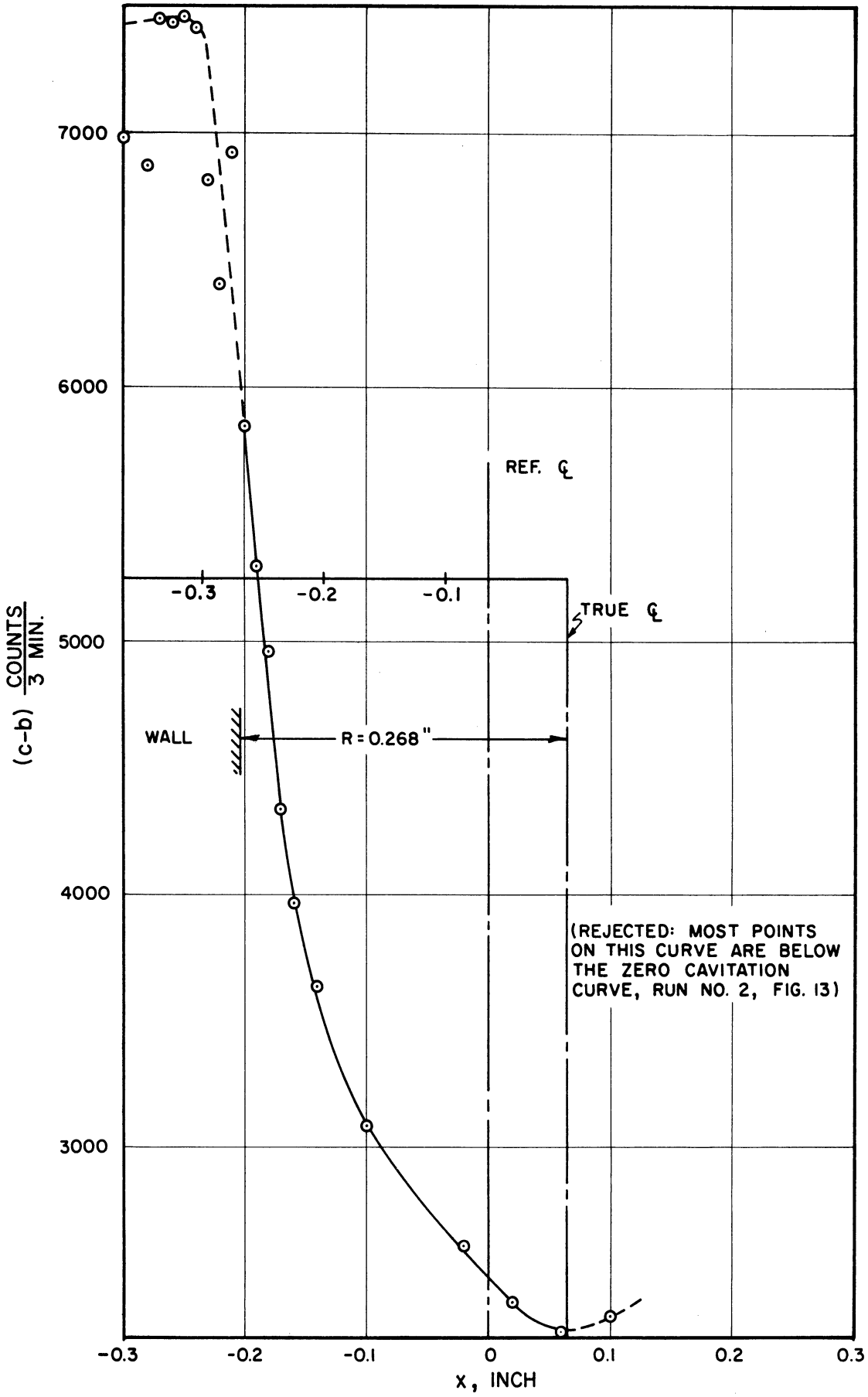

Figure 16. Run N°16, Visible Initiation Cavitation. Z = 0.25, R = 0.268, D = 2.5.

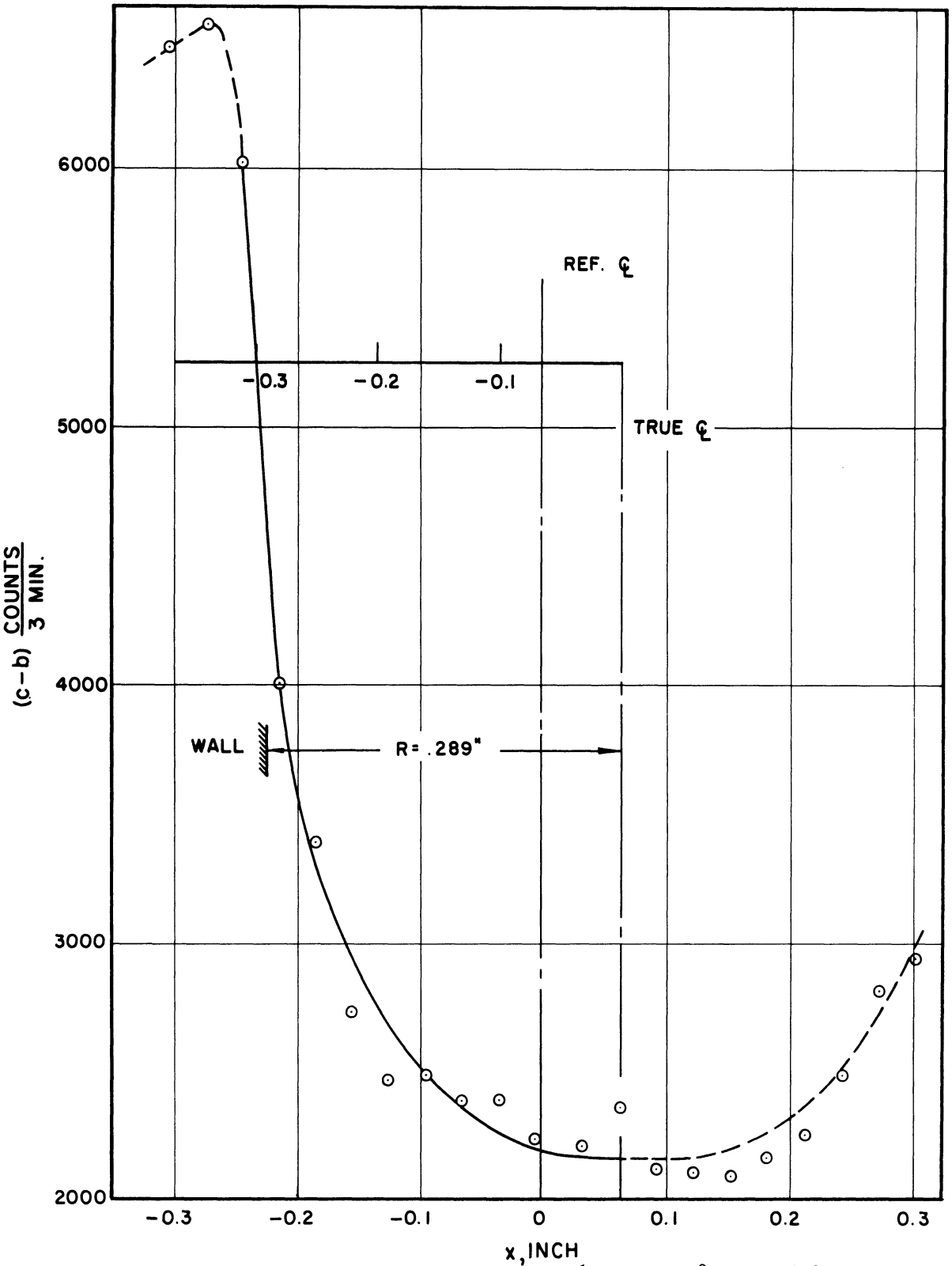

Figure 17. Run N°3, Zero Cavitation. Z = 0.625, R = 0.289, D = 1.0.

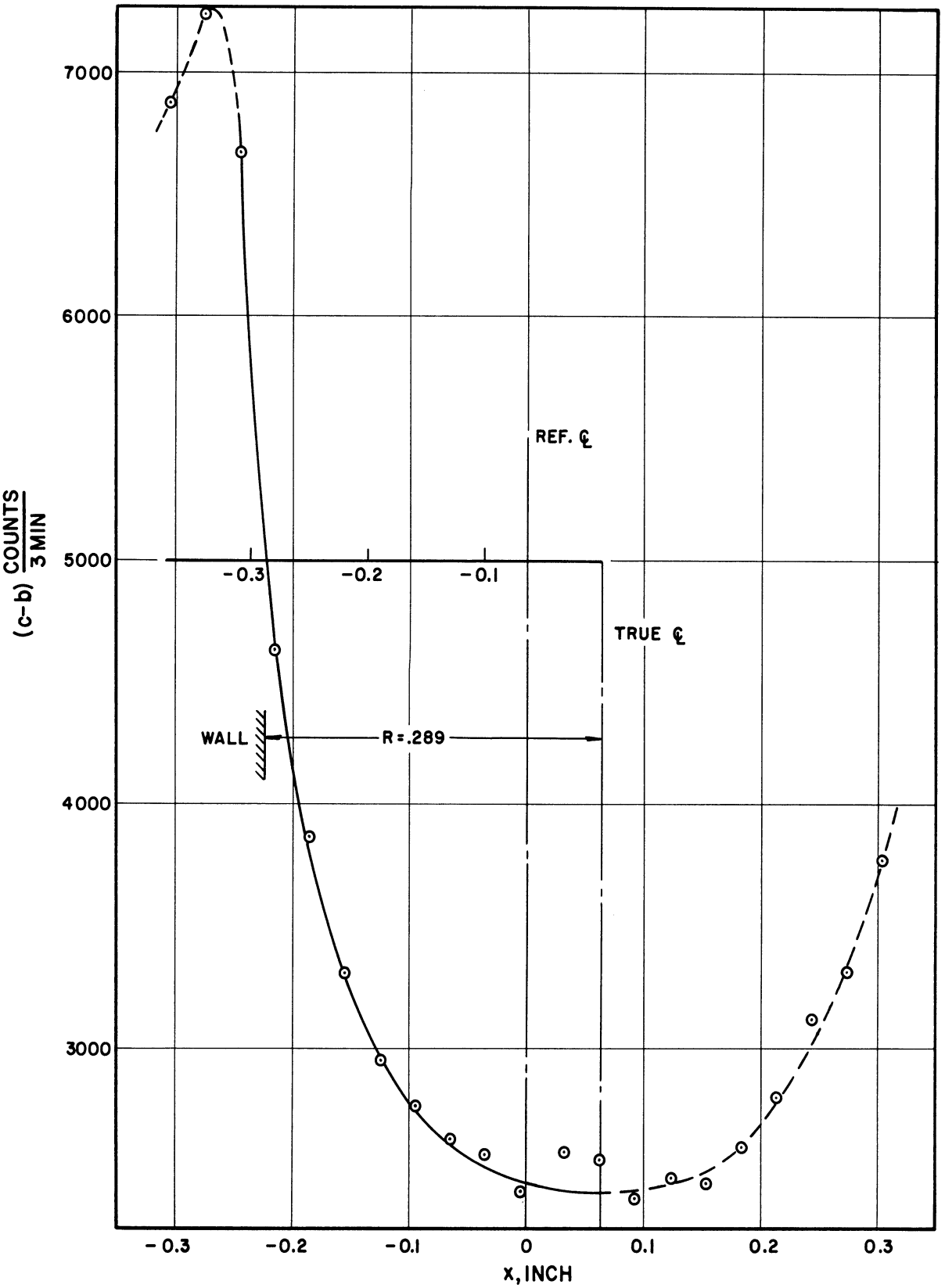

Figure 18. Run N°4, Cavitation to Nose. Z = 0.625, R = 0.289, D = 2.5.

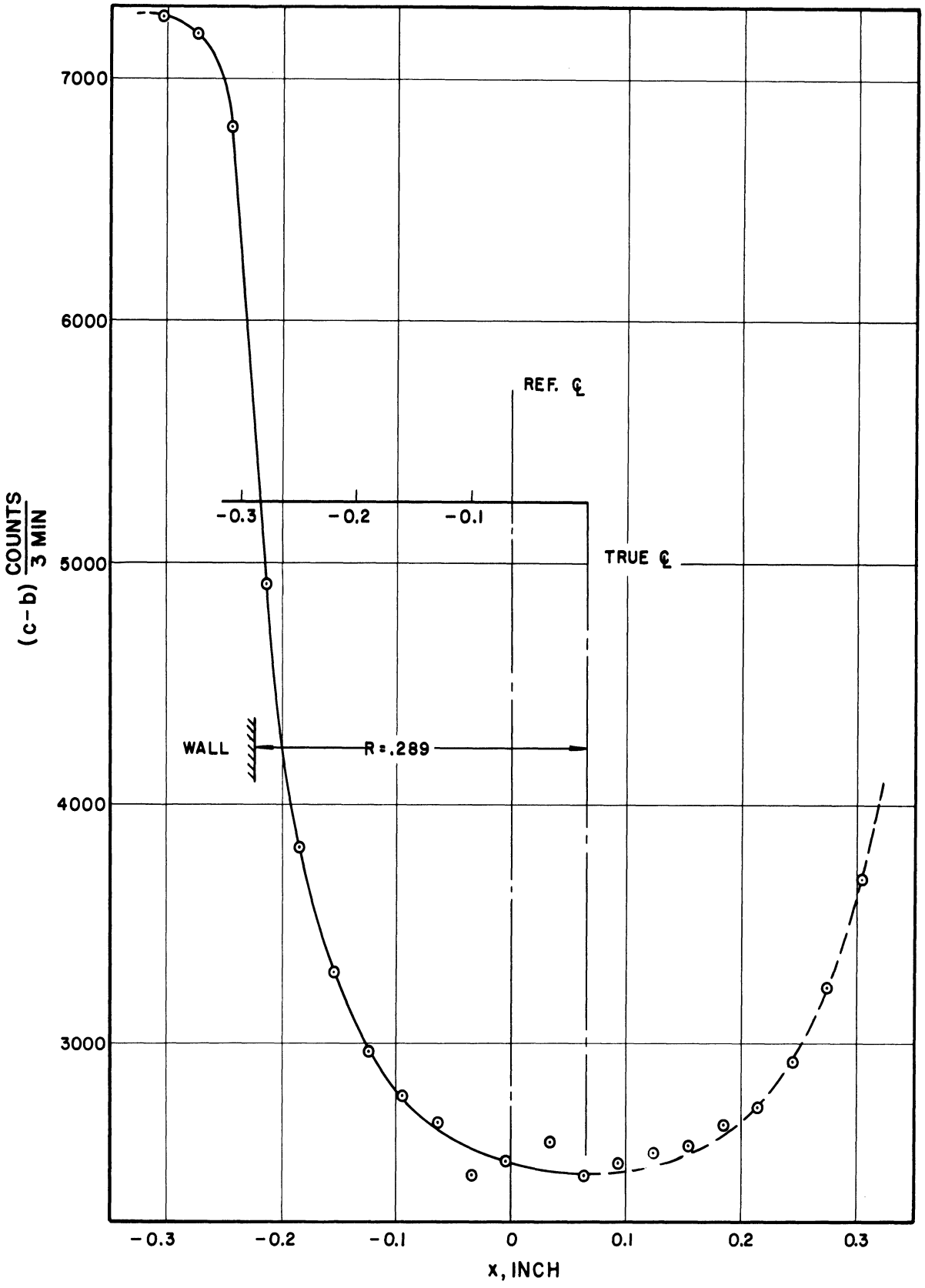

Figure 19. Run N°6, Standard Cavitation. Z = 0.625, R = 0.289, D = 2.5.

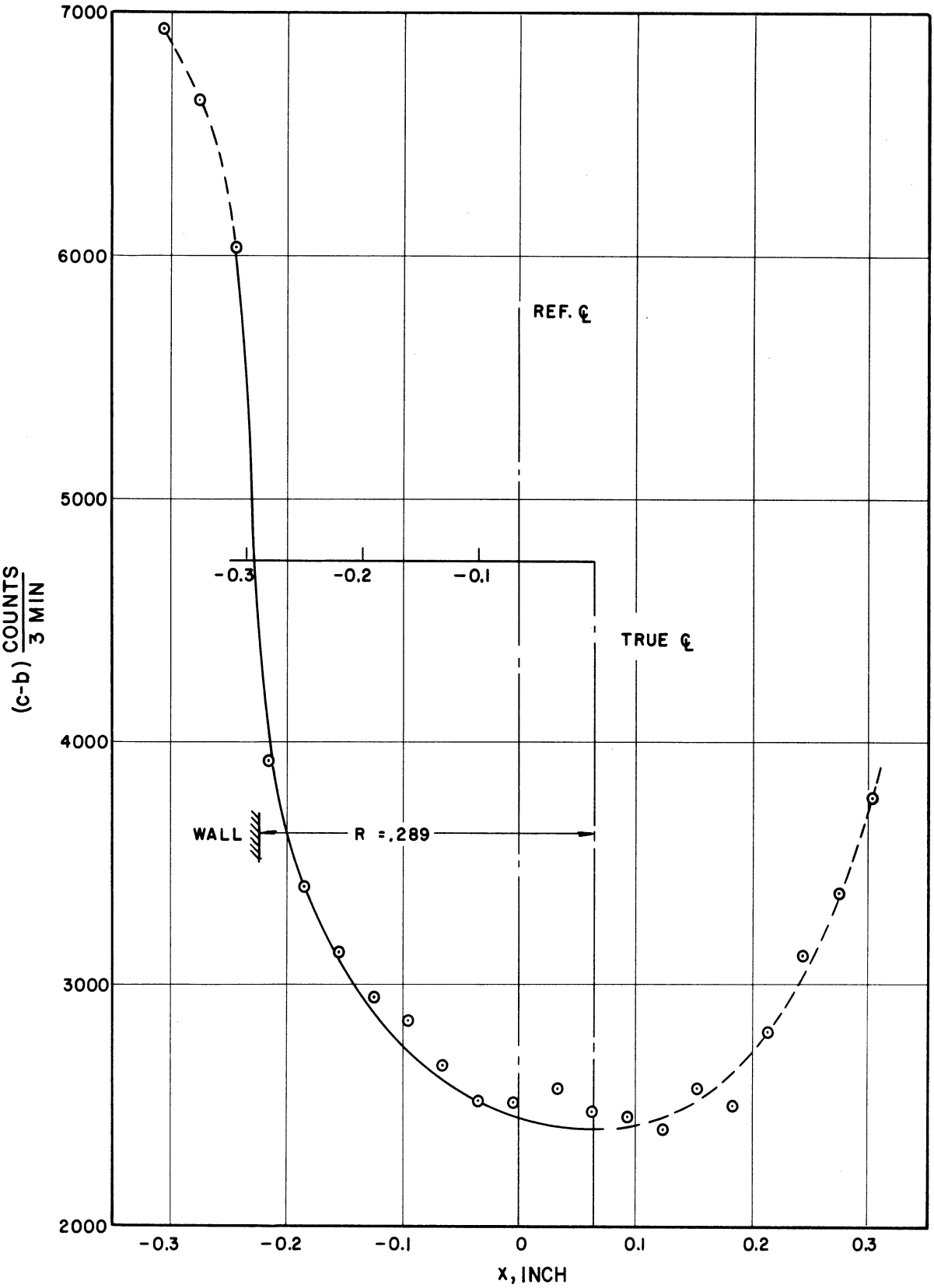

Figure 20. Run N°5, Visible Initiation Cavitation. Z = 0.625, R = 0.289, D = 2.5.

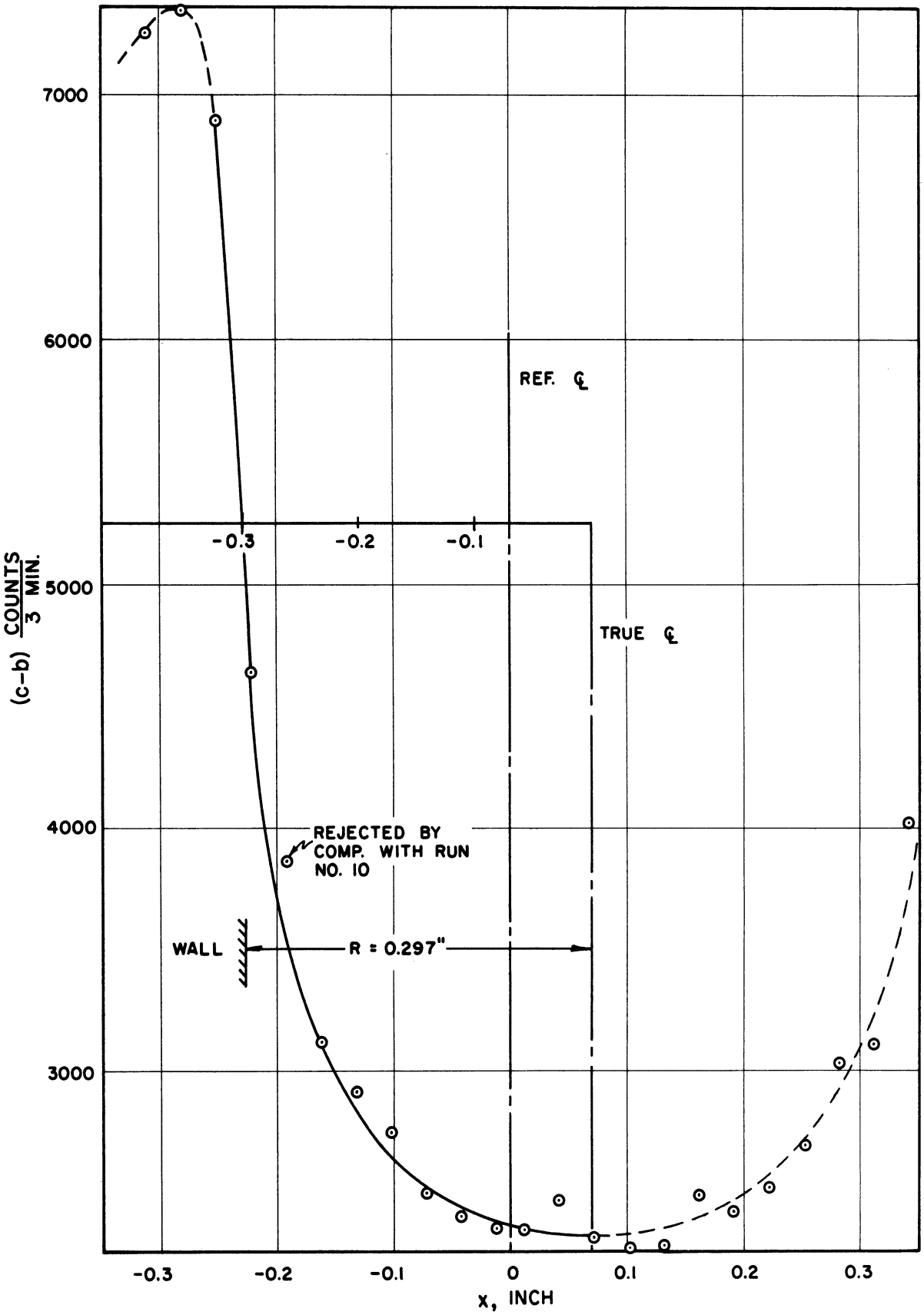

Figure 21. Run N°8, Zero Cavitation. Z = 0.786, R = 0.297, D = 1.0.

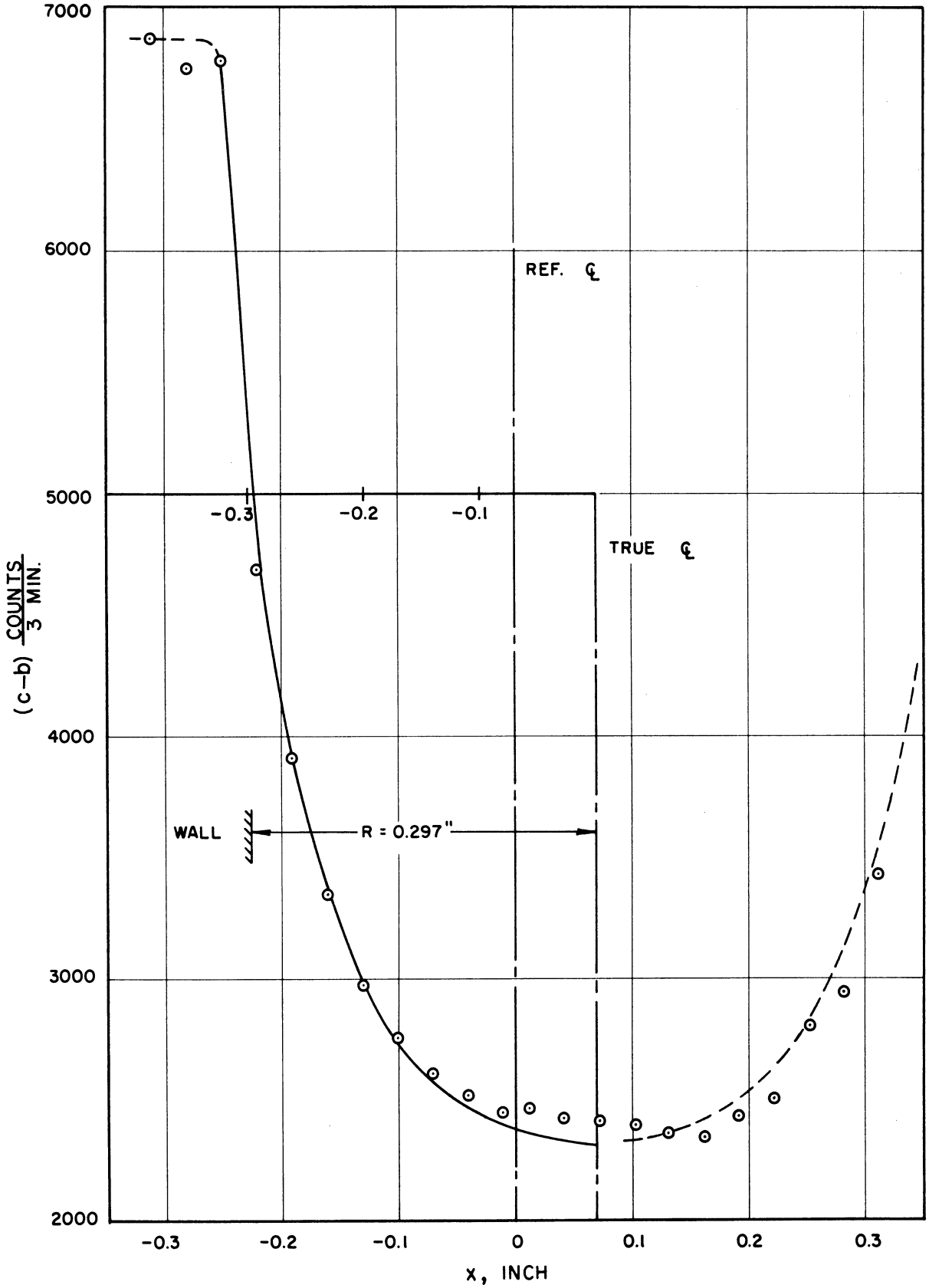

Figure 22. Run N°7, Standard Cavitation. Z = 0.786, R = 0.297, D = 2,5.

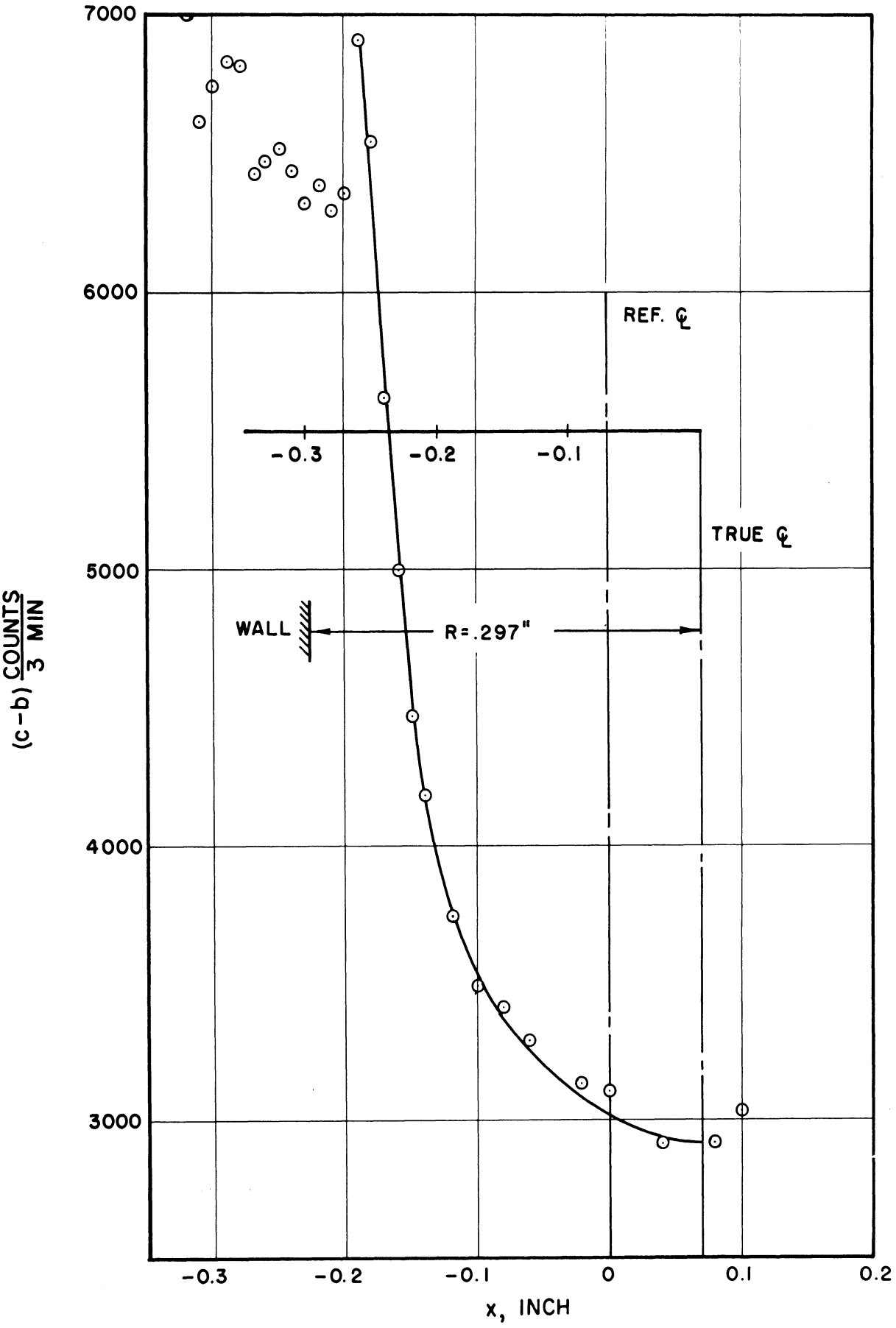

Figure 23. Run N°24, First Mark Cavitation. Z = 0.786, R = 0.297, D = 2.5.

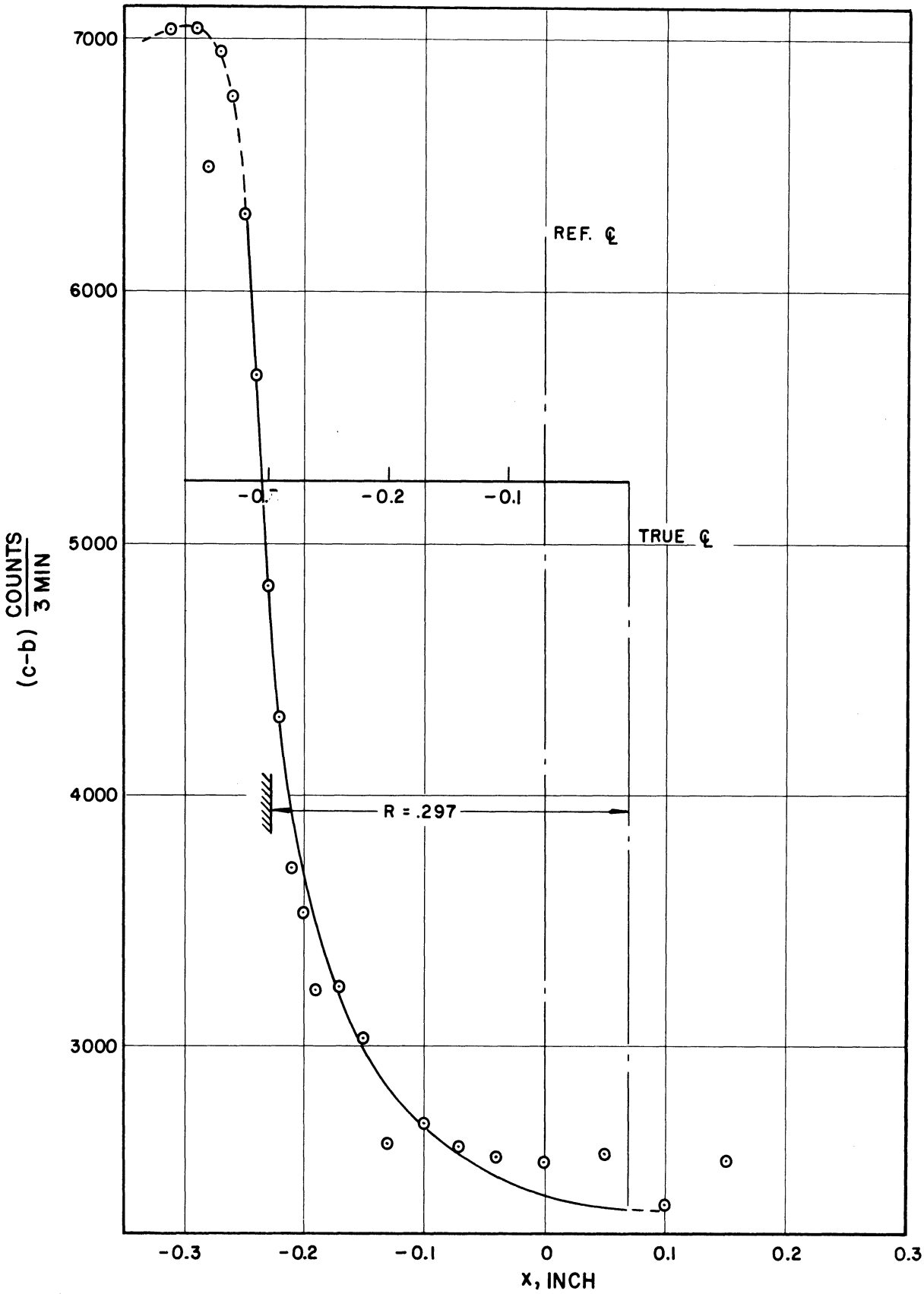

Figure 24. Run N°10, Visible Initiation Cavitation. Z = 0.786, R = 0.297, D = 2.5.

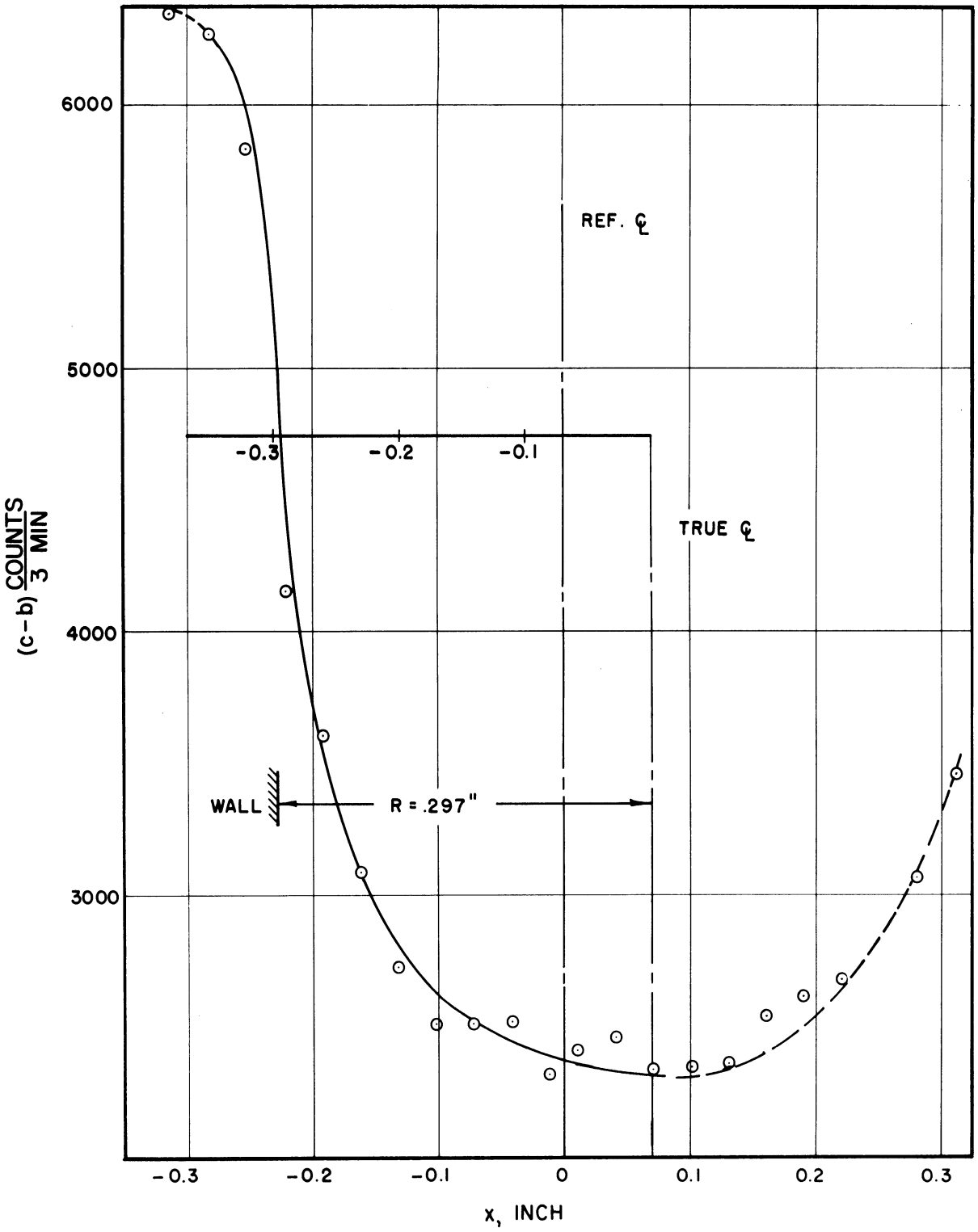

Figure 25. Run N°9, Cavitation to Nose. Z = 0.786, R = 0.297, D = 2.5.

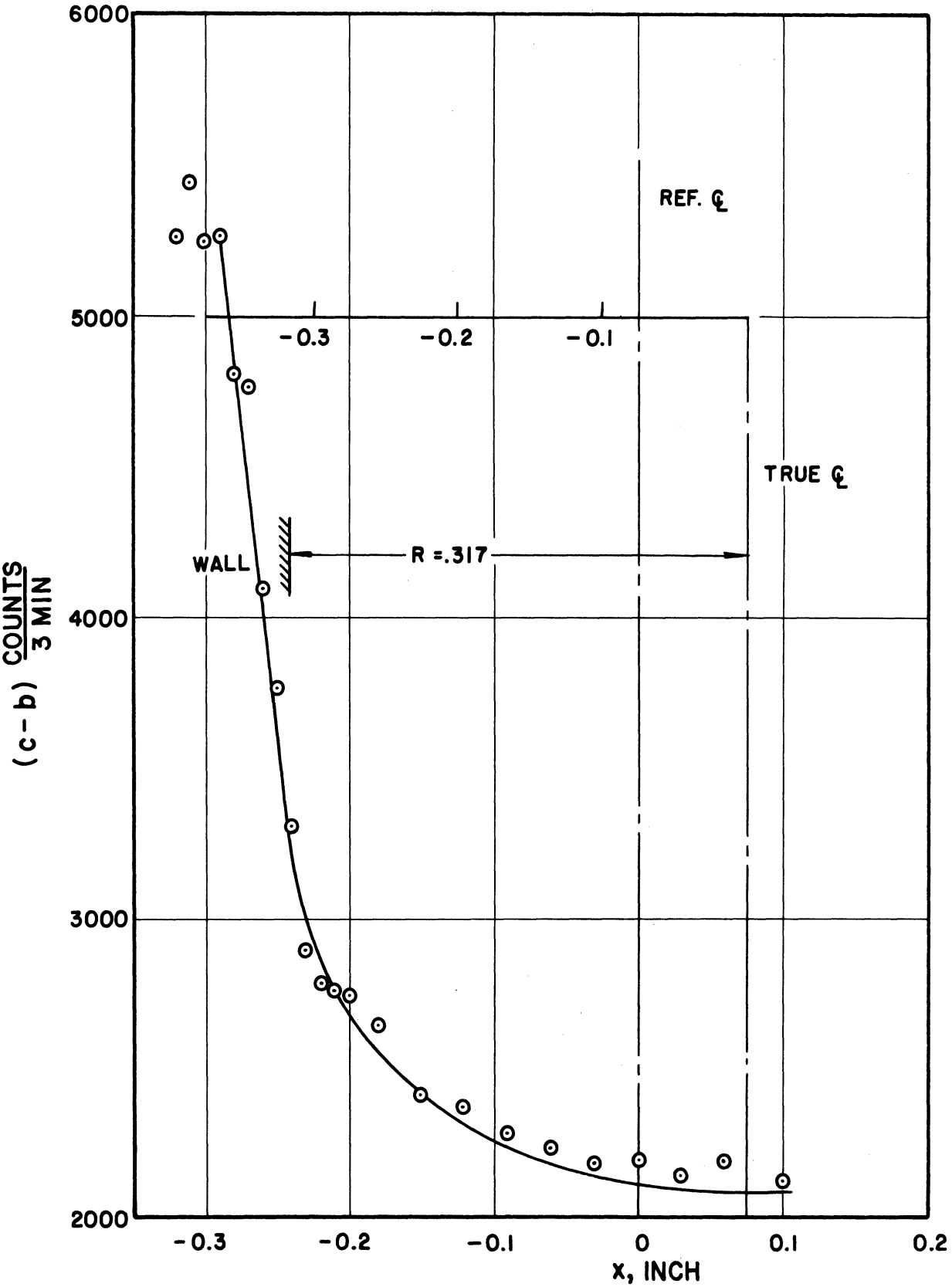

Figure 26. Run N°12, Zero Cavitation. Z = 1.163, R = 0.317, D = 1.0.

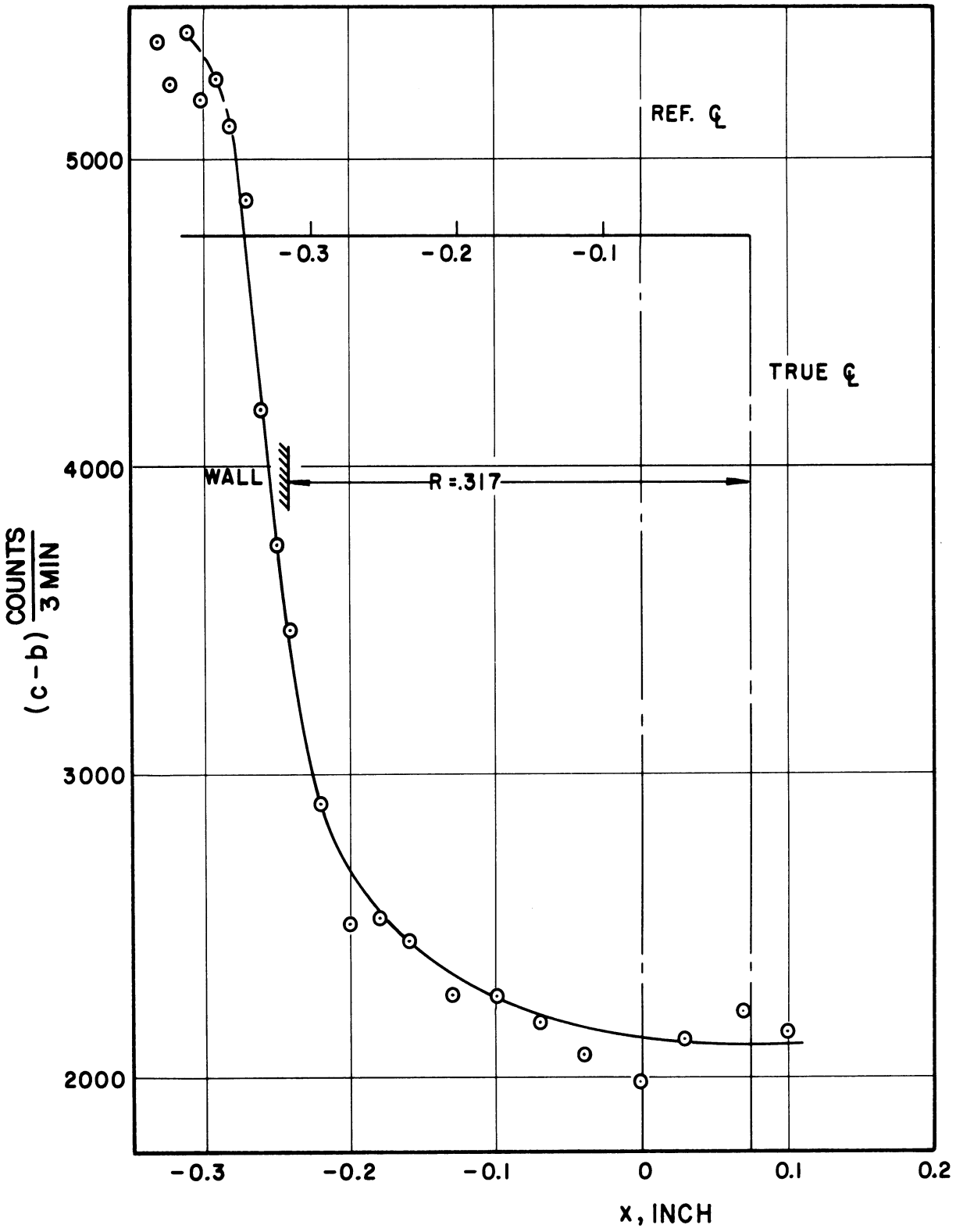

Figure 27. Run N°11, Visible Initiation Cavitation. Z = 1.163, R = 0.317, D = 2.5.

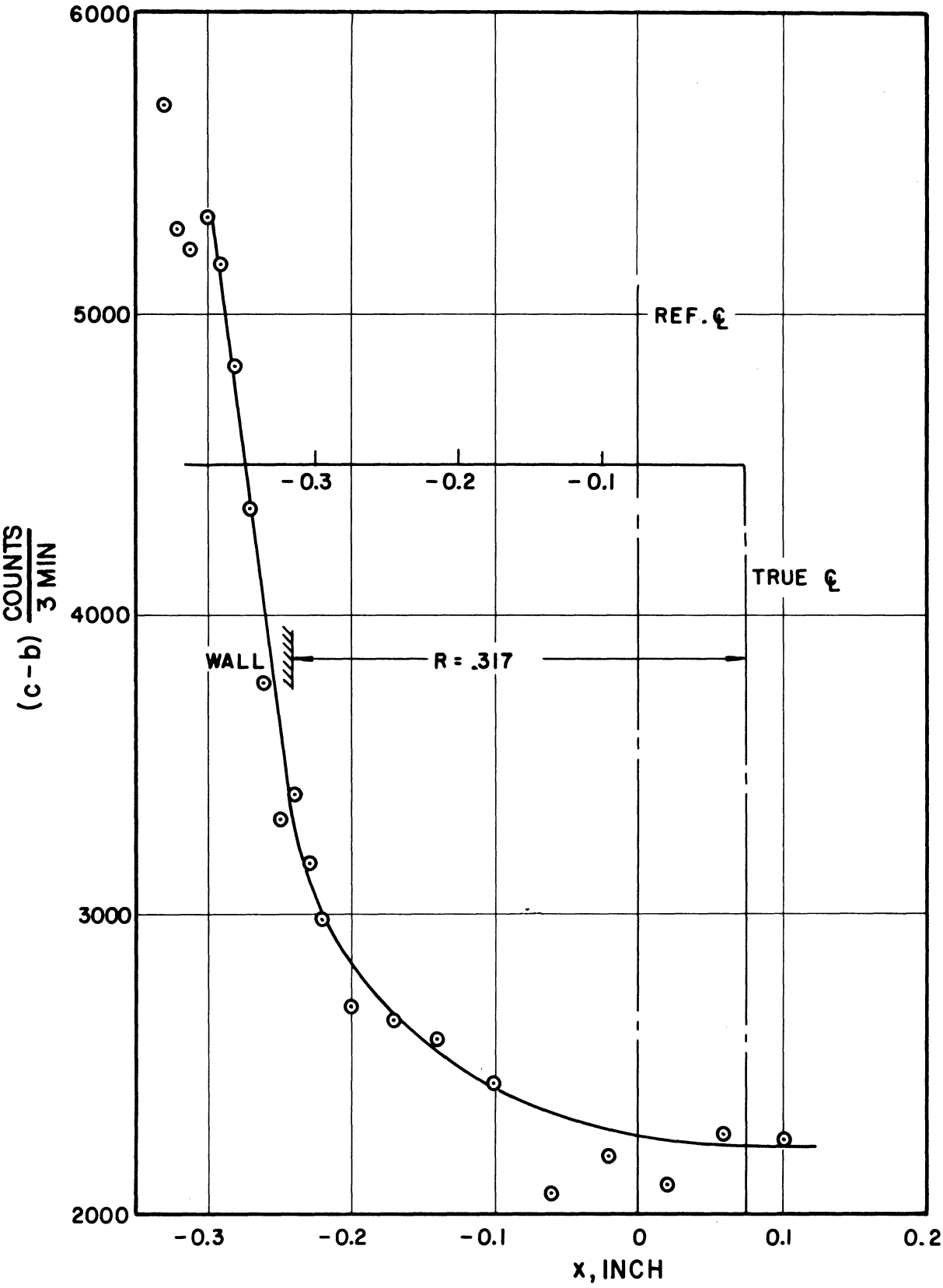

Figure 28. Run N°14, Standard Cavitation. Z = 1.163, R = 0.317, D = 2.5.

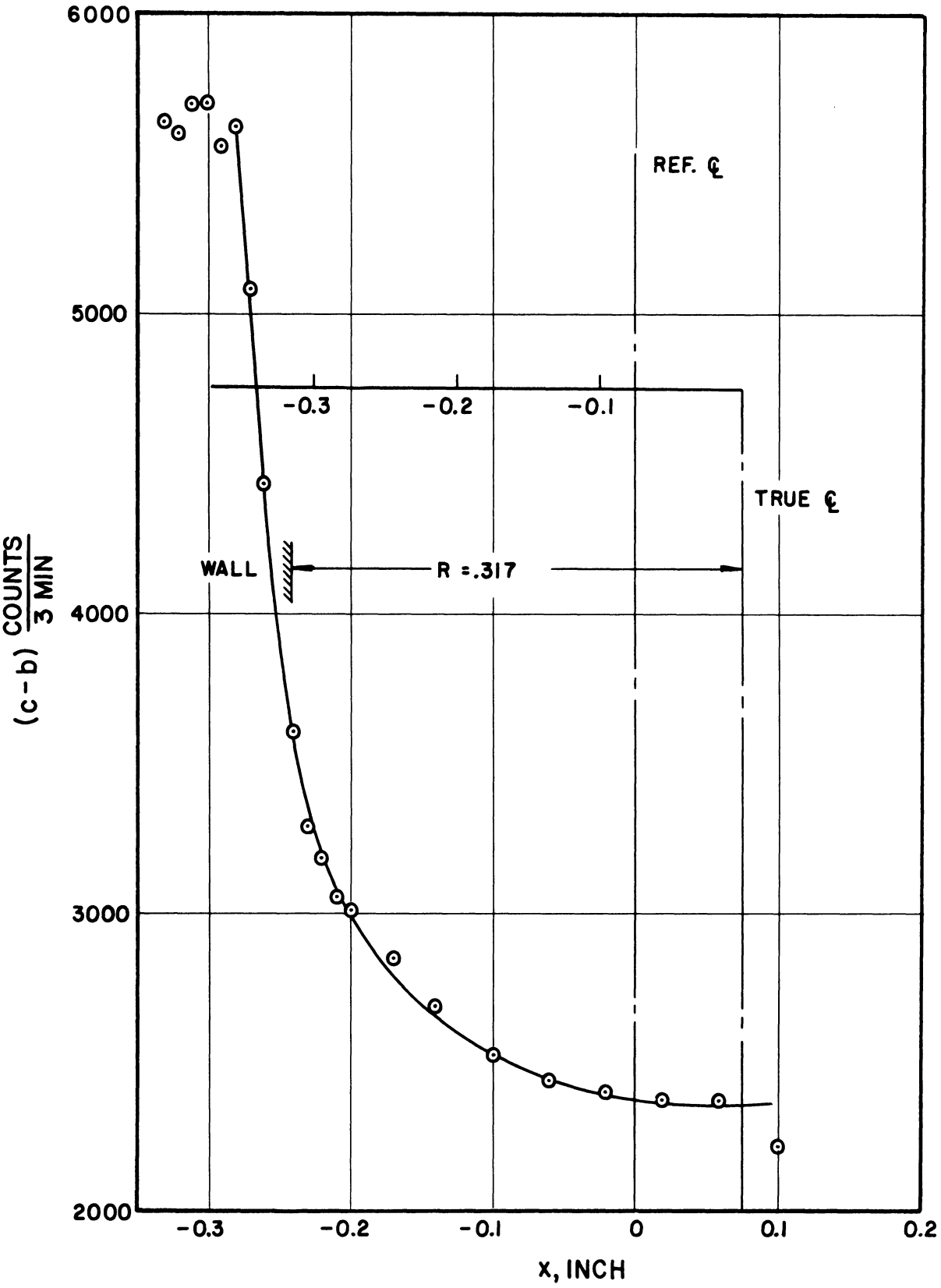

Figure 29. Run N°13, Cavitation to Nose. Z = 1.163, R = 0.317, D = 2.5.

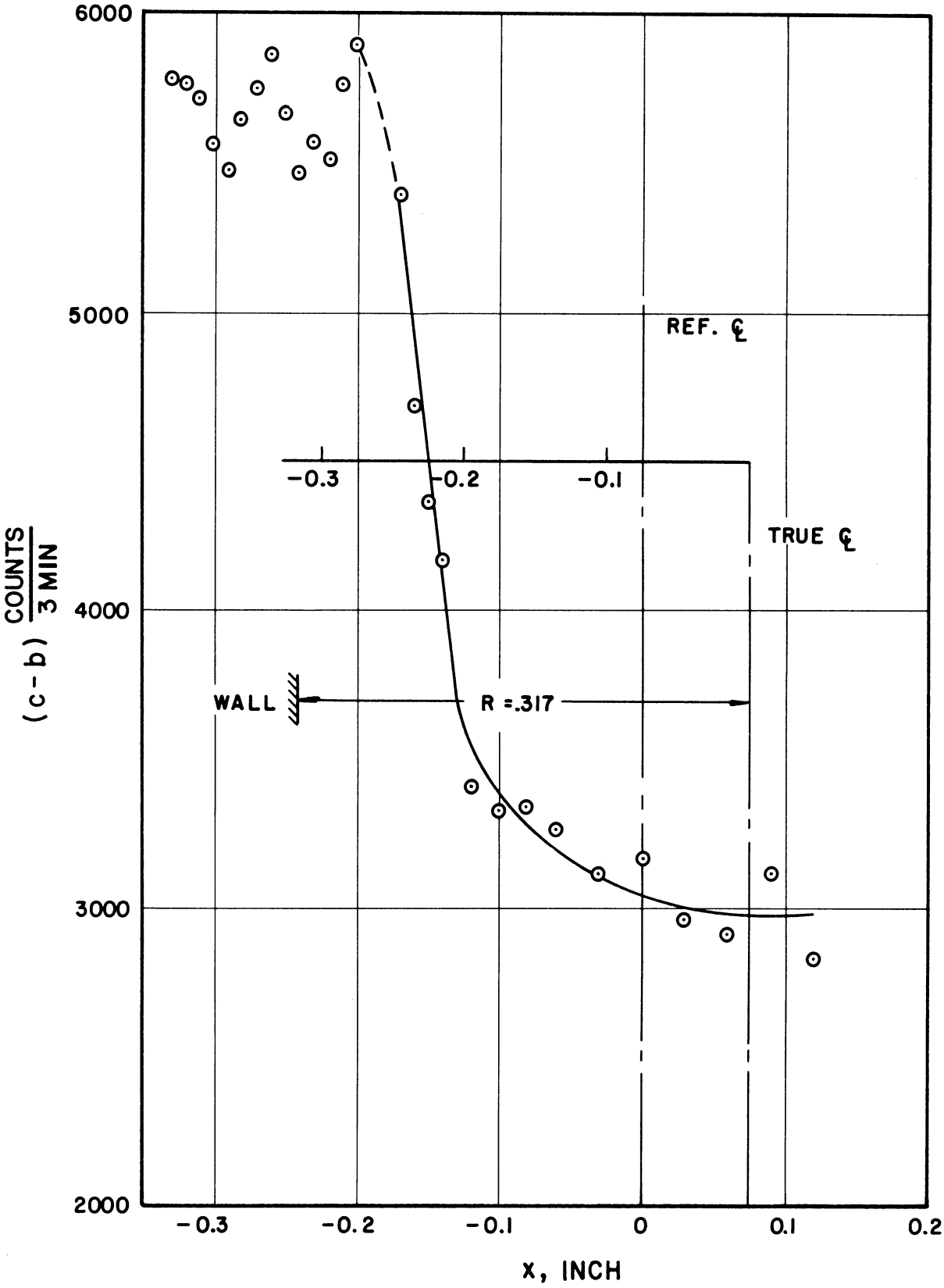

Figure 30. Run N°25, First Mark Cavitation. Z = 1.163, R = 0.317, D = 2.5.

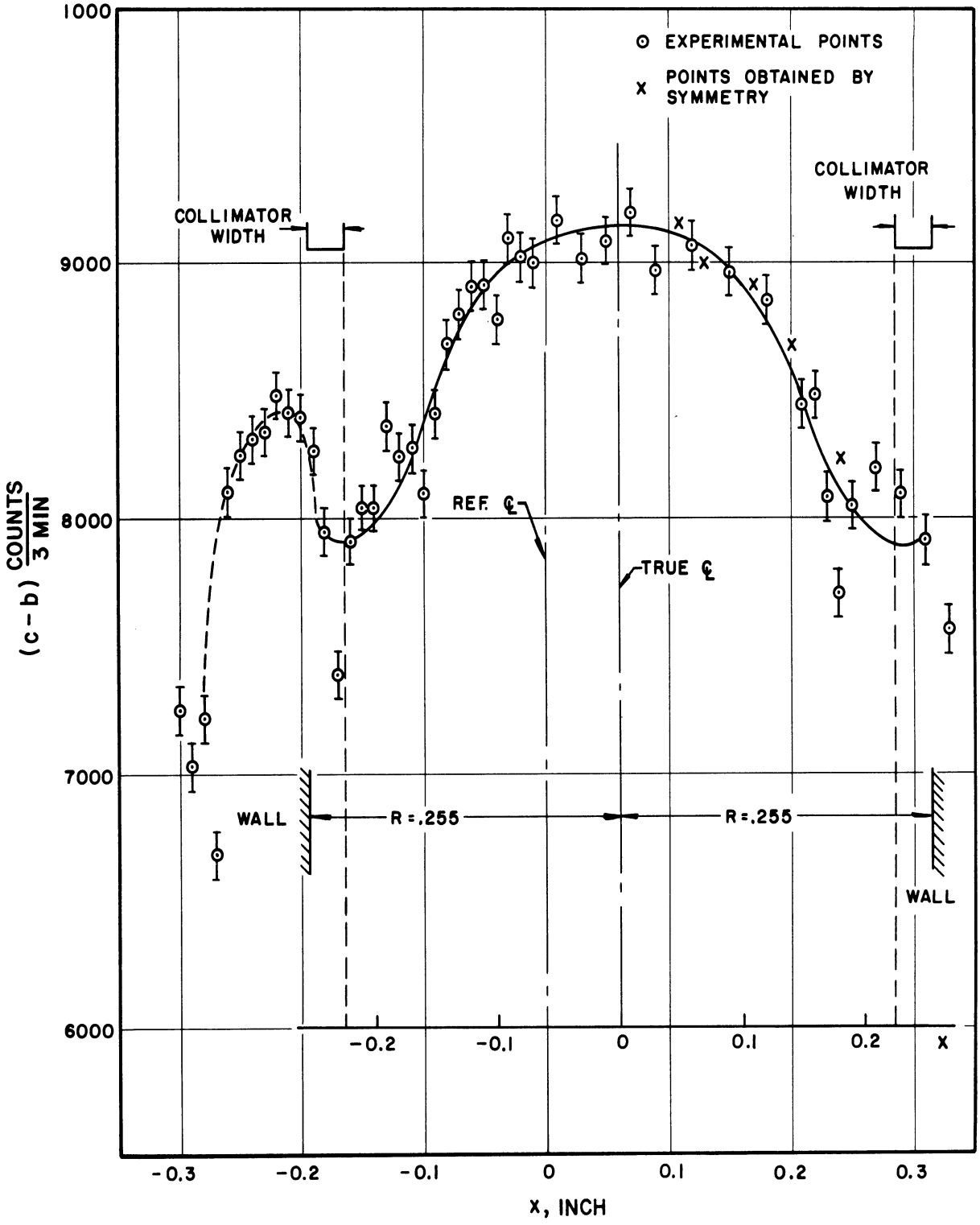

Figure 31. Run N°26, Venturi Filled With Air. Z = -0.25, R = 0.255.

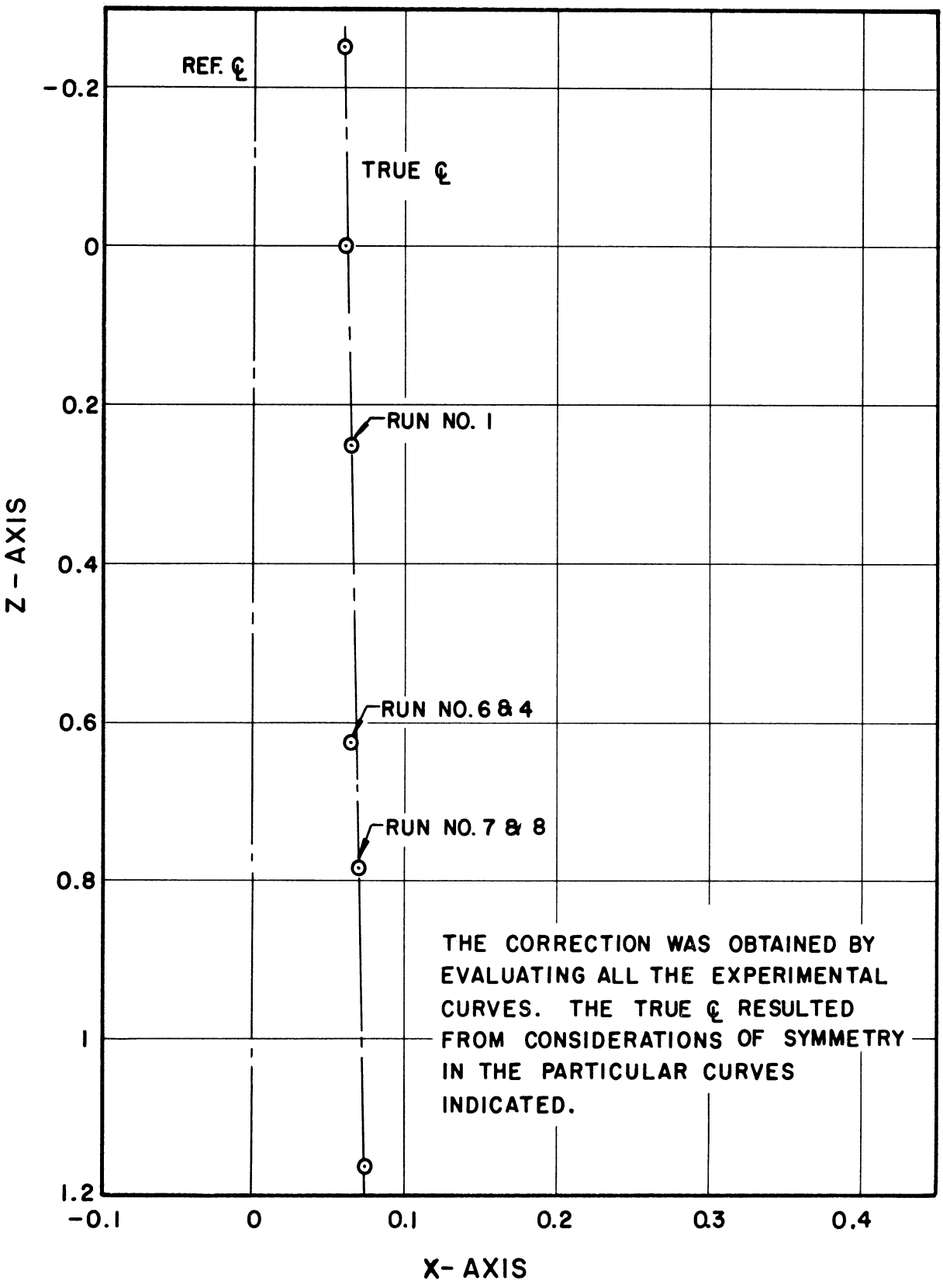

Figure 32. Centerline Correction.

the true center line. These values of correction or deviation from the reference center line were plotted for the various axial positions in Figure 32 to give the true center line of flow compared to the arbitrary reference center line used to take the data. The true center line was finally added to Figures 6 through 31.

It is observed that the standard deviation of a typical point on these curves represents a statistical error of less than 2%. Considerably more deviation than this was observed for points near or in the plastic walls of the venturi. This is considered to be due to the pitted condition of the wall surface, and the subsequent collection of a brownish oxidation material in the wall pores which radically changes the attenuation of gammas from point to point in this vicinity. Figure 31 shows a run made with the venturi containing only air and indicates a considerable deviation in the count rate at or near the walls, i.e., of the order of three or four standard deviations. It is noted that the curve is symmetrical with respect to the true center line.

The above irregularities could be reduced by the use of a new plexiglas test section which would not contain insert holes for wear testing. This would eliminate the possibility of a film of strongly attenuating material collecting on the boundaries of the wear inserts (Figure 2).

The cavitation conditions labelled visible initiation, cavitation to nose, standard cavitation and first mark have been previously defined[1,3]; however, the definitions are repeated here for convenience. Reference to Figure 2 will help to clarify the discussion.

"Visible Initiation" is that cavitation condition in which a continuous ring of cavitation only is visible at throat discharge. For "Cavitation to Nose," the cavitation terminates at the axial position corresponding to the location of the nose of the test specimens (which actually were not present in this experiment). "Standard Cavitation" has its termination at the position of the middle of the damage specimens. "First Mark Cavitation" has the termination 1 3/4 inches downstream of the throat exit, and thus also downstream of the specimens. The above conditions are listed in increasing extent of the cavitating region. They can be reproduced quite accurately by reproducing venturi inlet and outlet pressures.

Runs were made for each cavitation condition at several specified axial positions at a given flow-rate. For each run a traverse was made across the venturi using increments no greater than 0.030" and sometimes smaller. As will be shown later, with the assumption of axial flow symmetry, a single radial traverse is sufficient to delineate the mean density (or void fraction) as a function of radius.

IV. REDUCTION OF THE DATA

After correction of background, the experimental count rates were plotted as function of distance in Figures 6 through 31. In the same figures, the correction of the center line position was performed. The count-rate values for the various cavitation conditions, $N_1(x)$, were retabulated from these smoothed curves, and compared with the count rates, $N_2(x)$, from the corresponding non-cavitating curves. The use of smoothed curves, held at all times within the limits defined by the standard deviations of the experimental points, was desirable to produce consistent final results.

The method for computing void fraction from the count-rate data has been previously given[8], but it is repeated for convenience in Appendix C. The actual calculation was performed with the help of an IBM 709 computer using the program detailed in Appendix D. The final results are presented in Tables XI through XXVII, where F represents the void fraction in percentage and r the normalized radial distance with respect to the true center line.

Preliminary calculations were first performed taking a 0.030" increment between the points read from the smoothed curves. The first point was taken 0.015" inside the Hg to eliminate the possibility of a point involving partial attentuation in plastic and mercury. If the void fractions, so calculated were obviously in error, such as gross nonsymmetry, the smoothed curves were modified, always within the limit of the statistical error, to obtain more reasonable results. This was necessary in some

cases, since it was found that a small horizontal displacement resulted in a very large effect on the count-rate difference at a particular transverse position between the cavitating and non-cavitating conditions. This was particularly true in the neighborhood of the walls, where the count-rate drops steeply. When the computed void fraction versus normalized radius curve showed a fairly continuous nature, the count-rate curves were considered properly drawn (as they appear in Figures 6 to 30). At this point a more detailed machine calculation was made using increments of 0.010" between points. The results are shown in Tables XI to XXVII.

V. DISCUSSION OF RESULTS

A summary of the experimental runs is shown in Table X, and the reduced data, giving void fraction as a function of radius for the various cavitation conditions in Tables XI through XXVII. From the computed data the constant void fraction profiles for the various cavitation conditions are shown in Figure 43, which was constructed as a cross-plot from Figures 33 through 42 where the void fraction is shown as a function of distance from the centerline at various axial positions, and for the various cavitation conditions. The presentation of the data in the form of constant void fraction profiles is believed most useful for the present purpose, i.e., a representation of the various flow regimes in terms of void fraction.

The venturi outline between the throat discharge and the downstream end of the test specimens (actually not in place during these tests) is shown to scale with respect to the venturi center line in Figure 43 as well as the outline of the test specimens. Upon this diagram constant void fraction loci are superimposed for the different cavitation conditions covering the range from "Visible Initiation," where there is only a ring of vapor at the throat discharge, to "First Mark Cavitation" wherein the cavitation terminates visually downstream of the end of the test specimen (1.75 inches downstream of throat discharge and 0.56 inches downstream of the trailing end of the test specimen).

An examination of the void fraction profiles discloses various significant results:

1) The data presented in this fashion is quite smooth and consistent with the possible exception of the 10%* line in the "Visible Initiation" condition , giving confidence in the accuracy of the results.

2) The region of relatively pure liquid (less than ~10% void) is virtually a jet of uniform diameter downstream to the vicinity of cavitation termination. However, the diameter of this jet is substantially less than the throat diameter (~88%) for all the cavitation conditions. Thus even for "Visible Initiation" there is substantial vapor along the wall of the venturi, at least as far back as 0.25 inches into the throat and presumably further. This vapor film along the wall tends to obviate the often-made assumption that friction drop in such a throat is not a function of the cavitation condition.

3) In no case is there more than a few percent void caused by the overall cavitation field in the vicinity of the polished faces of the damage specimens.** Hence it is surmised that the damage is probably mainly caused by local cavitation generated by the presence of the specimens themselves, and it appears from the damage tests that the greatest damage occurs in regions of relatively small void.***

---

*The precision of the data for void fractions less than 10% seems questionable from an examination of Figures 33 through 42.

**See Reference 9 for a detailed description of the test specimens and the venturi.

***It should be possible to verify this assumption in future water tests which are planned with a two-dimensional venturi.

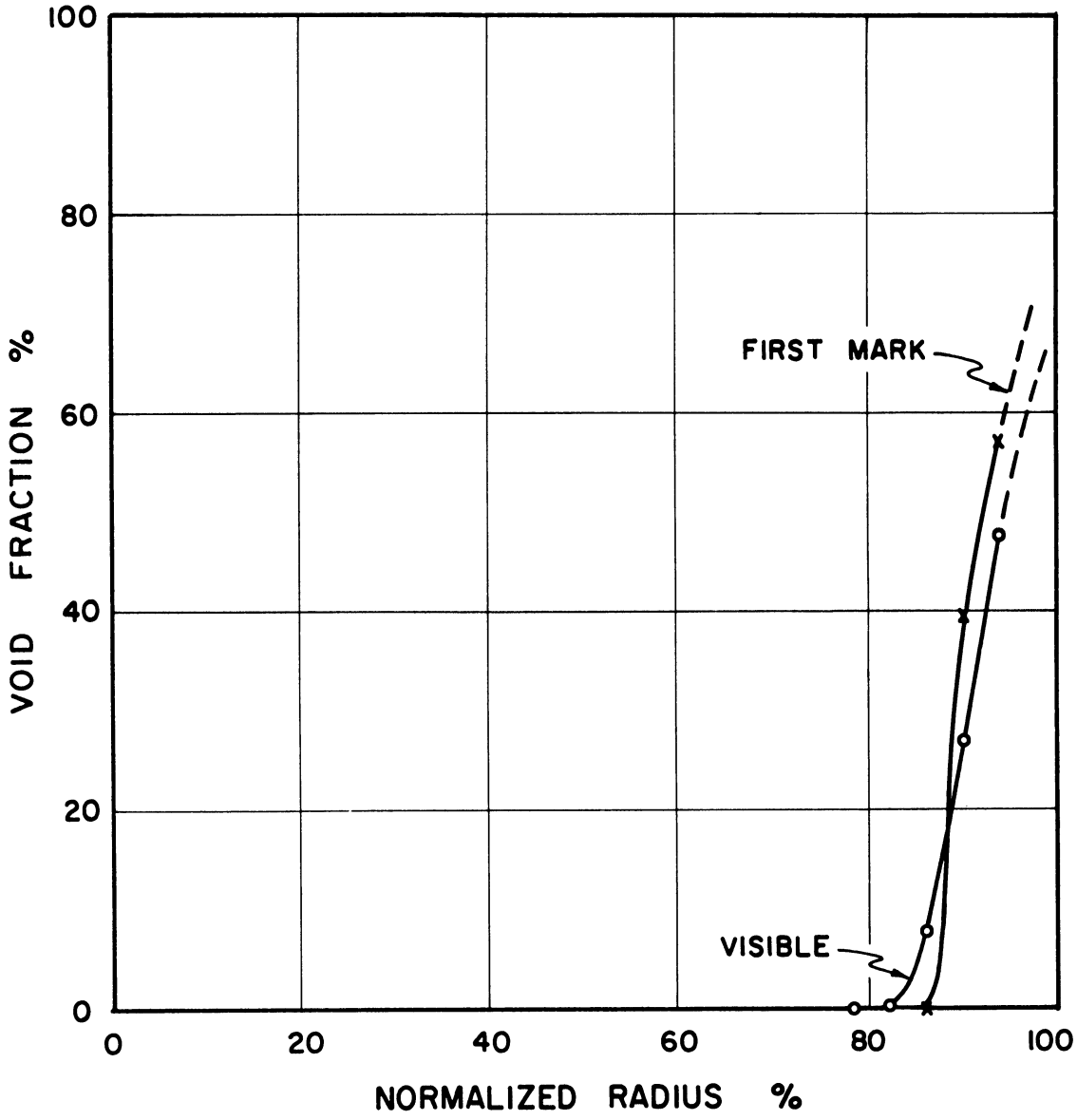

Figure 33. Void Fraction versus Normalized Radius.
Z = -0.25, R = 0.255.
Data from Computer Run N°24.

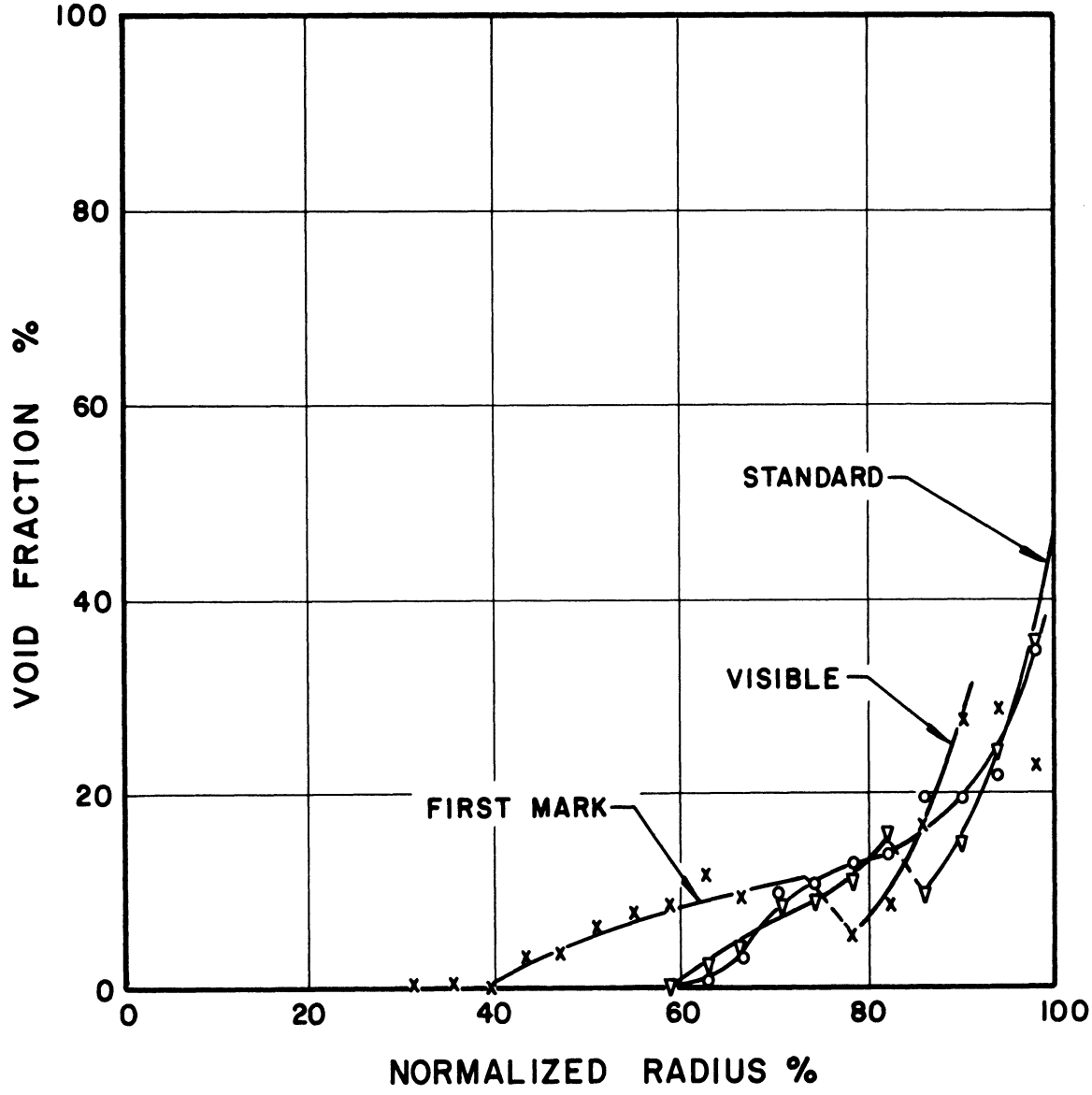

Figure 34. Void Fraction versus Normalized Radius.
Z = 0.00, R = 0.255.
Data from Computer Run N°25.

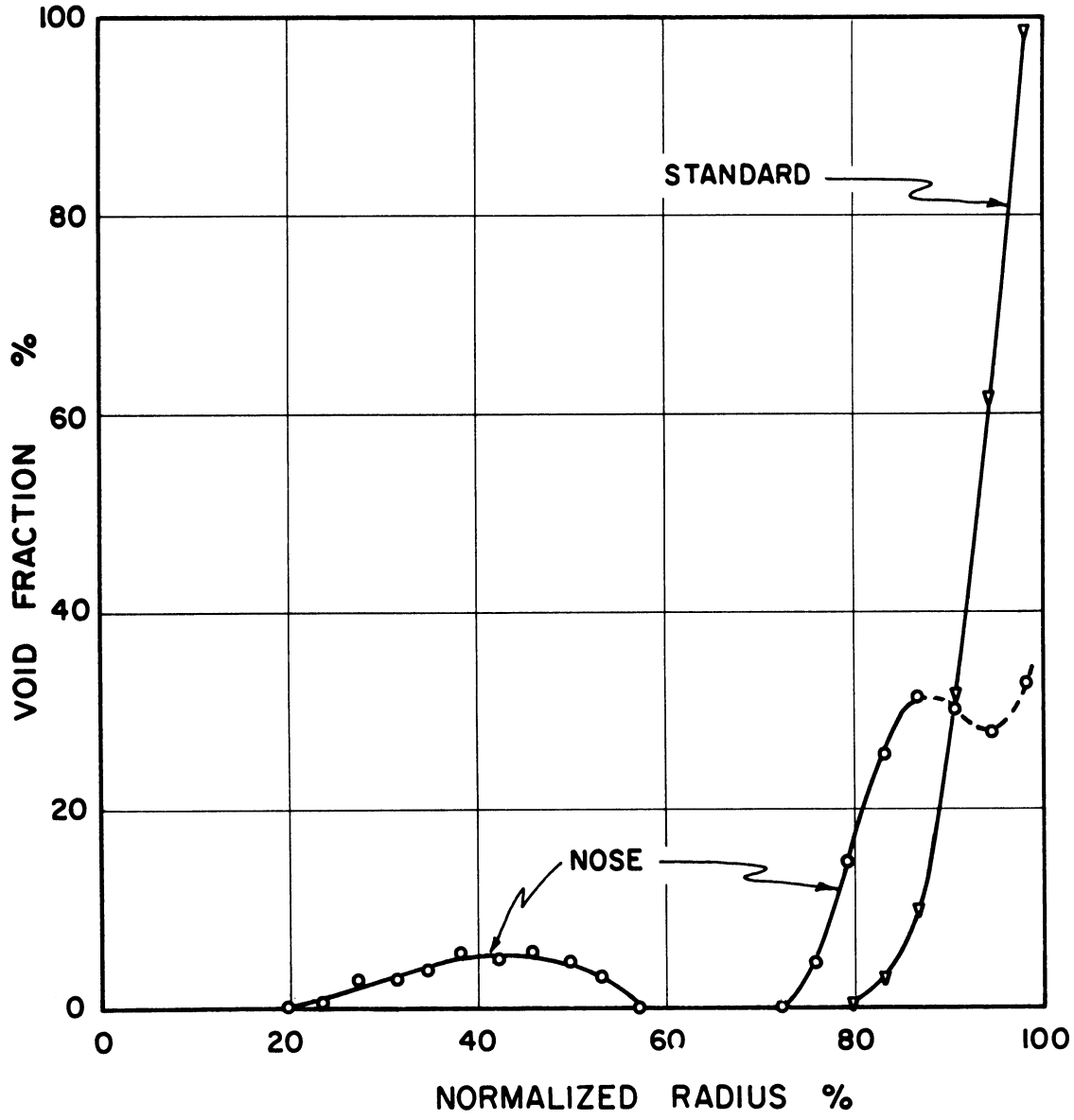

Figure 35. Void Fraction versus Normalized Radius.
Z = 0.25, R = 0.268
Data from Computer Run N°26.

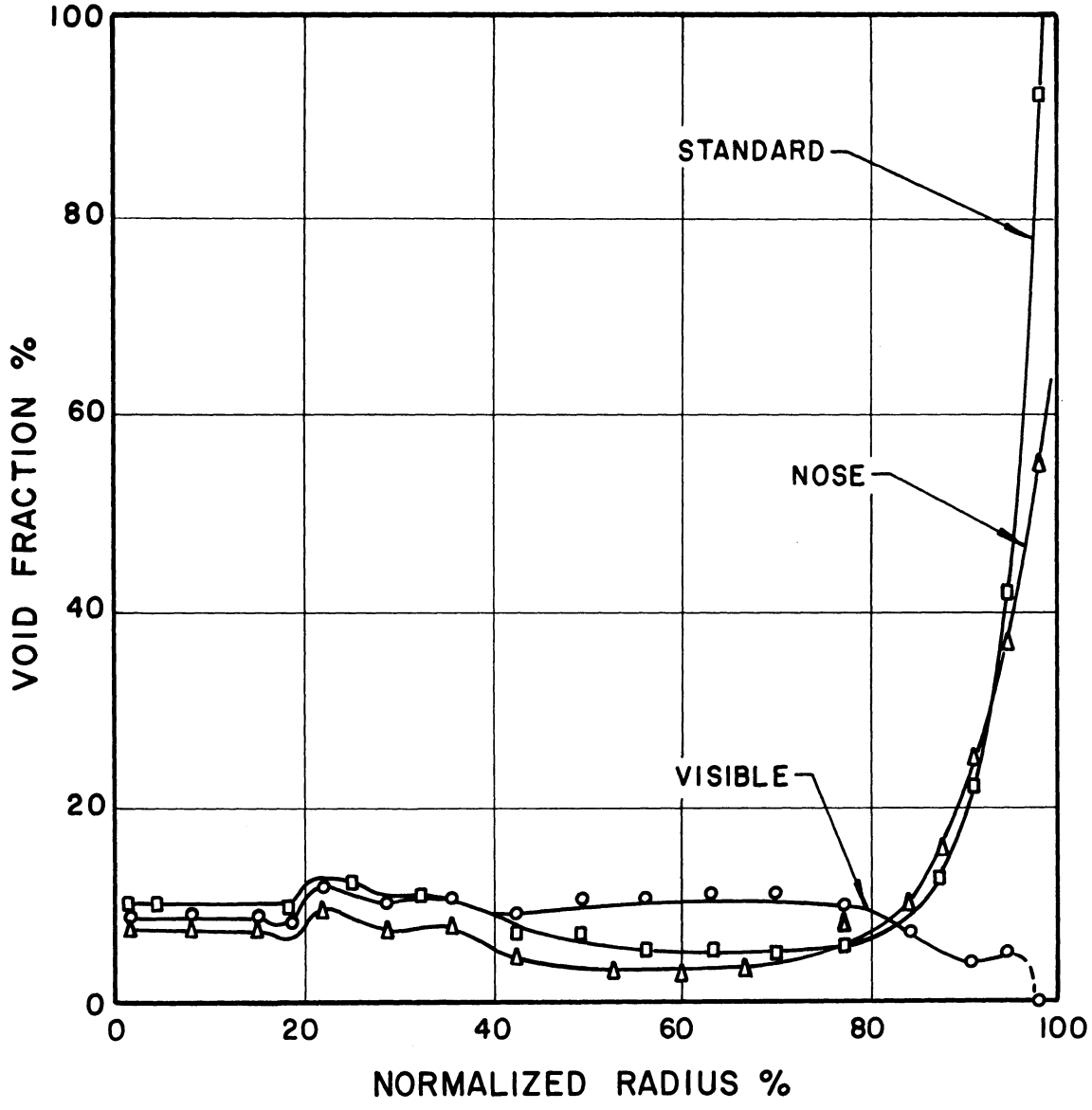

Figure 36. Void Fraction versus Normalized Radius.
Z = 0.625, R = 0.289.
Data from Computer Run N°18.

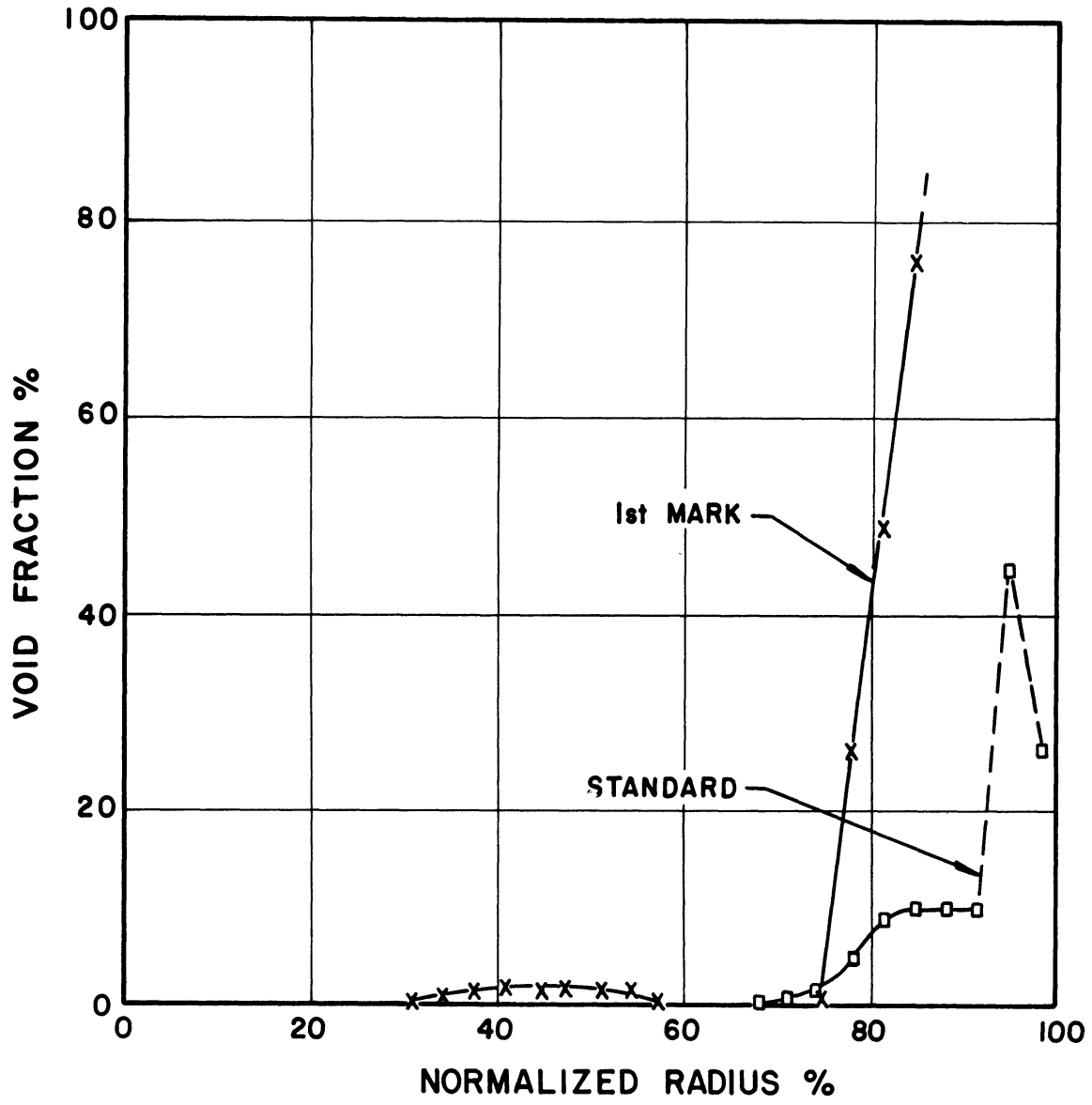

Figure 37. Void Fraction versus Normalized Radius.
Z = 0.786, R = 0.297.
Data from Computer Run N°27.

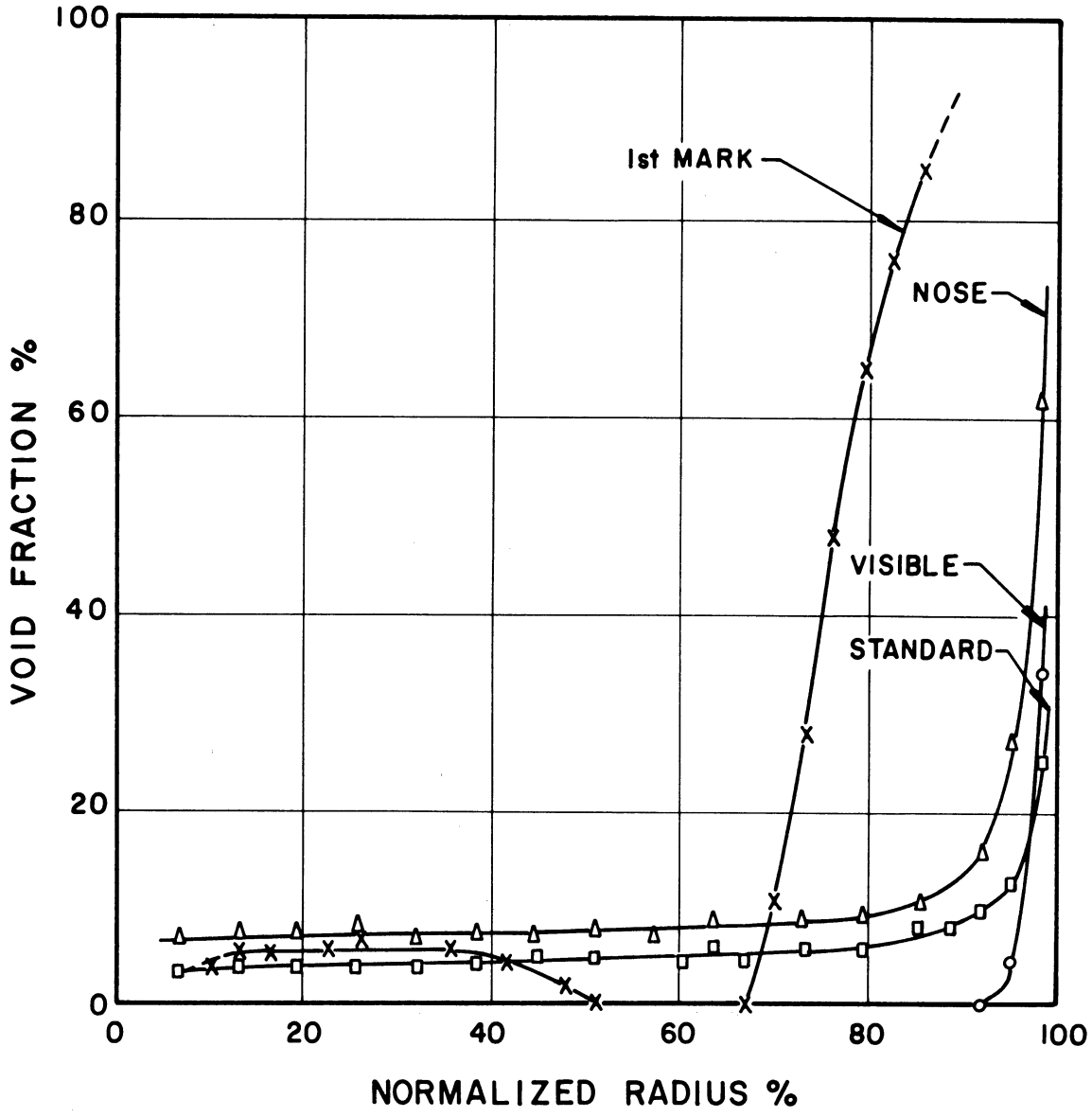

Figure 38. Void Fraction versus Normalized Radius.
Z = 1.163, R = 0.317.
Data from Computer Run N°19.

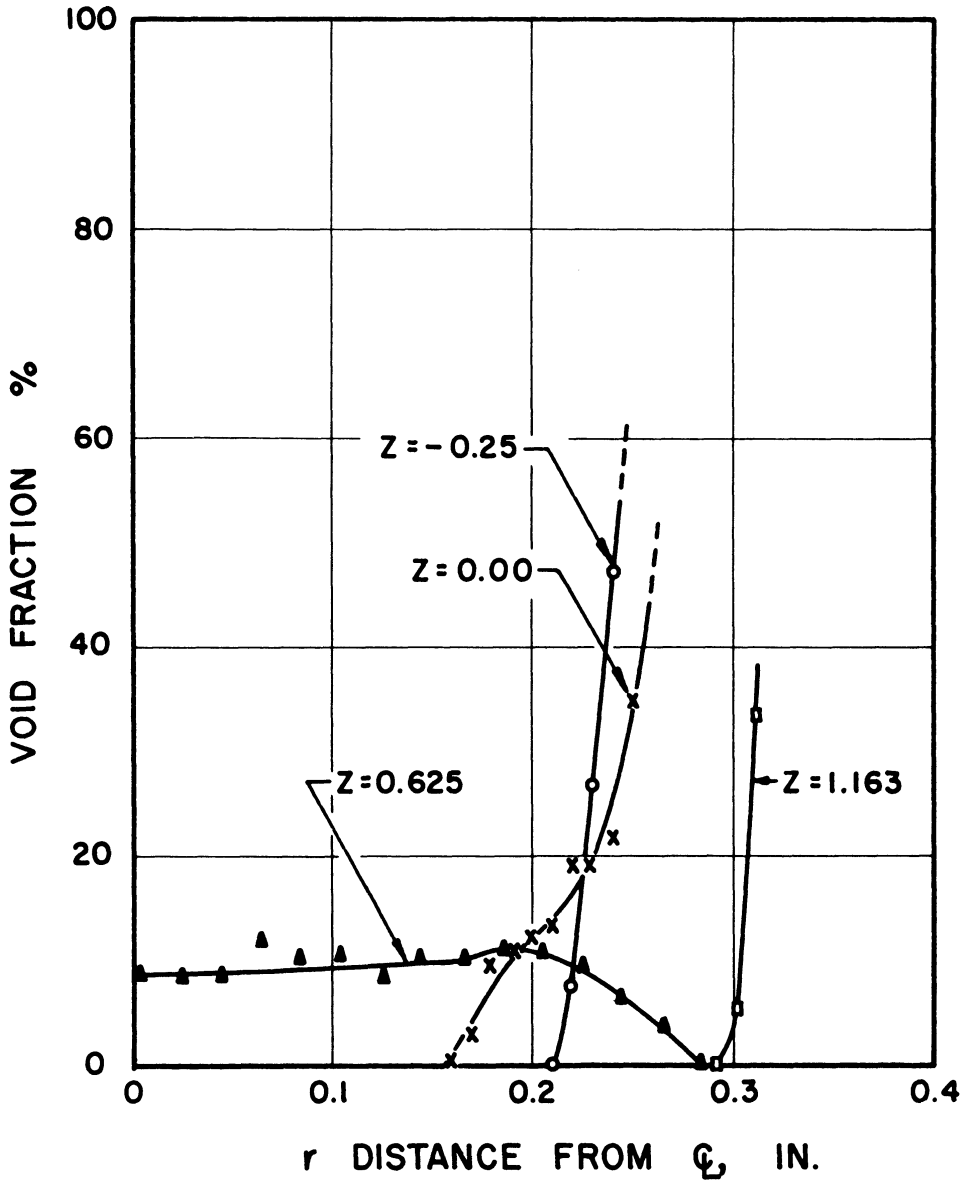

Figure 39. Void Fraction versus Radial Distance for Visible Initiation Cavitation.

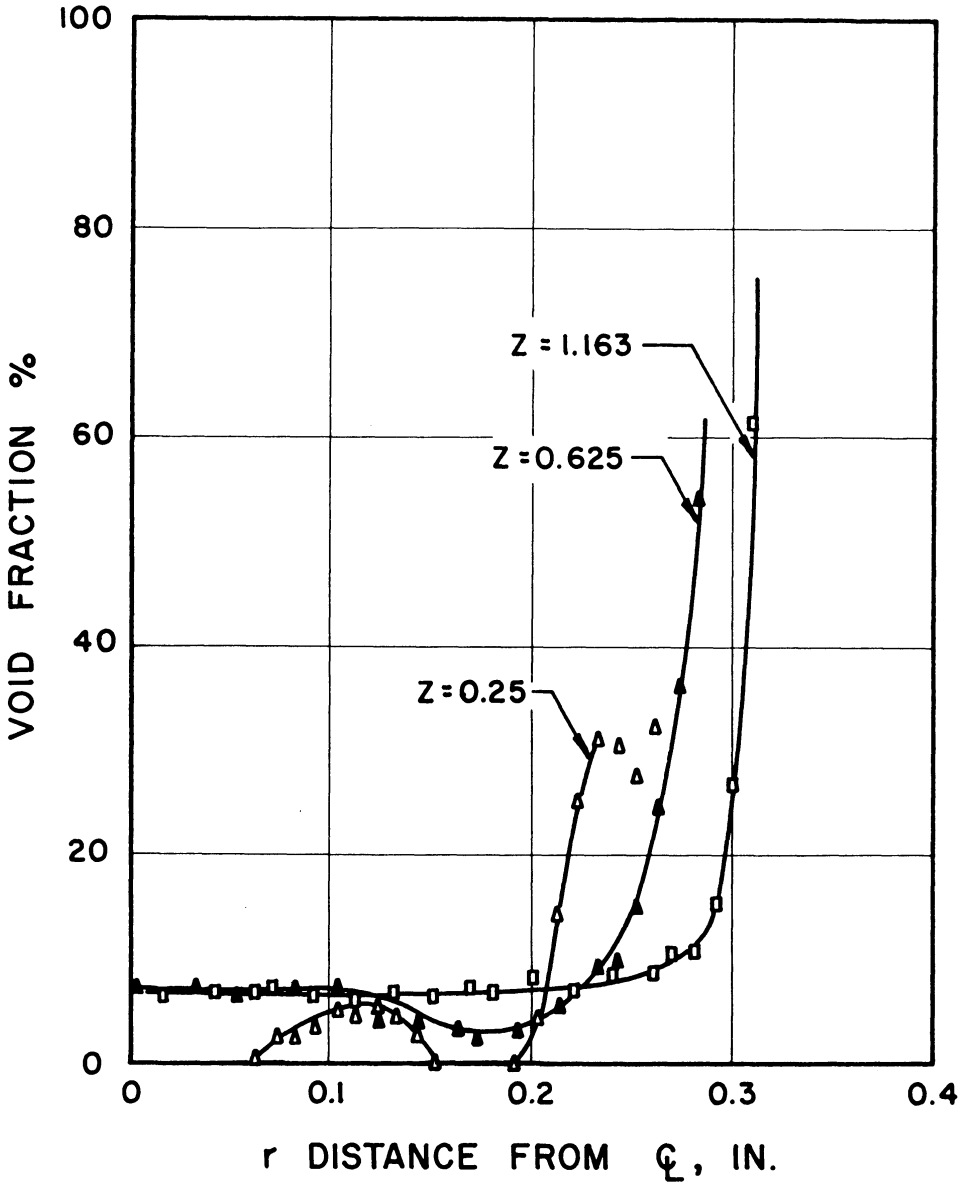

Figure 40. Void Fraction versus Radial Distance for Cavitation to Nose.

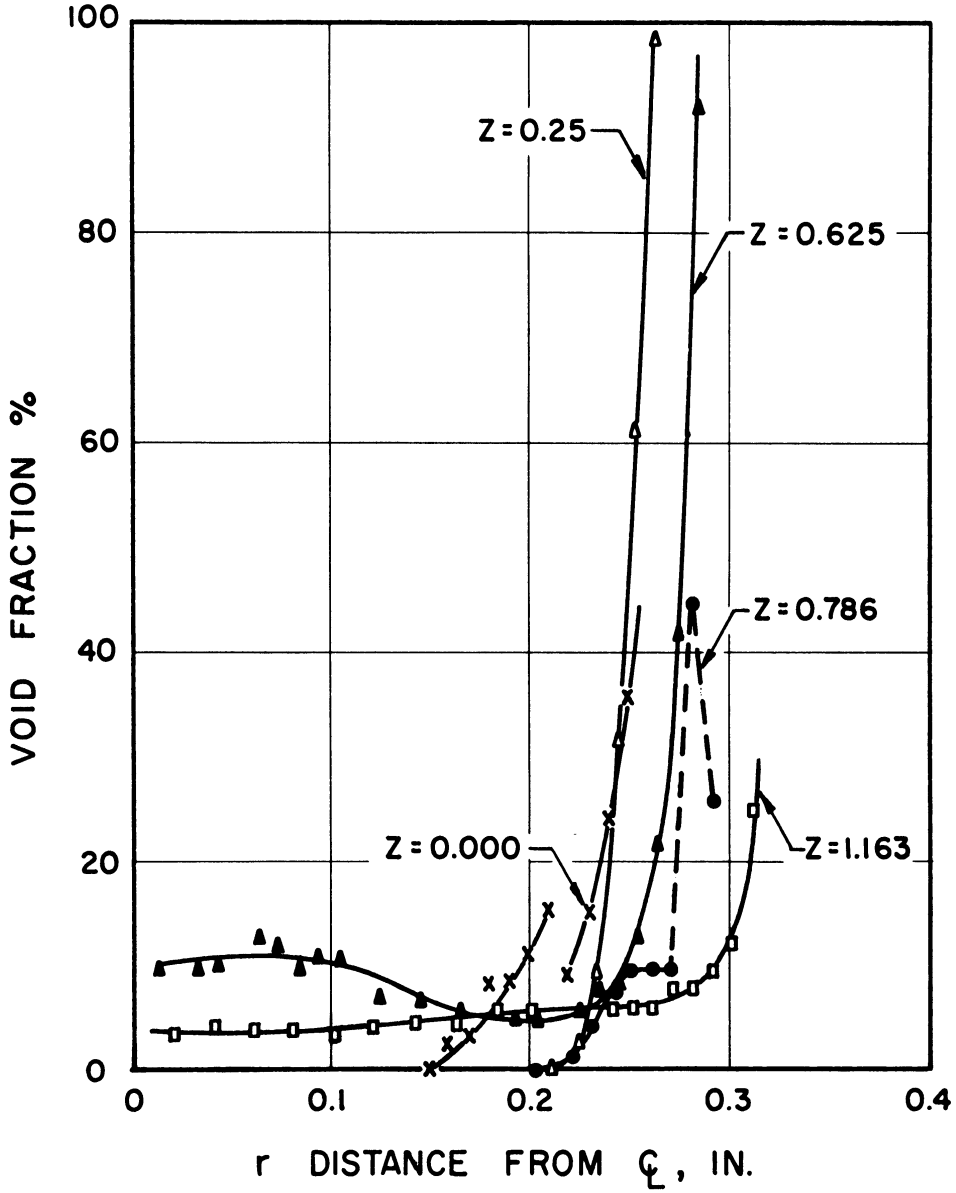

Figure 41. Void Fraction versus Radial Distance for Standard Cavitation.

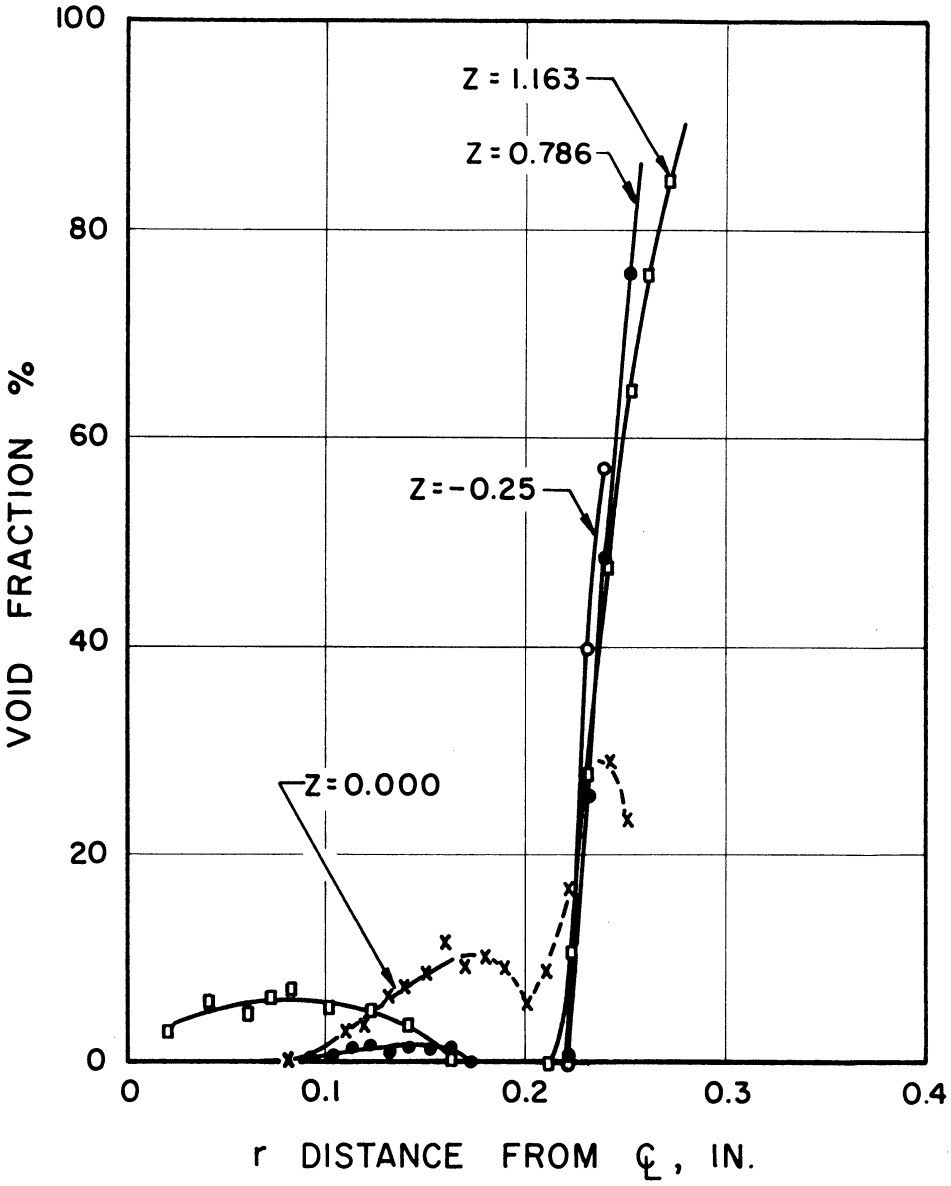

Figure 42. Void Fraction versus Radial Distance for Cavitation to First Mark.

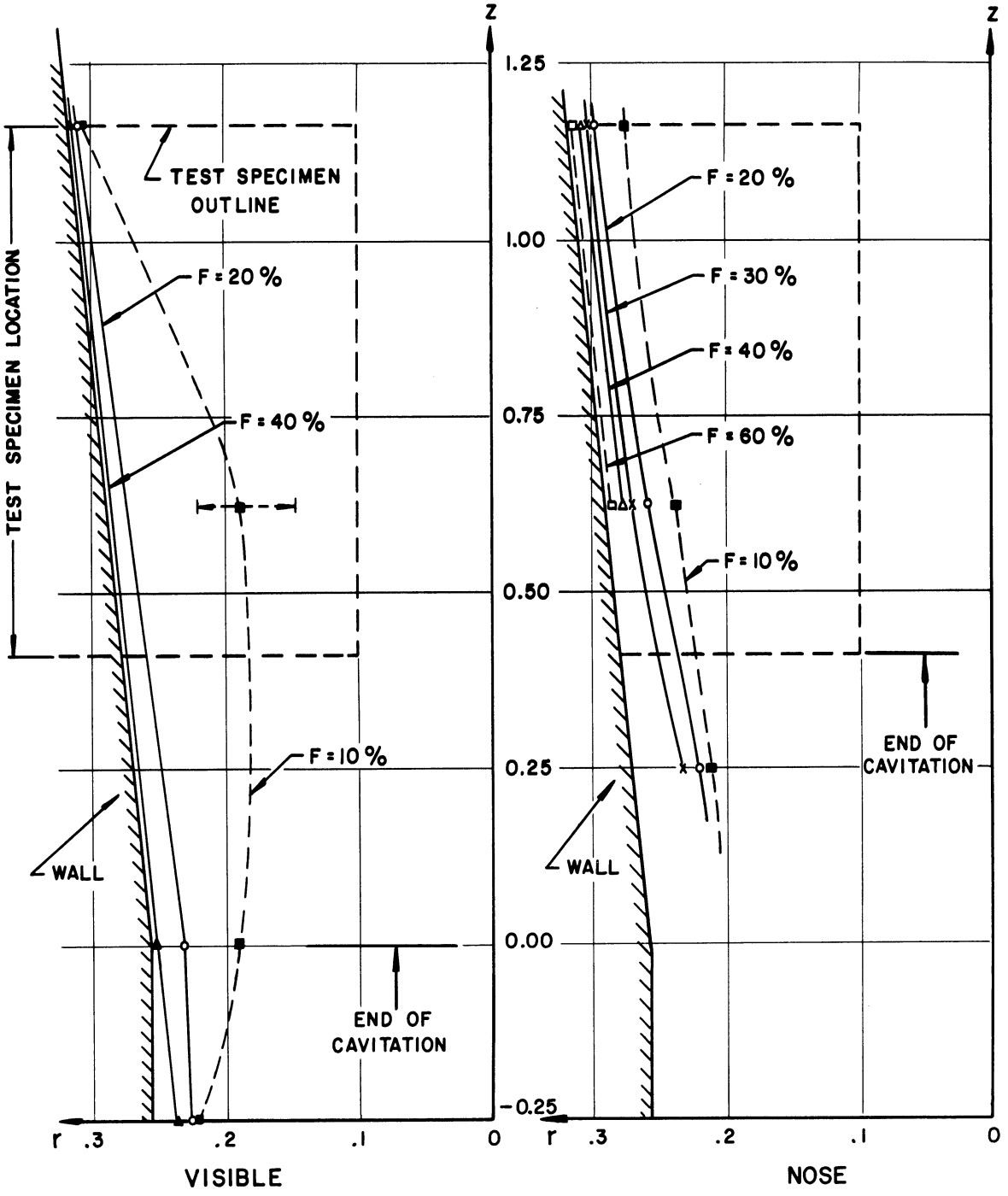

Figure 43. Void Fraction Profiles for Different Cavitation Conditions.

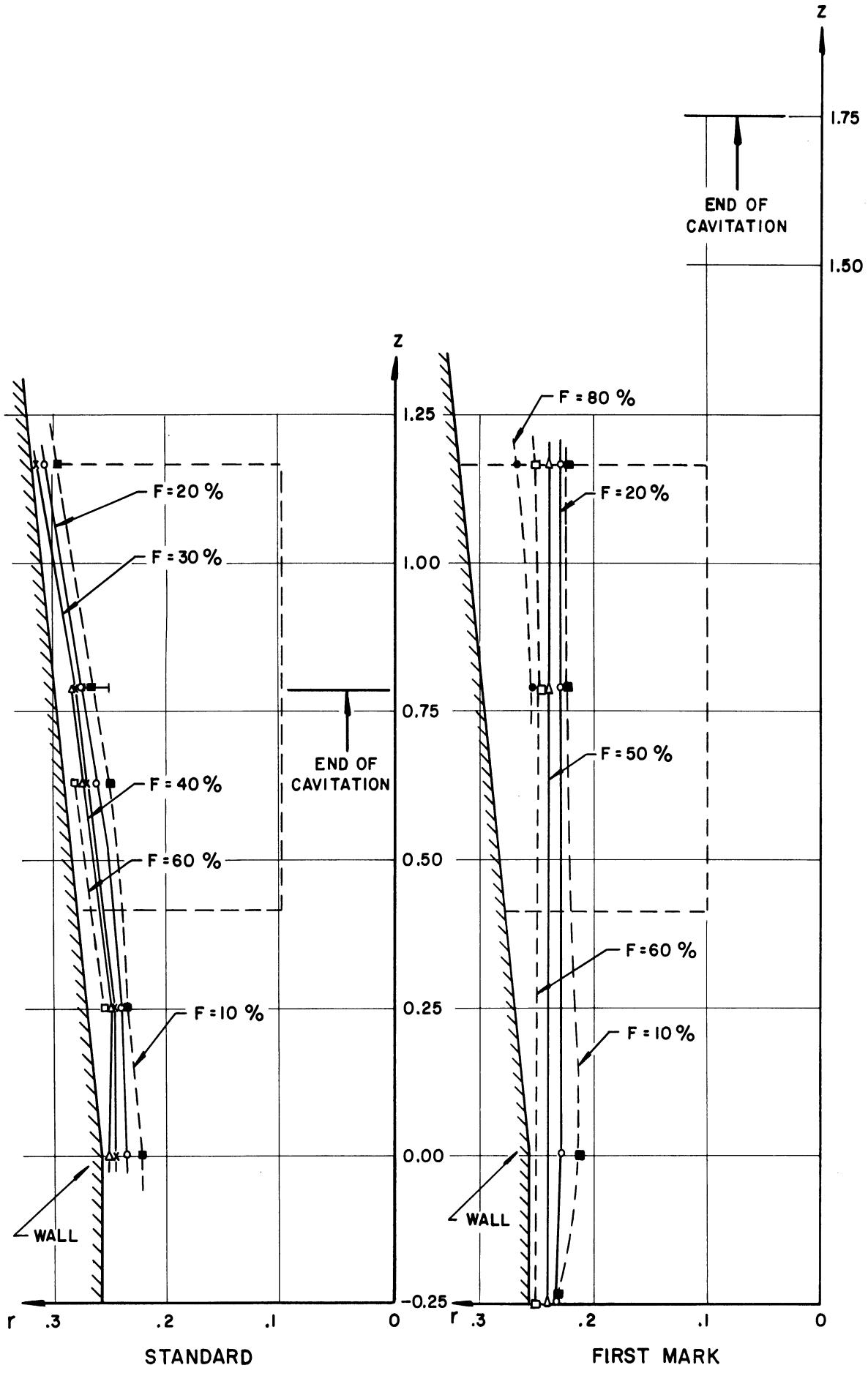

Figure 43 (Concluded)

However, it is certainly influenced by the overall cavitation field in that the local pressures are so influenced, and hence the collapse violence of the bubbles. The existence of such dependence has of course been demonstrated by the wear results.[9]

4) A direct comparison of void fraction profiles under the same cavitation condition between water and mercury is not at present possible, although runs similar to the mercury runs herein described are planned eventually for water. Water runs, using the present venturi, were made previously with a non-collimated densitometer [2,3], from which average void fraction, rather than void fraction as a function of radius, was determined, at a given axial location. From this the diameter of a hypothesized jet of pure liquid centered about the venturi center line was calculated. This data is shown in Figure 20 of Reference 2 and reproduced here for convenience (Figure 44). Also shown in the same figure are jet diameter curves based on pitot tube, rather than densitometer, measurements. It is noted that the results are fairly similar* at least for "First Mark Cavitation." Of interest in the present context is the gamma-ray densitometer curve for "First Mark Cavitation" with cold water. It is noted that in this case the diameter of the jet, if it were of pure liquid, is about 69% of the venturi diameter at the "First Mark" position. In the present tests with mercury, but under otherwise similar conditions, the locus of the 10% void fraction line is at about 63% of the diameter of this location, if it is assumed that a straight-line extrapolation in Figure 43 from the

*The possible reasons for the differences in results obtained from these independent measuring techniques were discussed previously.[2]

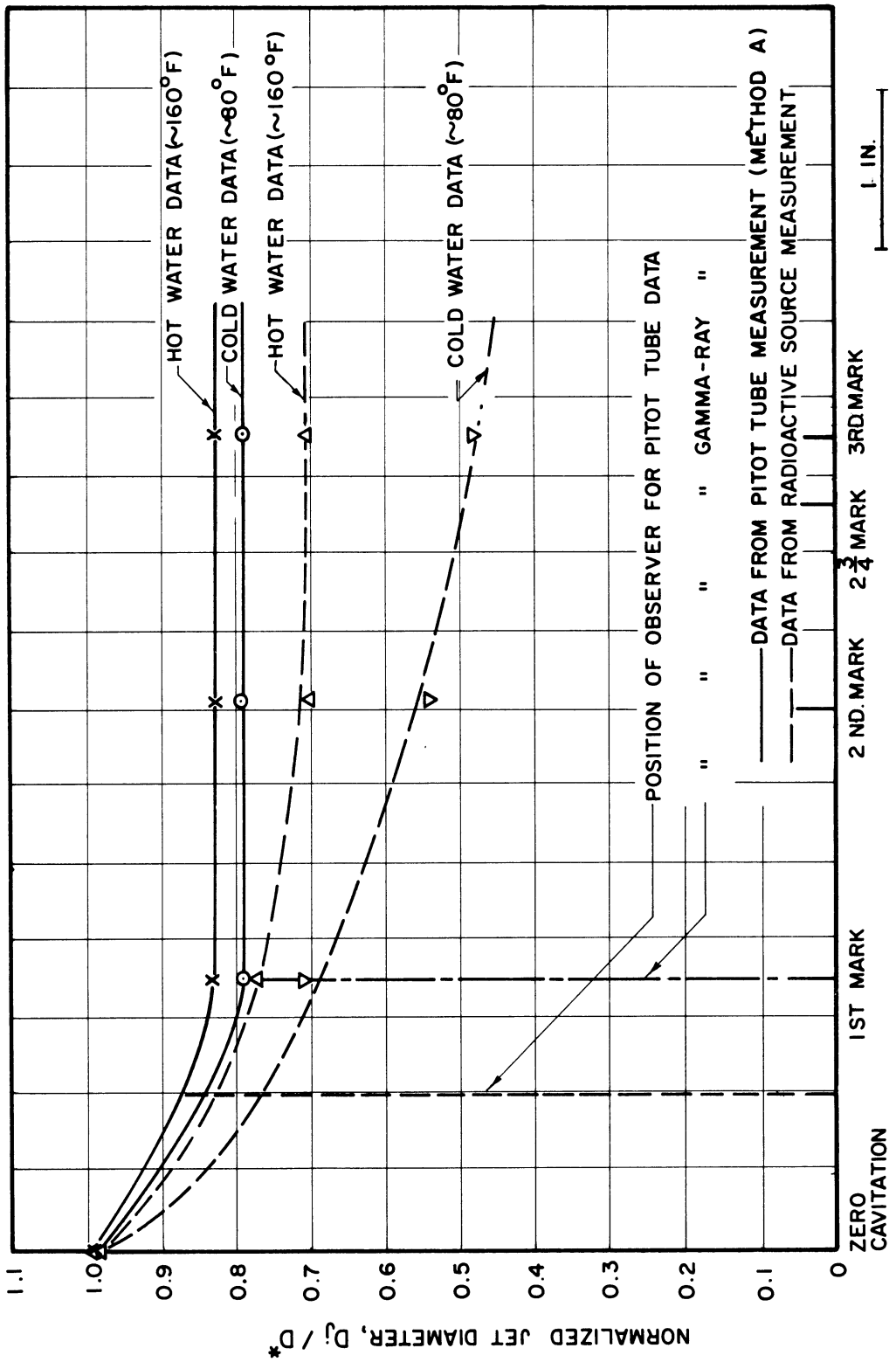

Figure 20. Comparison of Jet Diameters for Hot Water and Cold Water Runs*

* D = 0.603 For Pitot Tube Measurements
D = 0.687 For Radioactive Measurements

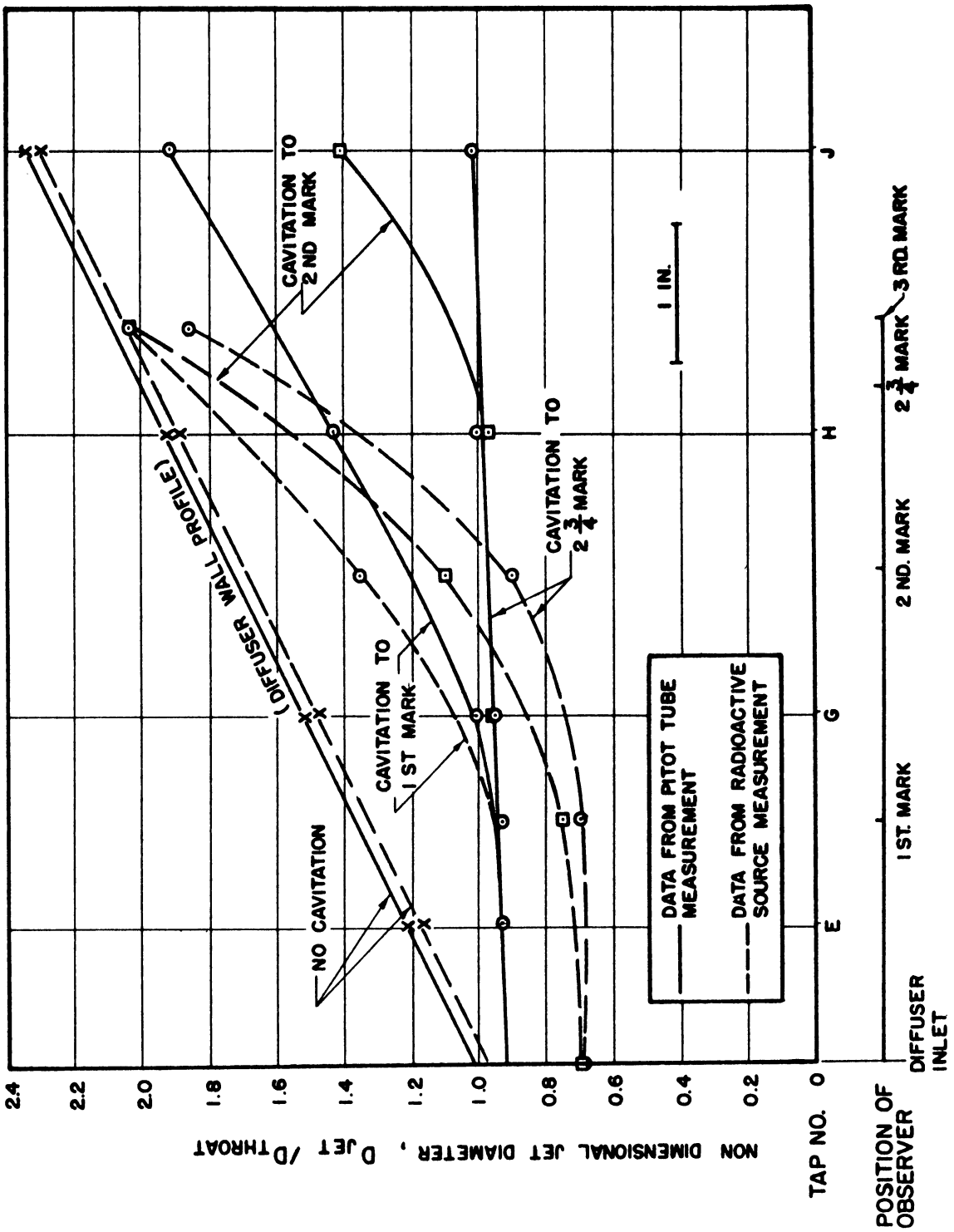

Figure 45. Non-Dimensional Liquid Jet Diameter as a Function of Axial and Cavitation Condition, Cold Water Data, 1/2" Test Section.

zone of measurement is valid. Actually, as shown in Figure 45 (reproduced from Figure 7 of Reference 3 for convenience), the hypothesized pure liquid jet diameter tends to increase substantially as the region of cavitation termination is approached. Hence the straight-line extrapolation value of 63% mentioned above is probably too small. On the other hand, the diameter of a pure liquid jet would be somewhat smaller than one containing a fringe area of ~10% void fraction, as well as some voids throughout. (An examination of the void fraction versus distance from center line plots of the present study, i.e., Figures 39 through 42, indicates the existence of perhaps 5% void even near the center line.)

Considering all the above, the present mercury tests seem consistent with the past water tests within the precision of the available data. However, this is not sufficient to prove the absence of possibly significant differences between water and mercury with respect to void fraction location and value. Further information on this point must await more precise water tests which are planned for the future.

VI. RECOMMENDATIONS FOR FUTURE TESTS

It is observed that all experimental count-rate vs. distance from center line curves are similar in the following aspect. They present an irregular pattern for positions of the collimator close to the venturi wall, drop suddenly when that distance increases, and level off for central positions of the collimator. The very rapid decrease of the count rates near the walls is of particular importance, since it is possible, within the standard deviation, to draw curves that satisfy the data and yet are significantly displaced horizontally from each other. Since the calculations are based on differences of values for a given ordinate of two of such curves, it is obvious that such horizontal displacement can become an important source of error. Moreover, in the present experiment, the possible uncertainty in the position of the center line of the venturi with reference to the table holding the collimator was about 30 mils. Using the computer program, an experimental calculation was performed by displacing the data of one of the curves by about half that amount. Results that were obtained were physically meaningless, while with a more suitable positioning of the curves the results of the computer were smooth and consistent. Fortunately, the correct position can be closely judged by symmetry considerations.

Therefore, in future tests, it is recommended that the collimator, gamma source, and scintillation detector should be fixed in a permanent way to the floor or walls, in such a manner that the center line of the venturi will coincide as perfectly as possible with the zero-line

(or other known reference) of the table, and will not move or vibrate during the experiment.

The required precise positioning is not easily obtained. However, the use of a beam of light is a possibility, provided that this beam is strictly normal to the free surface of the venturi, and that possible errors due to diffraction are eliminated.

Calculations show the statistical errors to be of the order of 2 or 3%. It was observed, however, that sometimes two successive counts of 3 minutes would yield values differing in more than the standard deviation. This was particularly true near the walls, and can be perhaps explained by actual irregularities in the flow of the mercury, that do not average out in the counting intervals adopted.

Hence, the counting times should be made as long as possible, to compensate for variations in the fluid flow. Of course, it is necessary that the nominal flow conditions (flow-rate and pressures) be maintained as nearly constant as possible during that period.

It is believed that some of the difficulties encountered in reproducing the results near the walls, when part of the gamma beam was passing through the plexiglas only, were due to the roughness of the internal surface of the venturi, which had been in operation, at the time of the experiment, for many hundreds of hours, and was severely pitted at certain locations. This damaged condition of the internal surface could result in local variations of the flow that would not average out in the counting interval.

Moreover, other obstructions to the gamma beam were present, such as the holders for the wear specimens, tap holes, etc. Thus, for new experiments, it would be desirable to use a new venturi in which specimen holders, taps, etc., had not yet been installed. Also, this would help in the accurate determination of the center line location.

VII. CONCLUSIONS

As described in this report, a method using a gamma-ray densitometer has been developed for obtaining precise measurements of local density (or void fraction) in an axially-symmetric cavitating flow wherein a dense test fluid such as mercury (or other heavy liquid metals) is used. The same technique can be adopted to light fluids as water or molten alkali metals; however, a source producing softer radiation than that used in the present investigation would be desirable. Such sources (promethium-tungstate for example) are available and have been previously used in the present cavitation work [2,3,6], although a much less precise densitometer was used.

Also significant information regarding the cavitation flow regime in a venturi has been obtained. This is summarized in Section V. Most significant from the viewpoint of the cavitation damage work is the observation that, for all degrees of cavitation used, there is only a very small void fraction (less than 10%) in the vicinity of the polished faces of the test specimens, excluding possible local cavitation caused by the test specimens themselves.

BIBLIOGRAPHY

1. Hammitt, F. G., "Observation of Cavitation Scale and Thermodynamic Effects in Stationary and Rotating Components," ASME Paper No. 62-Hyd-1, May 1962. (To be published in Trans. ASME Jour. Basic Engr.)

2. Hammitt, F. G., et al., "Fluid-Dynamic Performance of a Cavitating Venturi, Part I," UMRI Technical Report No. 03424-2-T, The University of Michigan, October 1960.

3. Hammitt, F. G., et al., "Observations and Measurements of Flow in a Cavitating Venturi," ORA Technical Report No. 03424-5-T, The University of Michigan, April 1962.

4. Hammitt, F. G., et al., "Observations of Cavitation Scale and Thermodynamic Effects in Stationary and Rotating Components with Water and Mercury," ORA Technical Report No. 03424-6-T, The University of Michigan, September 1962.

5. Cramer, V. F., et al., "High Speed Motion Picture Studies of Flow in a Cavitating Venturi," ORA Project No. 03424, Internal Report No. 12, The University of Michigan, May 1962.

6. Pérez, Simón, "Cavitation Degree Measurements by Radioactive Attenuation," M.S. Thesis, Department of Nuclear Engineering, The University of Michigan, January 1960.

7. Ivany, R., "Design of a Gamma-Ray Densitometer for Mercury or Molten Lead," ORA Project No. 03424, Internal Report No. 5, The University of Michigan, March 1961.

8. Adyanthaya, B. R., "Mercury Void Fraction Measurements Using a Collimated Gamma-Ray Beam," M.S. Thesis, Department of Nuclear Engineering, The University of Michigan, June 1961.

9. Hammitt, F. G., et al., "Cavitation Damage Tests with Water in a Cavitating Venturi," ORA Technical Report No. 03424-4-T, The University of Michigan, March 1962.

10. Etherington, Harold, editor, Nuclear Engineering Handbook, McGraw-Hill, 1958.

11. Hodgman, Charles D., Handbook of Physics and Chemistry, 33rd. Ed. Chemical Rubber Publishing Company, June 1951.

12. Storm, E., et al., "Gamma-Ray Absorption Coefficients for Elements 1 through 100 Derived from the Theoretical Values of the National Bureau of Standards, LA-2237, 1957.

APPENDIX A

CALIBRATION OF ELECTRONIC EQUIPMENT

CALIBRATION OF ELECTRONIC EQUIPMENT

The single channel analyzer and associated equipment used in this experiment were extensively calibrated to ensure their proper operation.

The single channel analyzer receives the pulses from the amplifier output. The pulse height region to be counted is selected (at a given amplifier setting) by using the E dial which has a range of 0-1000 arbitrary E dial units. The E dial is proportional to pulse height which is in turn proportional to the energy of the incident gamma. When the instrument is set on "Differential Count," the ΔE dial selects the energy increment above E over which the pulses will be counted. Hence, for a particular setting of the E and ΔE dials, only those pulses between E and $E + \Delta E$ are counted. All pulses below E and above $E + \Delta E$ are discriminated against and do not register a count. The range of the ΔE Dial is also 0-1000 units but the ΔE units are much smaller than the E dial units. The ΔE dial is calibrated in terms of E dial units, this value being referred to as window width.*

The calibration of the electronic equipment requires the determination of the linearity of the linear amplifier, calibration of the E dial with energy, and the calibration of the ΔE dial in terms of E dial units at various E dial settings.

A signal generator was used to put a 60 cycle square wave input into the linear amplifier and the output pulses were observed on a cathode

*Window width: Opening of the ΔE dial in terms of E dial units.

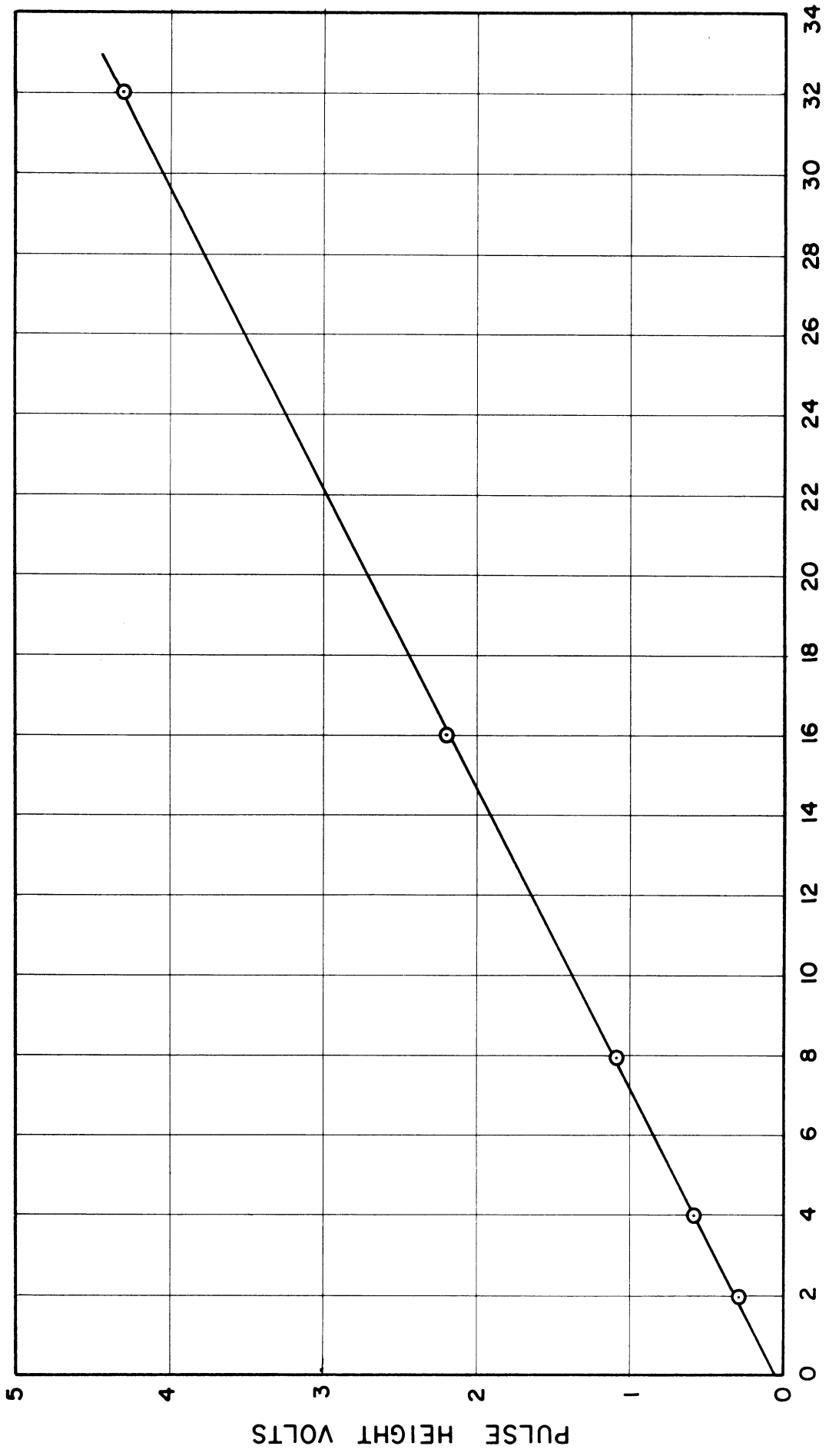

Figure A1. Linearity of Linear Amplifier.

ray oscilloscope. Table I presents the data plotted in Figure A1 which reveals that the amplifier is indeed linear.

The ΔE dial was calibrated in percent window width at E dial settings of 300, 500, 700, and 900. This was done with the input of the signal generator. The percent window width was computed by,

$$\% \text{ w. w.} = \frac{(E_2 - E_1) \text{ E dial units}}{1000 \text{ E dial units}} \times 100.$$

The data is presented in Table II and plotted in Figure A2. The plot reveals that the ΔE dial as a function of window width was non-linear but only to a moderate degree. The non-linearity was pronounced at the higher window widths. This did not introduce error into this experiment.

This information was of importance since a precise window width at a particular E dial was required in the determination of the linear absorption coefficient of only the 1.17 Mev Co^{60} gamma in mercury and in the data taken to calculate void fractions. When the E dial position was yet to be determined, the experimenter was able to calibrate the ΔE dial for various E dial settings and pick the required value from the graph when the required E dial value was decided. This calibration gives an insight into the condition of the single channel analyzer.

A very weak set of standard sources was used to determine roughly the photopeak positions of Co^{60} and Cs^{137} on the E dial. The differential spectrum data is presented in Table III and plotted in Figure A3. The position of the photopeaks was plotted versus E dial in Figure A4 which reveals the E dial is linear in energy. This, and the above calibrations, indicate that the single channel analyzer used was in good working condition.

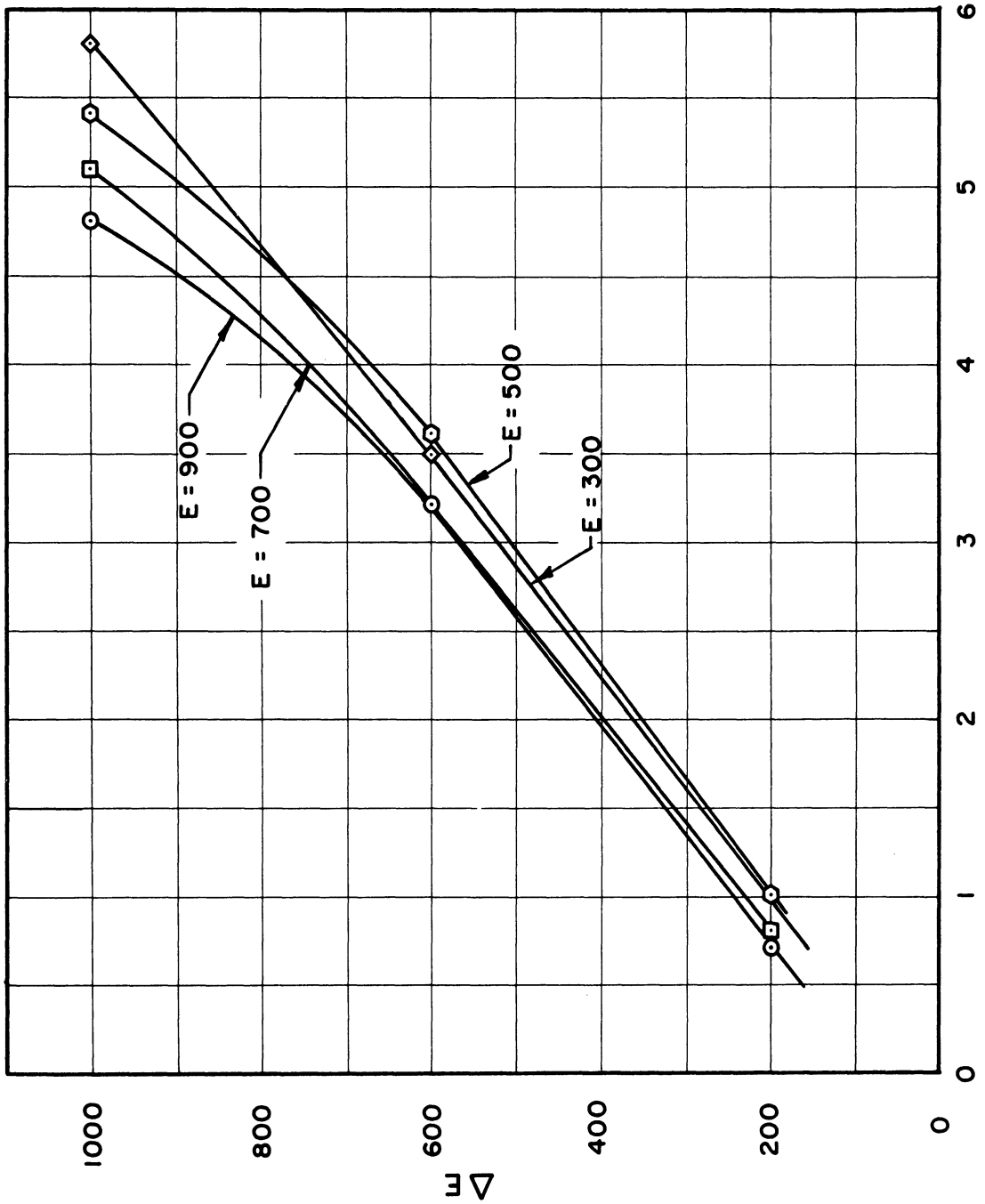

Figure A2. Calibration of ΔE Dial. Data From Table II.

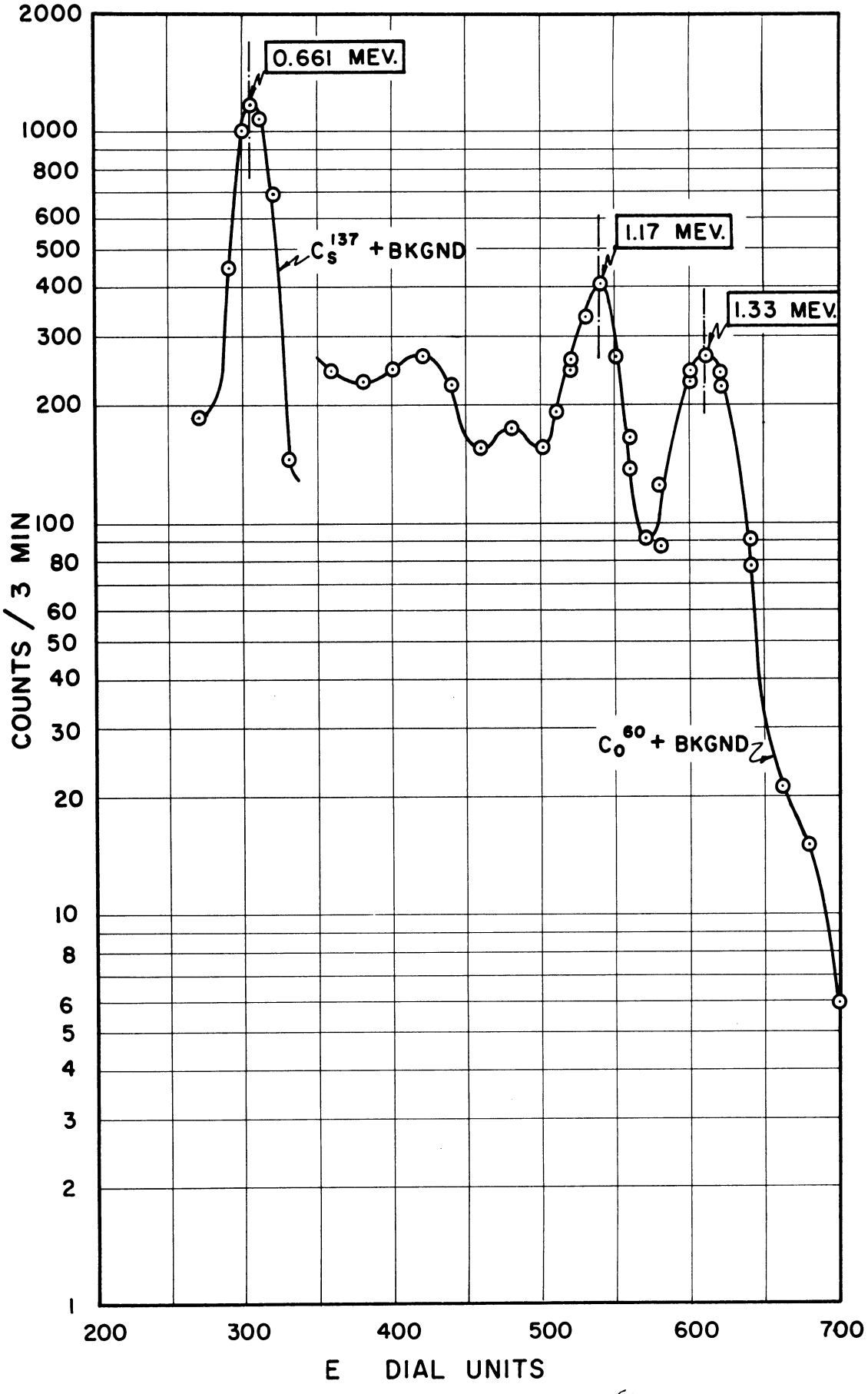

Figure A3. Differential Curves of C_o^{60} and C_s^{137}. Data from Table III.

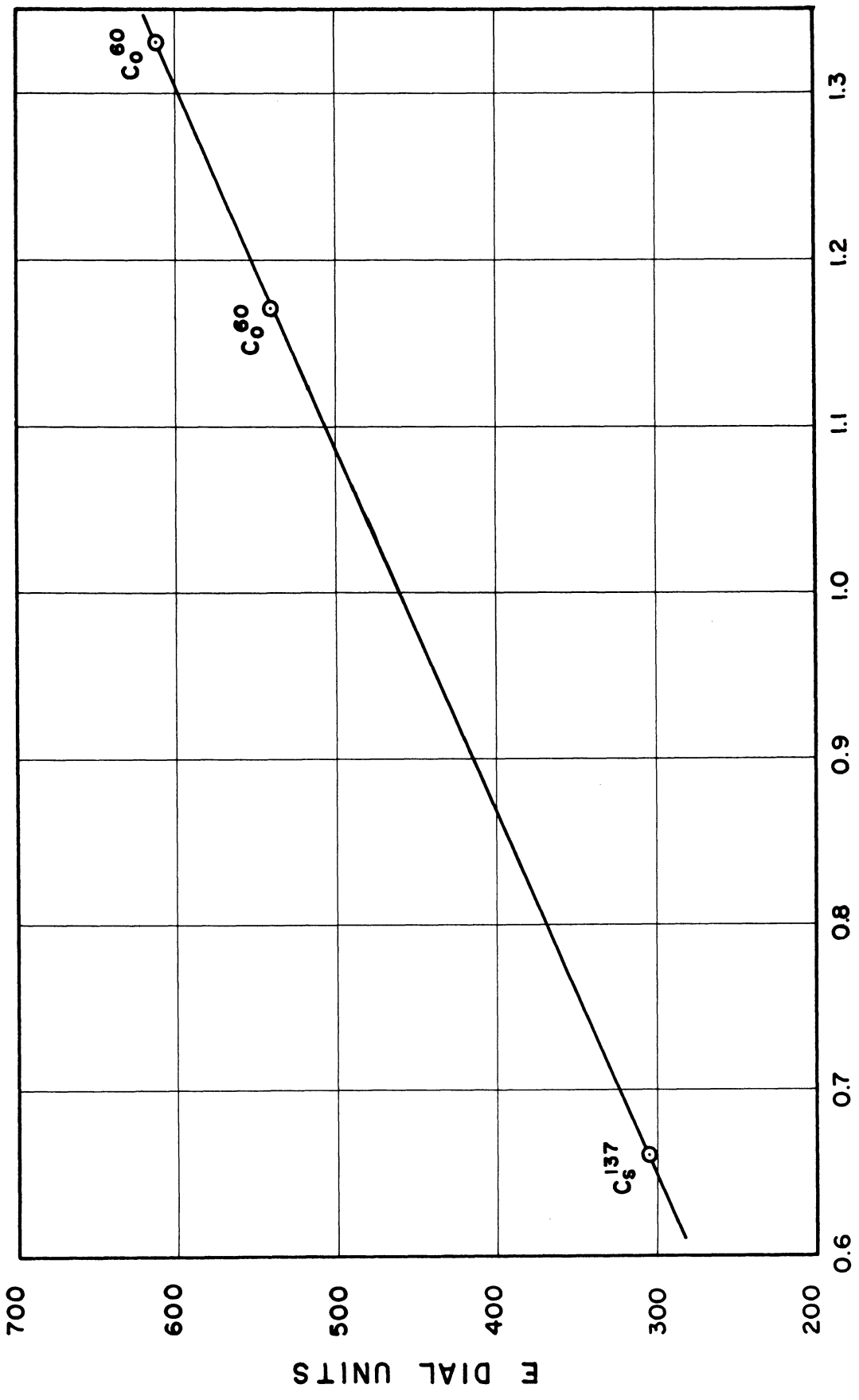

Figure A4. Energy Calibration of SCA. Amplifier Gain: 2 x 36.
Data from Figure A3.

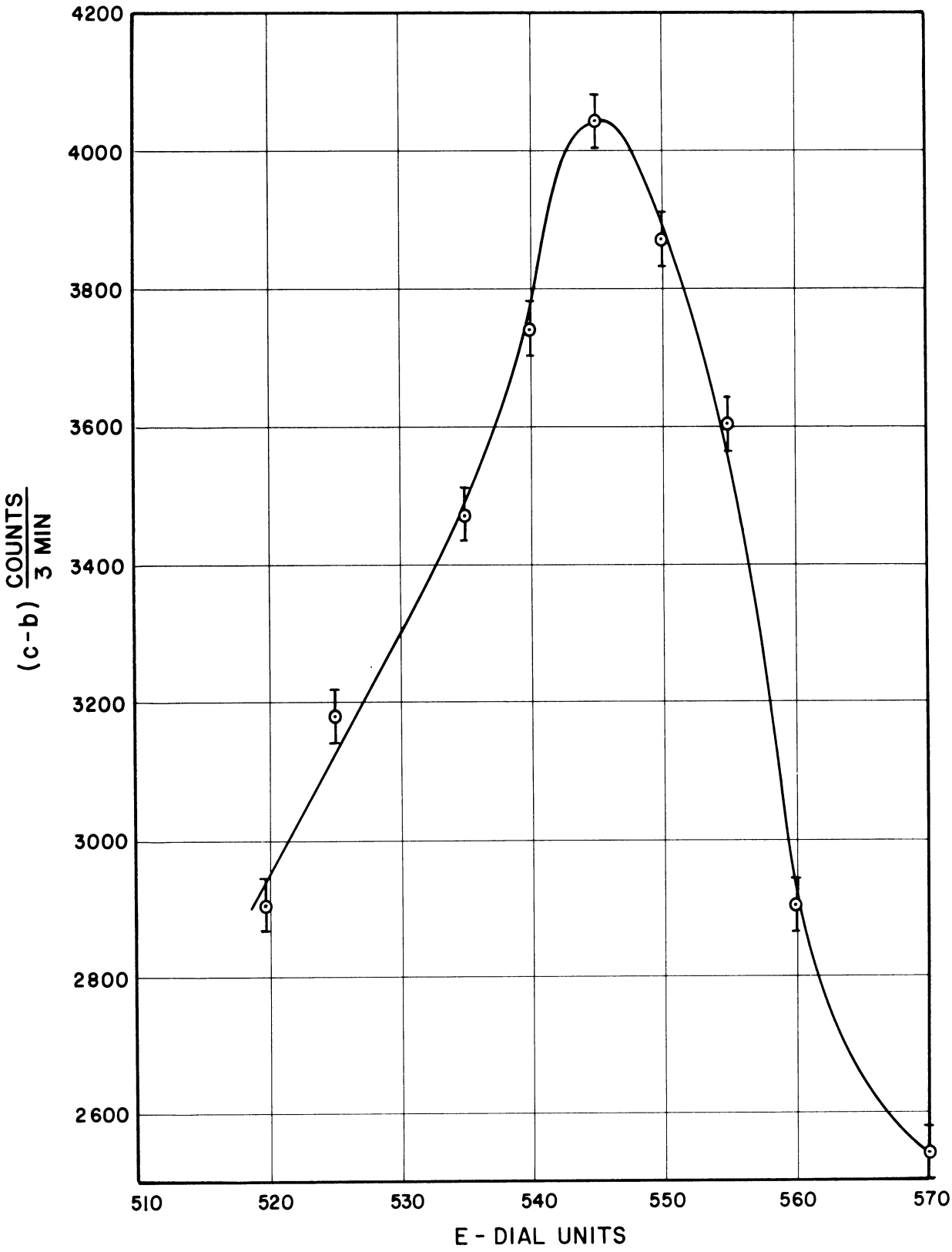

Figure A5. Precise Determination of Co^{60} 1.17 Mev Photopeak. Data from Table IV.

Since only the 1.17 Mev Co^{60} photopeak was used in the linear absorption coefficient and void fraction determinations, a very precise determination of its E dial position was required. The 20 mc Co^{60} source was placed in the collimator and the single channel analyzer was used with $\Delta E = 200$ ($\sim$1% window) to obtain the differential spectrum exactly. A precise background determination was also made. Table IV presents the data plotted in Figure A5 which shows that the 1.17 Mev photopeak is at 545 E dial units. The Compton effect due to the 1.33 mev gamma can clearly be seen on the low energy side of the 1.17 Mev peak.

Figure A5 indicates that an E dial of 530 with a ΔE dial corresponding to 30 E dial units would symmetrically include the peak and give enough counts to provide adequate statistics, i.e., about 1-2%. Thus, from Figure A2 a 3% window width at 530 E dial units required a ΔE dial setting of 490 units. These values were used throughout the rest of the experiment.

ELECTRONIC EQUIPMENT AND RADIOACTIVE

SOURCES USED IN THIS EXPERIMENT

NAME	MANUFACTURER	NUC. ENG. NO.	MODEL AND SERIAL NO.
1) Scintillation Detector	RCL	69	Model 11028 136
2) Super Stable High Voltage Supply	Atomic Instrument Company	108	Model 312 10972
3) Non-Overloading Amplifier	Baird Atomic	56	Model 215 528-N
4) Single Channel Analyzer	RCL	106	Model 2204 258
5) Scaler	Baird Atomic	359	Model 1283 241
6) Pulse Generator	Departmental	95	----
7) Oscilloscope	Type 592 Dual Beam (Mechanical Eng.)	MA 2001	Type 502 Dual Beam 767
8) Sources 1.) $Co^{60} \sim 10 - 20$ mc 2.) New England Nuc. Corp. Set C-18.			

APPENDIX B

LINEAR ABSORPTION COEFFICIENT OF Hg FOR 1.17 Mev GAMMAS

LINEAR ABSORPTION COEFFICIENT OF Hg FOR 1.17 Mev GAMMAS

A preliminary survey of the literature showed that there was some doubt as to the linear absorption coefficient of mercury for the 1.17 Mev gamma-ray, and that published values were based either on theoretical calculations or extrapolations of experimental results. Hence it seemed desirable to establish an experimental value of sufficient precision for the present investigation.

Cross section data from Reference 12 were listed in Table V and plotted in Figure B1. An interpolation was made at an energy of 1.17 Mev to give a value of 0.822 cm^{-1} for the linear absorption coefficient for mercury. This value reflects only extrapolated calculations based on theoretical considerations of attenuation effects as a function of atomic number.

Table VI gives the data taken from Reference 10 which is an experimental determination of μ for mercury. Figure B2 was used to interpolate the above data to 1.17 Mev which gave $\mu = 0.829$ cm^{-1}.

Since the density of mercury varies somewhat with temperature, data from Reference 11 (Table VII and Figure B3) was used. Since the temperature of the mercury in the loop during the tests was approximately 70°F, a value of 13.5435 gm/cm^3 was selected. The maximum variation from this temperature is estimated to be about 5°F (during the non-cavitating runs when the mercury flow rate was reduced to a minimum). As noted in Figure B3 such a temperature variation corresponds to a density variation of about 0.05%, and is considered a negligible source of error.

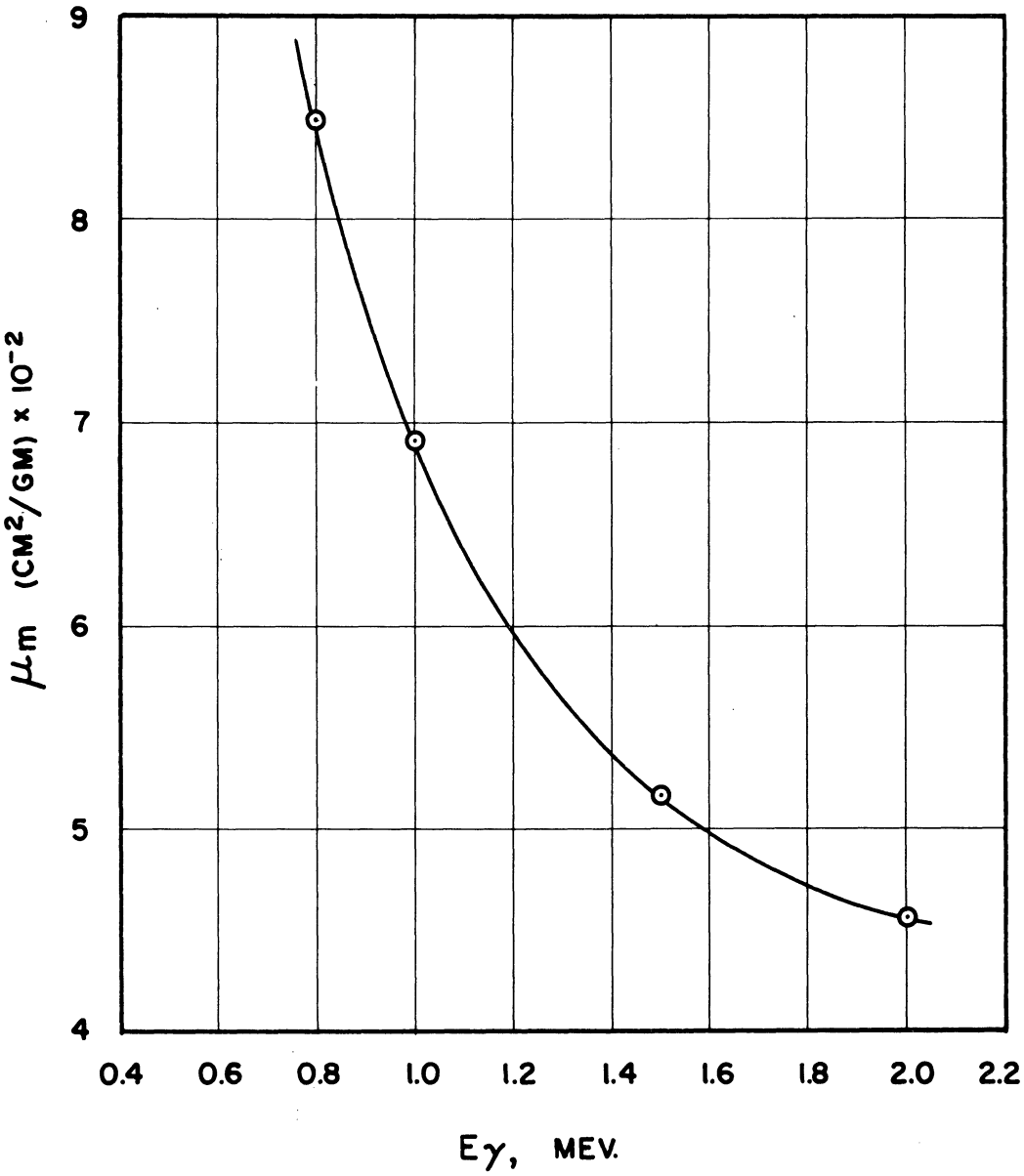

Figure B1. Mass Absorption Coefficient of Hg. (LA-2237, Ref. 12).

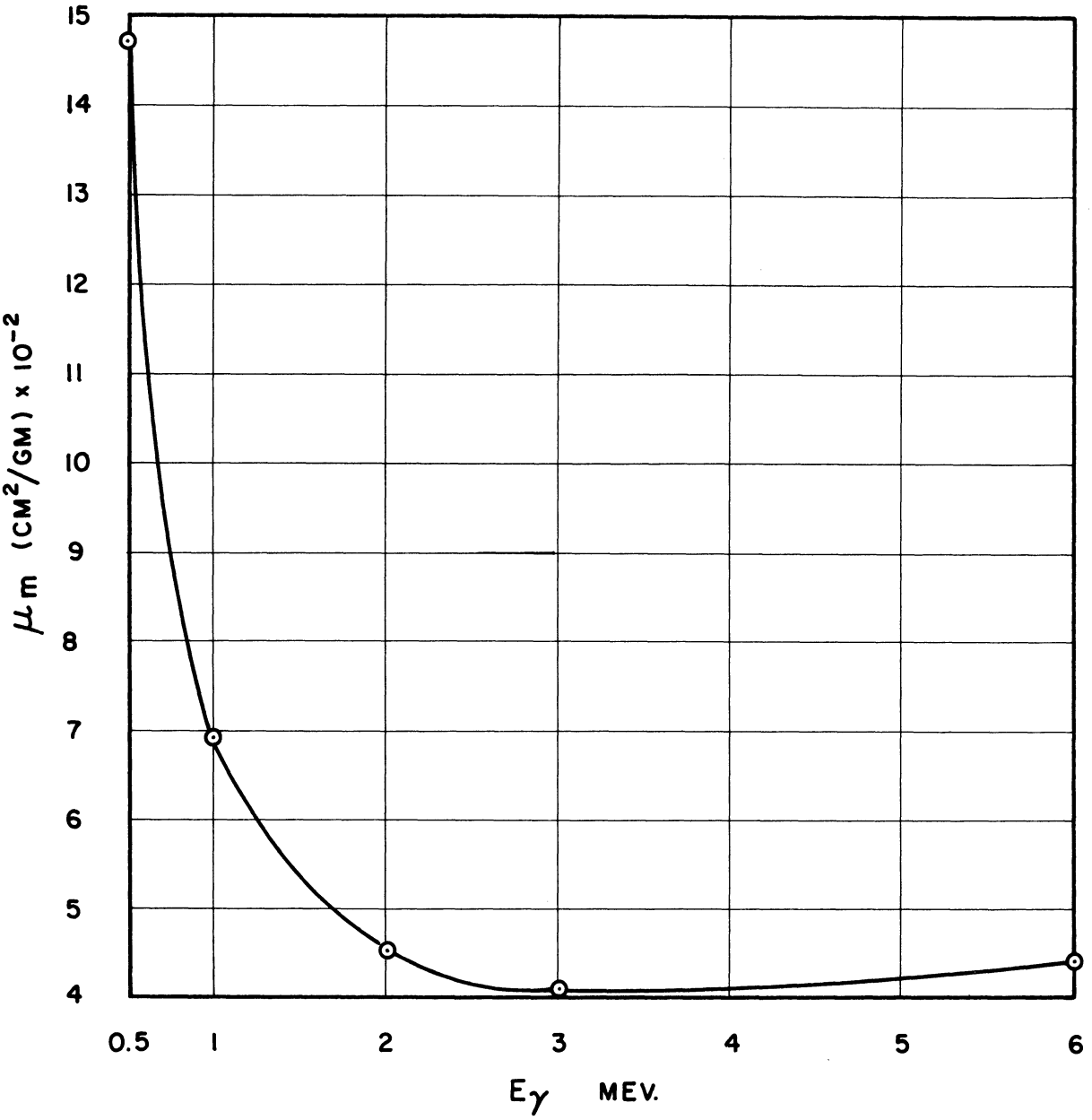

Figure B2. Mass Absorption Coefficient of Hg.
(Nuclear Engrg. Handbook, Ref. 10)

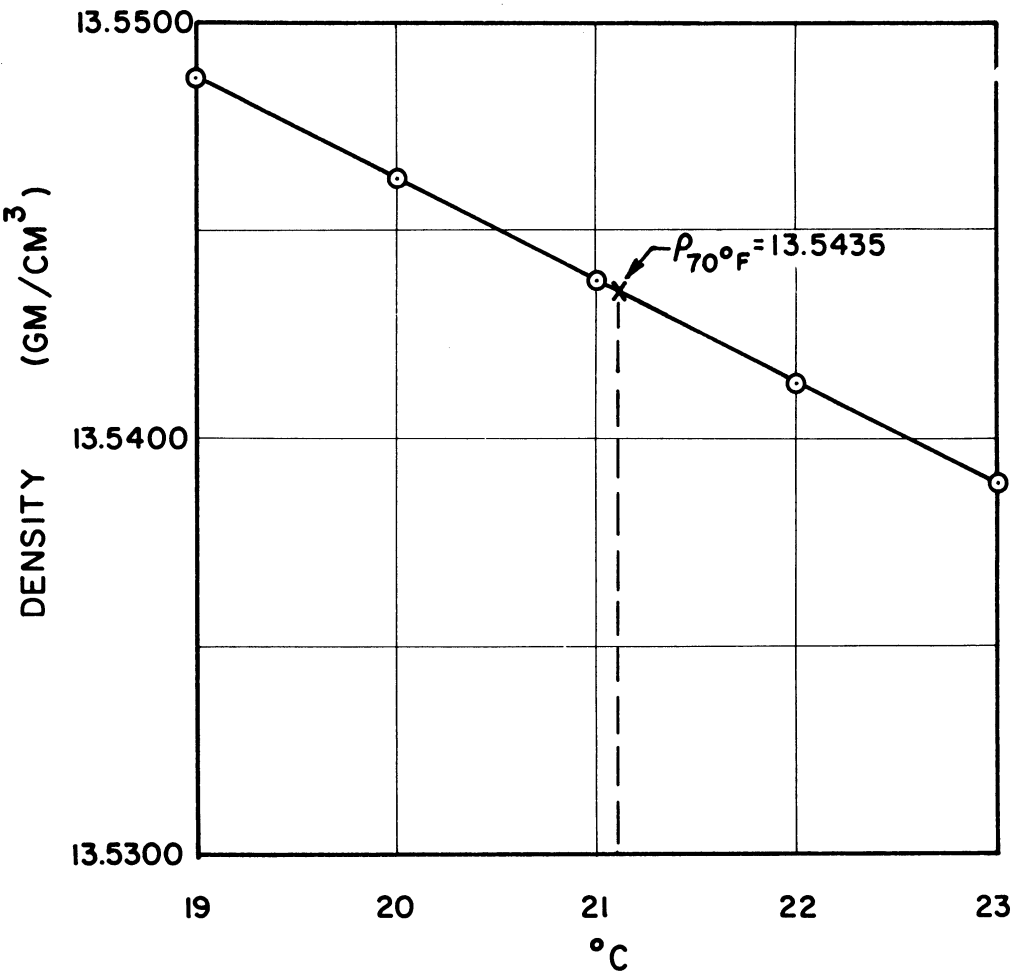

Figure B3. Density of Mercury versus Temperature. (Handbook of Chem. and Physics, Ref. 11).

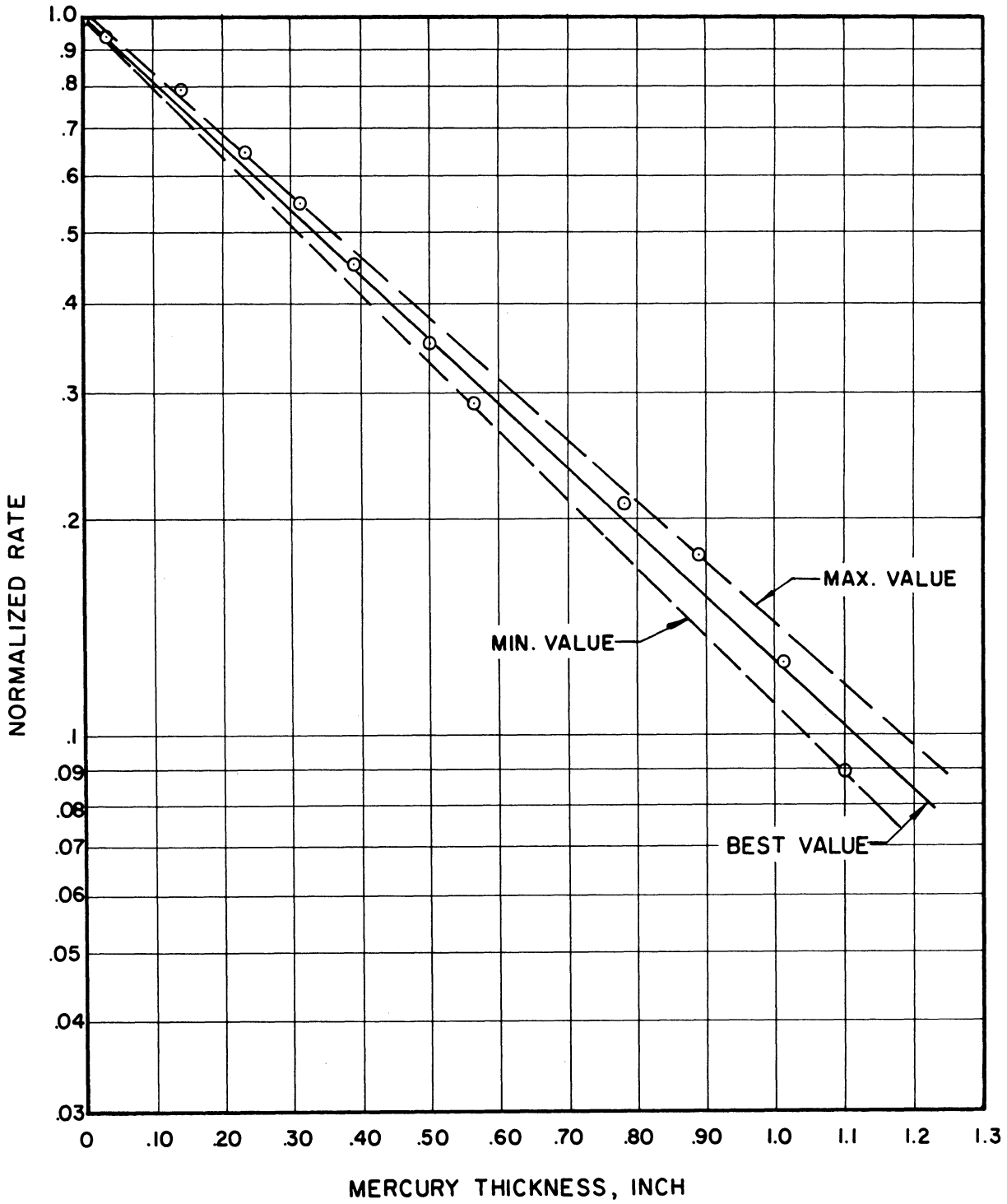

Figure B4. Linear Absorption Coefficient of Hg for Co^{60} 1.17 Mev Gammas. (Experimental data).

As a simple but suitable experimental set up for the measurement of μ, a glass beaker was used with a depth gauge attached to a metal cover platform to measure the depth of mercury within. This beaker was placed over the vertical collimator and three minute counts made with various mercury depths. With the proper E Dial and ΔE dial settings, using the 20 mc Co^{60} source. The data is presented in Table VIII and the count rates corrected for background are normalized to the first measurement as "zero" thickness and plotted in Figure B4.

The best straight line through the points was drawn. Considerable dispersion outside the statistical error of about $\pm$ 0.009 (normalized value) exists in the points, due presumably to error in reading the depth gauge. The lowest two points can be neglected since their count is very nearly of background magnitude. The straight line drawn appears to fit the remaining points quite well.

The linear absorption coefficient for mercury was then calculated from Figure B4, giving $\mu = 0.827\ cm^{-1} = 2.10\ in^{-1}$.

Figure B4 also shows lines drawn through the most divergent points to give the maximum error in μ due to the dispersion of the points. These values are 0.869 cm^{-1} and 0.784 cm^{-1} which give the maximum error in μ of $\pm$ 4.2%. The value of 0.827 cm^{-1} is considered to be determined to much greater accuracy than these values, which are the maximum errors, i.e., total statistical and experimental errors. This experimental value agrees closely with the literature. Both of the results found in the literature are within 0.4% and their average is within 0.2% of the value obtained in this experiment. Therefore the experimental value,

μ = 0.827 cm^{-1} (2.10 in^{-1}) from the present tests is considered the most reasonable value to be used since it is based on direct measurements whereas the values reported in the literature are not.

APPENDIX C

DERIVATION OF VOID FRACTION RELATIONS

DERIVATION OF VOID FRACTION RELATIONS

The basic relations required to express the void fraction in terms of the observed count-rates were developed by Adyanthaya.[8] The derivation will be reproduced here for convenience, since most of the intermediate equations are necessary for the computer program detailed in Appendix D.

Figure C1 represents the cross-section of the venturi at any particular axial position z. Let R be the venturi radius, t the path length of the radiation within the flow area, and x the horizontal distance from the venturi center line to the collimator center line. Also let:

n_o = number of photons/sec emitted by the source through the slit of area A of the collimator.

$n_1(x)$ = photons/sec passing through the entire test section, at a distance x, for any cavitation condition.

$n_2(x)$ = photons/sec passing through the entire test section, at a distance x, when there is no cavitation (i.e., stagnant mercury).

$\rho(x)$ = average density of the vertical column of fluid, located at a distance x, and which has cross-section equal to the area A of the collimator slit.

h = maximum transversal dimension of the test section, as shown in Figure C1.

Then:

$$n_1(x) = n_o \, e^{-\mu_p(h-t)} \, e^{-\beta\rho(x)t}$$

$$n_2(x) = n_o \, e^{-\mu_p(h-t)} \, e^{-\beta\rho t}$$

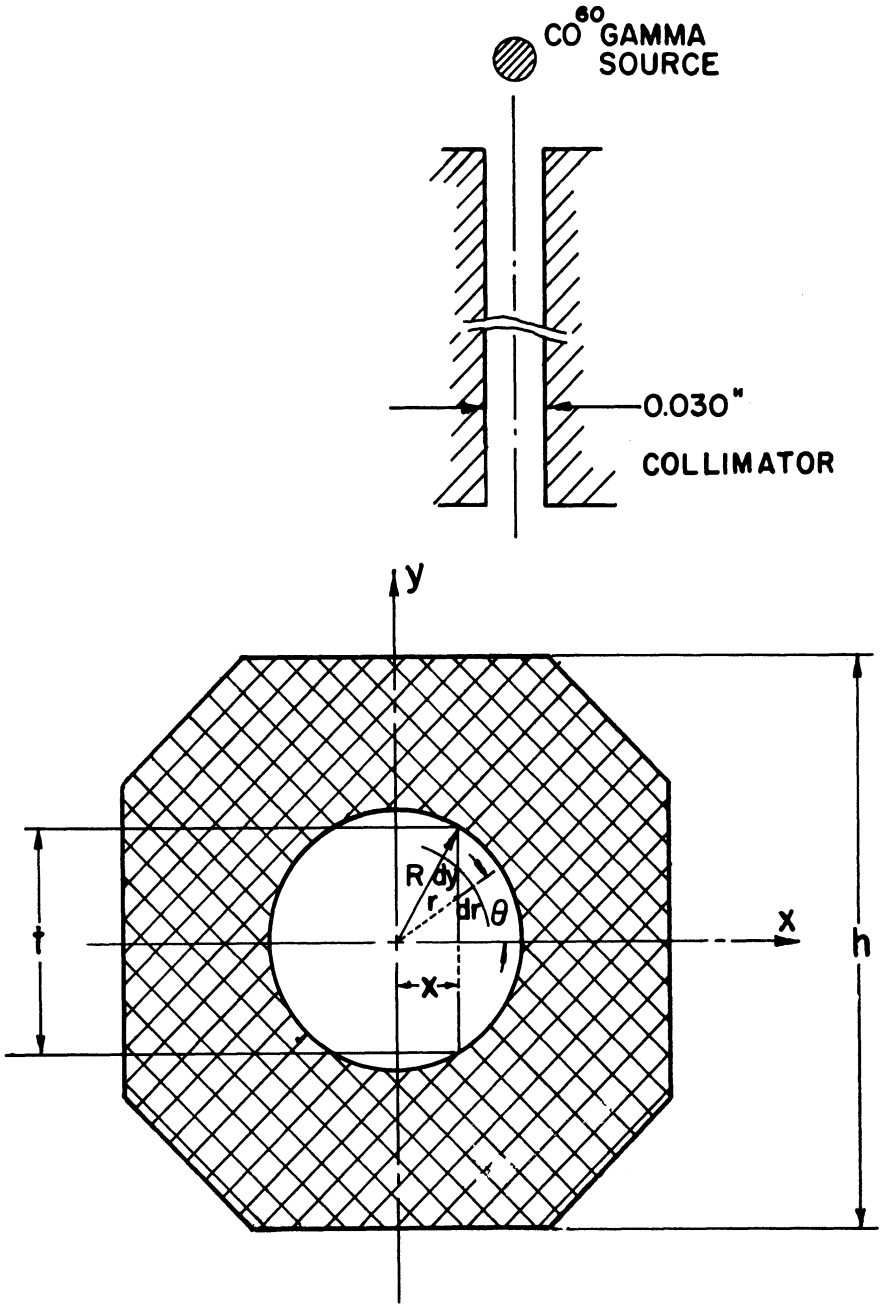

Figure C1. Venturi Cross-Section.

where:

ρ = density of mercury = 221.977 gm/in^3

μ = linear absorption coefficient for H_g = 2.1 in^{-1}

β = μ/ρ = mass absorption coefficient

μ_p = linear absorption coefficient of the plexiglas

Dividing the above equations and rearranging:

$$\ln \frac{n_2(x)}{n_1(x)} = \beta t[\rho(x) - \rho]$$

or:

$$\rho(x) = \rho + \frac{1}{\beta t} \ln \frac{n_2(x)}{n_1(x)}$$

But, from the geometry:

$$t = 2\sqrt{R^2 - x^2}$$

thus:

$$\rho(x) = \rho + \frac{1}{2\beta\sqrt{R^2 - x^2}} \ln \frac{n_2(x)}{n_1(x)} \qquad \text{(C-1)}$$

This average density, corresponding to a column of height t and cross-section equal to the collimator aperture, is always less than the density ρ of the liquid mercury, since $n_2 < n_1$. Moreover, the procedure is independent of the collimator opening provided this is small enough so that the average density can be considered as constant within the corresponding column. Thus, the average density is a function of the distance x only, and the displacements of the collimator can be arbitrarily chosen.

It is also worthwhile to notice at this point that the number of photons per second, n_1 and n_2, can be substituted by the actual counting rates, since the efficiency of the detector will cancel out in the equation above. A method has been found, then, to determine $\rho(x)$ experimentally by measuring $n_1(x)$ and $n_2(x)$.

One is interested, however, in obtaining the density as a function of the radial distance, r, rather than as a function of the transverse distance, x. For that purpose, two assumptions are made:

(a) The flow within the cavitating venturi is axially symmetrical, i.e., the density at any value of r is a function of r only, $\rho(r)$.

(b) Between r and r $+\Delta r$, the density $\rho(r)$ can be considered as constant, for small values of Δr. Naturally, the smaller Δr, the more accurate the calculations will be.

Then, $\rho(r)$ can be obtained from the values of $\rho(x)$ as follows. Let A be the area of the opening of the opening of the collimator, and hence, the area over which $\rho(x)$ is averaged. Thus:

$$\rho(x) = \frac{\int_o^y \rho(y)\ A dy}{\int_o^y A dy} = \frac{\int_o^y \rho(y)\ dy}{\int_o^y dy}$$

But, from Figure C1,

$$dr = dy \sin\theta = dy \frac{\sqrt{r^2 - x^2}}{r}$$

or:

$$dy = \frac{r\ dr}{\sqrt{r^2 - x^2}}$$

and the above equation becomes:

$$\rho(x) = \frac{\int_{r=x}^{R} \frac{r\ \rho(r) dr}{\sqrt{r^2-x^2}}}{\int_{r=x}^{R} \frac{rdr}{\sqrt{r^2 - x^2}}}$$

or:

$$\rho(x)\ \sqrt{R^2 - x^2} = \int_{r=x}^{R} \frac{r\ \rho(r)\ dr}{\sqrt{r^2 - x^2}} \qquad \text{(C-2)}$$

which is an exact relation between $\rho(x)$ and $\rho(r)$.

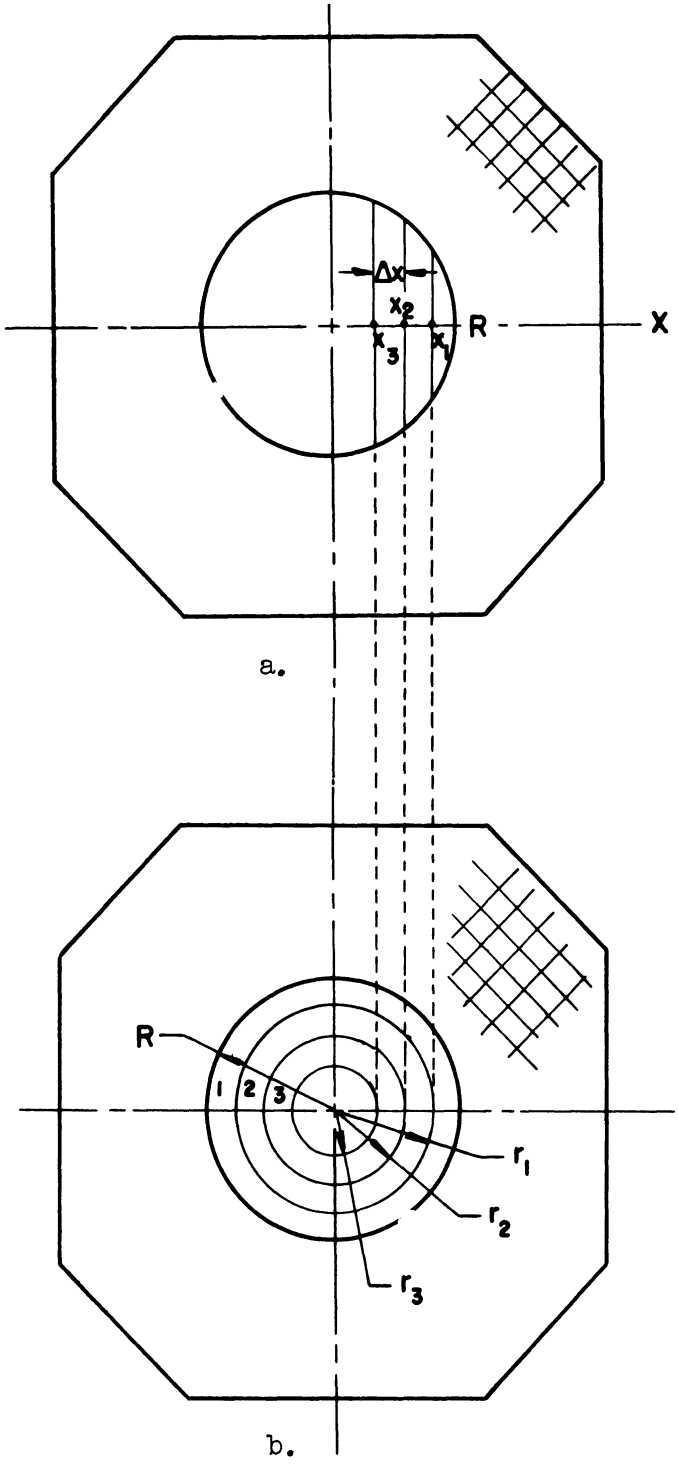

Figure C2. $\rho(r)$ from $\rho(x)$.

One observes then that at x_1, x_2, x_3, ... the values $n_1(x)$ and $n_2(x)$ are known, from the experimental work, and that using Equation (C-1) the corresponding values of $\rho(x)$ are readily calculated. The procedure is therefore to divide the flow section into different regions, as shown in Figure C2(b), where the different radii r_1, r_2, ... correspond to the transverse distances x_1, x_2, ... The outer radius of the first region is thus R, and the inner radius is x_1. As per assumption (b), within this region the radial density is constant, and from Equation (C-2) one obtains:

$$\rho(x_1)\sqrt{R^2 - x_1^2} = \int_{x_1}^{R} \rho(r_1) \frac{rdr}{\sqrt{r^2 - x^2}} = \rho(r_1) \int_{x_1}^{R} \frac{rdr}{\sqrt{r^2 - x^2}} = \rho(r_1)\sqrt{R^2 - x_1^2}$$

or:

$$\rho(r_1) = \rho(x_1) \qquad (C\text{-}3)$$

For region 2, similarly:

$$\rho(x_2)\sqrt{R^2 - x_2^2} = \int_{x_2}^{R} \frac{\rho(r)r\ dr}{\sqrt{r^2 - x_2^2}} =$$

$$= \int_{x_2}^{x_1} \frac{\rho(r)\ dr}{\sqrt{r^2 - x_2^2}} + \int_{x_1}^{R} \frac{\rho(r)\ dr}{\sqrt{r^2 - x_2^2}} =$$

$$= \rho(r_2) \int_{x_2}^{x_1} \frac{rdr}{\sqrt{r^2 - x_2^2}} + \rho(r_1) \int_{x_1}^{R} \frac{rdr}{\sqrt{r^2 - x_2^2}} =$$

$$= \rho(r_2) \left[\sqrt{r^2 - x_2^2}\right]_{x_2}^{x_1} + \rho(r_1) \left[\sqrt{r^2 - x_2^2}\right]_{x_1}^{R}$$

Thus:

$$\rho(x_2)\sqrt{R^2 - x_2^2} = \rho(r_2)\sqrt{x_1^2 - x_2^2} + \rho(r_1)\left[\sqrt{R^2 - x_2^2} - \sqrt{x_1^2 - x_2^2}\right] \qquad (C\text{-}4)$$

Here, all values except $\rho(r_2)$ are known, which becomes now determined.

The general expression for the n-th region can be written now as:

$$\rho(x_n)\sqrt{R^2 - x_n^2} = \rho(r_n)\sqrt{x_{n-1}^2 - x_n^2} +$$

$$+ \rho(r_{n-1})\left[\sqrt{x_{n-2}^2 - x_n^2} - \sqrt{x_{n-1}^2 - x_n^2}\right] + \ldots. +$$

$$+ \rho(r_2)\left[\sqrt{x_1^2 - x_n^2} - \sqrt{x_2^2 - x_n^2}\right] +$$

$$+ \rho(r_1)\left[\sqrt{R^2 - x_n^2} - \sqrt{x_1^2 - x_n^2}\right] \qquad (C\text{-}5)$$

where all values except $\rho(r_n)$ are known. Thus, from this expression, the value of $\rho(r_n)$ can be calculated.

The repetitive nature of the calculations of $\rho(r)$ make a high-speed digital computer a valuable tool for the reduction of the experimental data. As detailed in Appendix D, a program for an IBM 709 computer was prepared, and the values $\rho(r)$ obtained.

Once the values of $\rho(r)$ are known, the void fraction, f, for a small fluid region (control volume) defined as:

$$f = \frac{\text{volume of voids}}{\text{total volume}} = \frac{V_v}{V}$$

is easily calculated.

Let: V_v = volume of mercury in vapor phase in control volume

V_m = volume of mercury in liquid phase in control volume

M = mass of mercury in control volume.

Then:

$$V = V_v + V_m$$

$$\rho(r) = \frac{\text{mass of mercury}}{\text{total volume}} = \frac{M}{V}$$

$$\rho = \frac{\text{mass of mercury}}{\text{liquid volume}} = \frac{M}{V_m}$$

and:

$$\frac{\rho(r)}{\rho} = \frac{V_m}{V}$$

The void fraction is thus expressed:

$$f = \frac{V_v}{V} = 1 - \frac{V_m}{V}$$

or finally:

$$f = 1 - \frac{\rho(r)}{\rho} \qquad (C\text{-}6)$$

where ρ is the density of the liquid mercury.

The values computed following the above procedure are summarized in Tables XI through XXVII.

APPENDIX D

COMPUTER PROGRAM

COMPUTER PROGRAM

To facilitate the computation of the void fraction in terms of the radial distance r, a program for an IBM 709 digital computer was prepared. The program was written in the MAD language (Michigan Algorithm Decoder) currently used at the University of Michigan, and it is based on the equations developed in Appendix C.

It was intended to make the program as general as possible. Thus, to facilitate future changes, the following three parameters were incorporated in the program as internal information on separate cards.

(1) ΔX = width of vertical bands in which the flow area is divided.

(2) ρ = density of fluid (gm/in^3).

(3) μ = linear absorption coefficient of fluid (in^{-1}).

It is observed that (1) will be changed according to the accuracy desired, and in fact, during the present experiment, the values $\Delta X = 0.030"$ and $0.010"$ were used, as explained in Section IV. The other two parameters depend essentially on the fluid under consideration, and for μ, on the energy of the gamma rays emitted by the radioactive source.

The input data are as follows:

i) the axial distance from the throat of the venturi, Z

ii) the radius of the venturi at distance Z. For this particular venturi, the radius R is given by the expression:

$$R = \frac{0.495}{9.217} Z + 0.255 \quad \text{in.} \qquad \text{(D-1)}$$

iii) the number of regions in which the flow area is divided, M, obtained from the relation:

$$M = \frac{R(Z)}{\Delta X} \qquad \text{(D-2)}$$

and taken to be an integer

iv) N1(I) = number of counts corresponding to the I^{th} vertical band (see Figure C2) in venturi cross-section, under cavitation conditions.

v) N2(I) = number of counts corresponding to the I^{th} vertical band in venturi cross-section, when filled with stagnant fluid.

Thus I is an integer varying between 1 and M.

vi) D = a parameter, related to the flow condition of the fluid, which does not appear in the calculations.*

During the first runs with the computer, the value $\Delta X = 0.030"$ was used, and, as indicated in Section IV, the first point was taken 0.015" inside the wall position to eliminate the possibility of a point involving partial attenuation in plastic. Then, the values of X(I) are given by the formula:

$$X(I) = R(Z) - \frac{(2I-1)\ \Delta X}{2} \qquad \text{(D-3)}$$

which was also used, for no particular reason, for the case $\Delta X = 0.010"$.

The average fluid density corresponding to the I^{th} vertical band is given by:

$$\rho(I) = \rho + \frac{\rho}{2\mu\sqrt{R^2 - X(I)^2}} \ln \frac{N2(I)}{N1(I)} \qquad \text{(D-4)}$$

which is identical to formula (C-1).

It is desired to obtain the average density as a function of the radius, r. For that, formulas (C-3), (C-4) and (C-5) are used, after rewriting them in a slightly different form as follows:

For I = 1: $\rho_r(1) \cong \rho(r_1) = \rho(1)$ (D-5)

*See Figure D2 for flow rate in GPM corresponding to values of D.

For I = 2:

$$\rho_r(2) \equiv \rho(r_2) = \rho(2)\,\frac{\sqrt{R^2 - X(2)^2}}{\sqrt{X(1)^2 - X(2)^2}} - \rho(r_1)\,\frac{\sqrt{R^2 - X(2)^2} - \sqrt{X(1)^2 - X(2)^2}}{\sqrt{X(1)^2 - X(2)^2}} \qquad \text{(D-6)}$$

and, in general, for I = I:

$$\begin{aligned}
\rho_r(I) = {} & \rho(I)\,\frac{\sqrt{R^2 - X(I)^2}}{\sqrt{X(I-1)^2 - X(I)^2}} \\
& - \rho_r(1)\,\frac{\sqrt{R^2 - X(I)^2} - \sqrt{X(1)^2 - X(I)^2}}{\sqrt{X(I-1)^2 - X(I)^2}} \\
& - \rho_r(2)\,\frac{\sqrt{X(1)^2 - X(I)^2} - \sqrt{X(2)^2 - X(I)^2}}{\sqrt{X(I-1)^2 - X(I)^2}} \\
& - \cdots\cdots\cdots\cdots\cdots\cdots\cdots\cdots\cdots\cdots \\
& - \rho_r(J)\,\frac{\sqrt{X(J-1)^2 - X(I)^2} - \sqrt{X(J)^2 - X(I)^2}}{\sqrt{X(I-1)^2 - X(I)^2}} \quad \left.\begin{array}{l}\text{generic}\\ \text{term:}\\ 2 \le J \le I-1\end{array}\right\} \\
& - \cdots\cdots\cdots\cdots\cdots\cdots\cdots\cdots\cdots\cdots \\
& - \rho_r(I-1)\,\frac{\sqrt{X(I-2)^2 - X(I)^2} - \sqrt{X(J-1)^2 - X(I)^2}}{\sqrt{X(I-1)^2 - X(I)^2}}
\end{aligned} \qquad \text{(D-7)}$$

where, for example, one means:

$$X(I-1)^2 \equiv [X(I-1)]^2 \equiv X_{I-1}^2$$

Following the calculation of the radial densities $\rho_r(I)$, the void fractions in terms of r are obtained from the formula:

$$F(I) = 1 - \frac{\rho_r(I)}{\rho} \qquad \text{(D-8)}$$

The output of the program was planned to provide not only the desired void fraction, but also the average density as a function of the radial distance, $\rho_r(I)$, and the average density as function of the transversal distance, $\rho(I)$.

A flow chart of the MAD program is shown in Figure D1 where the numbers refer to the statement number in the program. A copy of the program, as obtained from the printer, is also included, where ρ is represented by the symbol RO, while ρ_r is indicated by ROR.

```
$COMPILE MAD, EXECUTE
          DELTAX = 0.030                                                    1
          MU = 2.10                                                         2
          RO =221.977                                                       3
START     READ DATA  Z,R,D,M,  N2(1)...N2(M),N1(1)...N1(M)                  4
          THROUGH BACK, FOR  I = 1, 1,  I.G.M                               5
          X(I) = R - (2*I-1)*DELTAX/2                                       6
BACK      RO(I)=RO-RO*ELOG.(N1(I)/N2(I))/(2.*MU*SQRT.(R*R-X(I)*X(I)))       7
          ROR(1) = RO(1)                                                    8
          I = 2                                                             9
NANCY     AUX = RO(I)*SQRT.(R * R     -X(I)*X(I))/SQRT.(X(I-1)*X(I-1)-      10
         1X(I)*X(I))-ROR(1)*(SQRT.(R * R     -X(I)*X(I))-SQRT.(X(1)*        11
         2X(1)-X(I)*X(I)))/SQRT.(X(I-1)*X(I-1)-X(I)*X(I))                   12
          WHENEVER I.G.2                                                    13
          THROUGH MARY, FOR J = 2, 1, J.G.I-1                               14
          T=-ROR(J)*(SQRT.(X(J-1)*X(J-1)-X(I)*X(I))-SQRT.(X(J)*X(J)-        15
         1X(I)*X(I)))/SQRT.(X(I-1)*X(I-1)-X(I)*X(I))                        16
MARY      AUX = AUX + T                                                     17
          ROR(I) = AUX                                                      18
          OTHERWISE                                                         19
          ROR(2) = AUX                                                      20
          END OF CONDITIONAL                                                21
          WHENEVER  I.L.M                                                   22
          I = I + 1                                                         23
          TRANSFER TO NANCY                                                 24
          OTHERWISE                                                         25
          THROUGH JEAN, FOR  I =1,1,     I.G.M                              26
          WHENEVER  ROR(I) .GE. RO                                          27
          F(I) = 0                                                          28
          OTHERWISE                                                         29
          F(I) = 1.-ROR(I)/RO                                               30
JEAN      END OF CONDITIONAL                                                31
          END OF CONDITIONAL                                                32
          INTEGER I,M,J                                                     33
          DIMENSION N1(30),N2(30),RO(30),ROR(30),X(30),F(30),NOR(30)        34
          PRINT COMMENT  $1VOID FRACTION MEASUREMENTS FOR MERCURY$          35
          PRINT COMMENT $-PARAMETERS$                                       36
          PRINT RESULTS  DELTAX, MU, RO                                     37
          PRINT COMMENT $0CAVITATION CONDITIONS                             38
         1                STANDARD AND NOSE,NEW DATA DEC.1961$              39
          PRINT RESULTS Z,R,D,M                                             40
          PRINT COMMENT $-REDUCED DATA$                                     41
          PRINT RESULTS N1(1)...N1(M),N2(1)...N2(M)                         42
          PRINT COMMENT $-                          COMPUTED VALUES$        43
          PRINT RESULTS   RO(1)...RO(M)                                     44
          PRINT RESULTS  X(1)...X(M),ROR(1)...ROR(M), F(1)...F(M)           45
          TRANSFER TO START                                                 46
          END OF PROGRAM                                                    47
$DATA
```

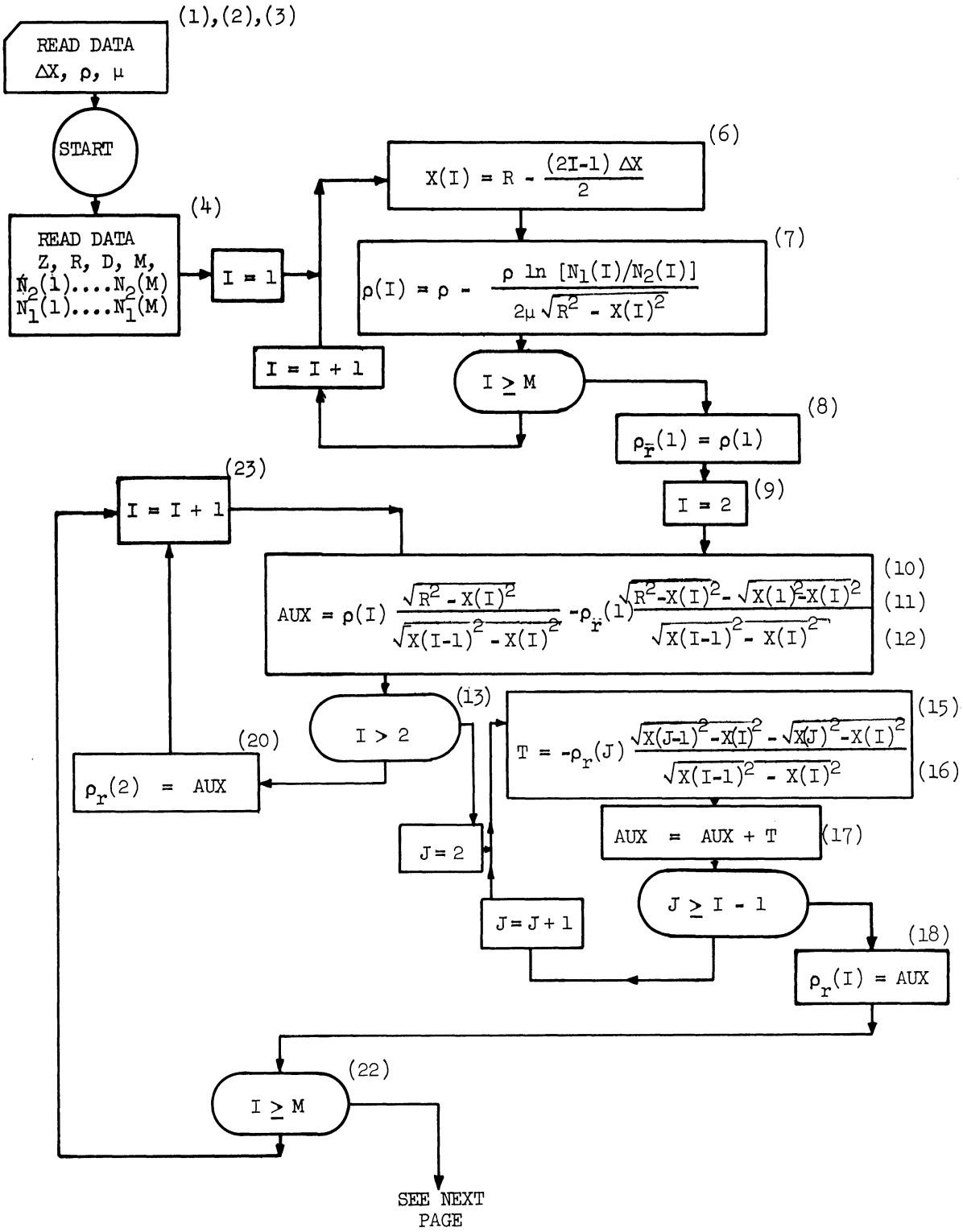

Figure D1. MAD Flow Chart.

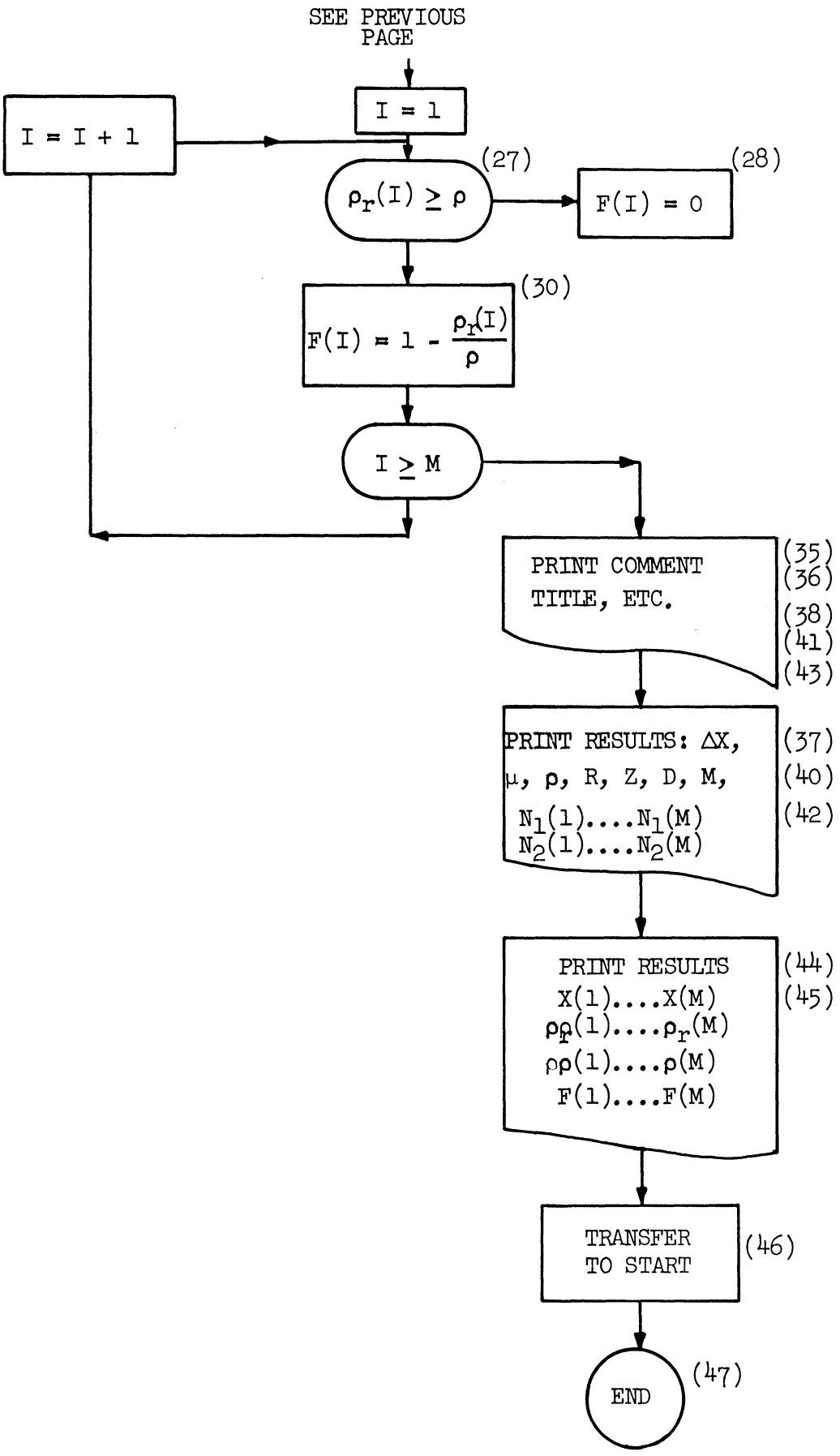

Figure D1. MAD Flow Chart (Continuation).

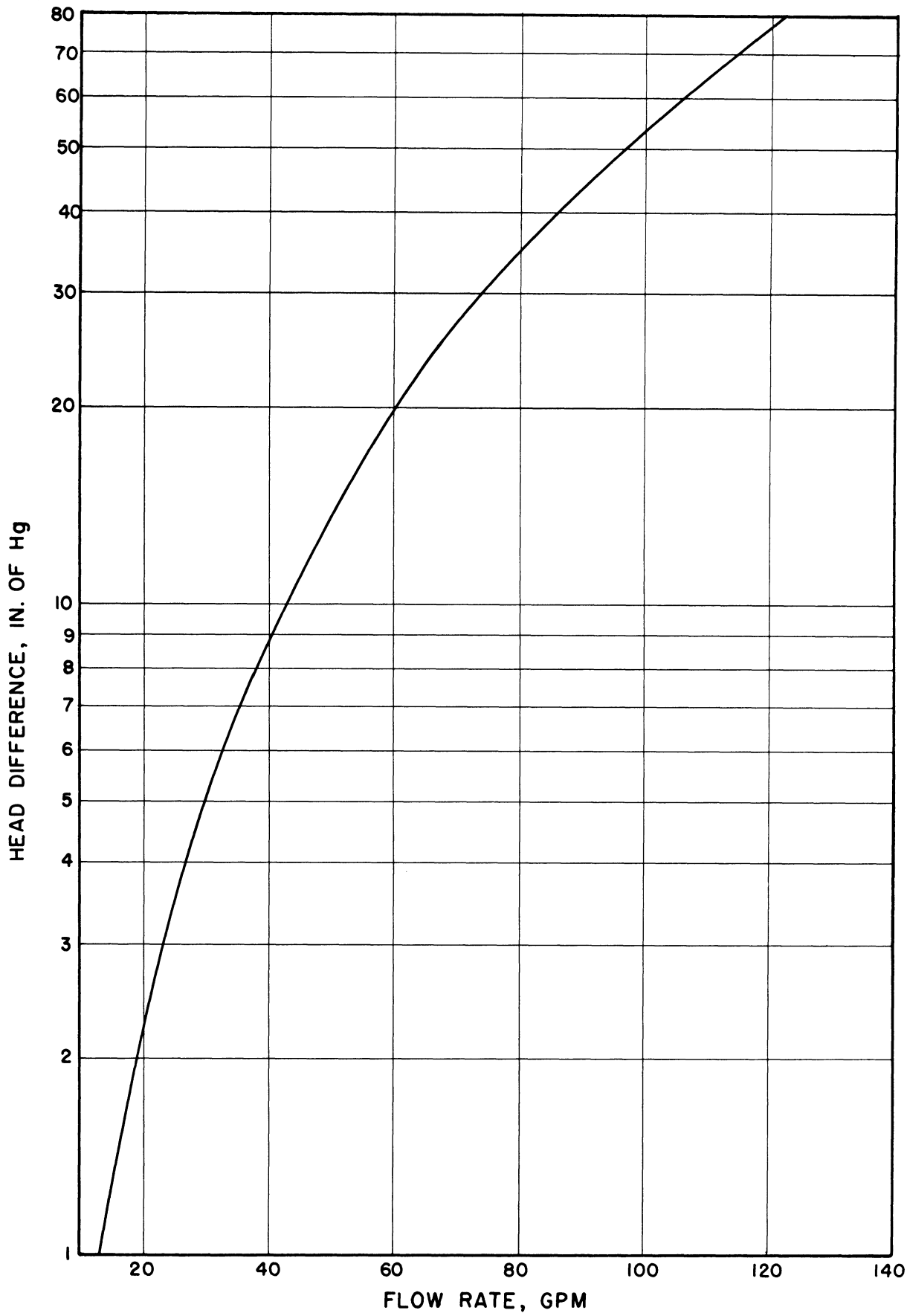

Figure D2. Flow Rate Calibration Curve. (Metering Venturi).

APPENDIX E

TABLES

TABLES

TABLE I

LINEARITY OF LINEAR AMPLIFIER

Gain		Pulse Height Volts
Coarse	Fine	
2	36	0.30
4	36	0.60
8	36	1.10
16	36	2.20
32	36	4.30
63	36	5.8

See Figure A1

TABLE II

CALIBRATION OF ΔE DIAL

E_{Dial}	ΔE_{Dial}	E_2	E_1	% Window
900	1000	915	867	4.8
	600	917	885	3.2
	200	918	911	0.7
700	1000	750	699	5.1
	600	749	717	3.2
	200	741	740	0.8
500	1000	516	462	5.4
	600	516	480	3.6
	200	516	506	1.0
300	1000	312	254	5.8
	600	312	277	3.5
	200	313	303	1.0

See Figure A2

TABLE III

PRELIMINARY DIFFERENTIAL SPECTRUM

Co^{60}				Cs^{137}	
E Dial	c/min	E Dial	c/min	E Dial	c/min
1000	6	440	227	330	146
980	5	420	267	310	1072
960	6	400	249	290	450
940	-	380	230	270	185
700	6	360	241	300	1003
680	15	640	91	320	692
660	21	620	244	305	1175
640	78	600	242		
620	225	580	126		
600	232	560	139		
580	87	550	267		
560	167	540	410		
540	381	530	339		
520	245	520	261		
500	154	510	193		
480	173	570	92		
460	155	610	264		

H.V. = -1000 volts

ΔE = 200, Gain 2 x 36

See Figure A3

TABLE IV

PRECISE DET. OF Co^{60} 1.17 Mev PEAK

E Dial	c/3 min	Background	Net Co^{60} c/3 min
560	3054	151	2903 ± 31
555	3754	149	3605 ± 35
550	4014	144	3870 ± 36
545	4195	148	4047 ± 37
540	3850 3882	142	3740 ± 35
535	3621	146	3475 ± 34
530	3407	139	3268 ± 33
525	3299	124	3175 ± 33
520	3038	131	2907 ± 31
570	2698	155	2543 ± 29
510	2691	105	2586 ± 29

H. V. = -1000, ΔE = 200, Gain { C-2 / f-36

Differential count, scalar discriminator - 1.5.
See Figure A5

TABLE V

LINEAR ABSORPTION COEFFICIENT OF Hg FOR Co^{60} GAMMA-RAYS ENERGY.*

E, Mev	τ	K_T	$\sigma = \sigma_\alpha + \sigma_I + \sigma_c$	$\tau + K_T + \sigma$
0.80	2.50×10^{-2}		5.930×10^{-2}	8.48×10^{-2}
1.00	1.70×10^{-2}		5.248×10^{-2}	6.41×10^{-2}
1.50	0.81×10^{-2}	0.15×10^{-2}	4.201×10^{-2}	5.161×10^{-2}
2.00	0.52×10^{-2}	0.48×10^{-2}	3.567×10^{-2}	4.567×10^{-2}

See Figure B1. All values are in cm^2/gm

Notation:

τ = photoelectric effect cross-section
σ_α = Compton absorption cross-section
σ_I = Compton scattering cross-section
σ_c = Thompson cross-section
K_T = pair production cross-section

* Reference [12]: LA-2237, "Gamma-Ray Absorption Coefficients for Elements 1 through 100 Derived from the Theoretical Values of the National Bureau of Standards," 1957.

TABLE VI

μ IN Hg. DATA FROM NUCLEAR ENGINEERING HANDBOOK[10]

Energy - Mev	μ/ρ - cm^2/gm	μ - cm^{-1}*
.5	0.147	1.993
1.0	0.0692	0.939
2.0	0.0451	0.611
3.0	0.0411	0.557
6.0	0.0441	0.598

* μ values computed using $\rho_{70\,°F} = 13.5435\ gm/cm^3$. See Figure B2

TABLE VII

MERCURY DENSITY AS A FUNCTION OF TEMPERATURE*

Temp - °C	ρ - gm/cm^3
0	13.5955
19	13.5487
20	13.5462
21	13.5438
22	13.5413
23	13.5389

* Data from Handbook of Chemistry and Physics[11] See Figure B3

TABLE VIII

ABSORPTION OF 1.17 Mev γ IN Hg

Hg Height-in	Δh-in	Δh-in	Total Hg Height, in	c/3 min	Background c/1 min	Net Co^{60} c/3 min	Normalized Rate
2 7/64	0	0	0	8931	153	8472	1.0
2 $\frac{4\ 1/2}{64}$	5/128	.0391	.0391	8457	172	7941	.937
1 62/64	13/128	.1018	.1409	7211	171	6698	.790
1 56/64	6/64	.0937	.2346	5935	173	5416	.640
1 51/64	5/64	.0782	.3128	5147	171	4634	.547
1 46/64	5/64	.0782	.3910	4335	169	3828	.452
1 39/64	7/64	.1095	.5005	3467	167	2963	.350
1 35/64	4/64	.0625	.5630	2966	173	2453	.289
1 21/64	14/64	.2190	.7820	2286	172	1770	.209
1 14/64	7/64	.1095	.8915	2012	165	1517	.179
1 6/64	8/64	.1205	1.0120	1626	188	1062	.126
1	6/64	.0937	1.1057	1313	186	755	.089
52/64	12/64	.1875	1.2932	912	168	408	.048

H. V. = -1000, ΔE = 490, Gain 2 x 36, E Dial = 530

Differential Count.

See Figure B4

TABLE IX

BACKGROUND INFORMATION

Date	Time	No. Counts	Counting Time	Counting Rate	Standard Deviation
Dec. 21	9:00	330	10	33 CPM	±1.81 CPM
Dec. 21	14:10	426	10	42.6 CPM	±2.06 "
Dec. 21	16:09	329	10	32.9 CPM	±1.81
Dec. 21	20:30	296	10	29.6 CPM	±1.71
Dec. 22	8:30	383	10	38.3 CPM	±1.95
Dec. 22	13:10	376	10	37.6 CPM	±1.93
Dec. 26	8:30	289	10	28.9 CPM	±1.69
Dec. 26	13:20	438	10	43.8 CPM	±2.09
Dec. 26	19:10	446	10	44.6 CPM	±2.11
Dec. 27	8:25	363	10	36.3 CPM	±1.90
Dec. 27	13:55	301	10	30.1 CPM	±1.73
Dec. 27	20:30	342	10	34.2 CPM	±1.84
Dec. 28	14:00	411	10	41.1 CPM	±2.02

Background corrections will be performed as follows:

Dec. 21 runs: use background closest to actual run time

Dec. 22 runs: as above: 115 counts/3 min

Dec. 26 runs: morning: use closest background determination; afternoon and evening, use:

$$\frac{438 + 446}{20} = 44.2 \text{ CPM}$$

Dec. 27 runs: use average value: $\frac{363 + 301 + 342}{30} = 33.5$ CPM

Dec. 28 runs: 41.1 CPM or 123 counts/3 min.

TABLE X

VOID FRACTION RUNS

December, 1961

Cavitation Condition	Run N°	Z, inch	R, inch
First mark	21	-0.250	0.255
	20	0.000	0.255
	24	0.786	0.297
	25	1.163	0.339
	--	1.750	0.349
	--	2.250	0.376
	--	2.750	0.402
Visible	22	-0.250	0.255
	17	0.000	0.255
	16	0.250	0.268
	5	0.625	0.289
	10	0.786	0.297
	11	1.163	0.317
Nose	1	0.250	0.268
	4	0.625	0.289
	9	0.786	0.297
	13	1.163	0.317
Standard	18	0.000	0.255
	15	0.250	0.268
	6	0.625	0.289
	7	0.786	0.297
	14	1.163	0.317
No cavitation (one run for each Z value)	26	-0.250	air only
	23	-0.250	0.255
	19	0.000	0.255
	2	0.250	0.268
	3	0.625	0.289
	8	0.786	0.297
	12	1.163	0.317
	--	1.375	0.339
	--	1.750	0.349
	--	2.250	0.376
	--	2.750	0.402

Remarks: Total N° of scheduled runs...32
Actually performed.....26

TABLE XI

Cavitation Condition: Visible
Axial Position: Z = - 0.250
R = 0.255 in.

r (in)	Reduced Data		Computed Values	
	N_2	N_1	F%	r%
.250	5600	7180		98.04
.240	4975	6200	47.46	94.12
.230	4375	5325	26.94	90.20
.220	4150	4825	7.79	86.27
.210	4000	4505	0.30	82.35
.200	3885	4265	0	78.43
.190	3770	4065	0	74.51
.180	3675	3875	0	70.59
.170	3580	3725	0	66.67
.160	3490	3590	0	62.74
.150	3410	3480	0	58.82
.140	3335	3390	0	54.90
.130	3260	3315	0	50.98
.120	3190	3250	0	47.06
.110	3115	3185	0	43.14
.100	3050	3130	0	39.22
.090	3005	3080	0	35.29
.080	2965	3040	0	31.37
.070	2925	3005	0	27.45
.060	2905	2975	0	23.53
.050	2885	2950	0	19.61
.040	2870	2930	0	15.69
.030	2855	2910	0	11.76
.020	2850	2895	0	7.84
.010	2845	2885	0	3.92
.000	2845	2880	0	1.46

TABLE XII

Cavitation Condition: lst. mark
Axial Position: Z = - 0.250
R = 0.255 in.

r (in)	Reduced Data		Computed Values	
	N_2	N_1	F%	r%
.250	5600	7100		98.04
.240	4975	6350	57.03	94.12
.230	4375	5575	39.80	90.20
.220	4150	4800	0	86.27
.210	4000	4440	0	82.35
.200	3885	4190	0	78.43
.190	3770	4015	0	74.51
.180	3675	3880	0	70.59
.170	3580	3760	0	66.67
.160	3490	3640	0	62.74
.150	3410	3550	0	58.82
.140	3335	3455	0	54.90
.130	3260	3365	0	50.98
.120	3190	3280	0	47.06
.110	3115	3210	0	43.14
.100	3050	3135	0	39.22
.090	3005	3070	0	35.29
.080	2965	3005	0	31.37
.070	2925	2945	0	27.45
.060	2905	2905	0	23.53
.050	2885	2865	0	19.61
.040	2870	2830	0	15.69
.030	2855	2805	0	11.76
.020	2850	2790	0	7.84
.010	2845	2775	0	3.93
.000	2845	2770	0	1.46

TABLE XIII

Cavitation Conditions: Visible
Axial Position: Z = 0.000
R = 0.255 in.

r (in)	Reduced Data		Computed Values	
	N_2	N_1	F%	r%
.250	6550	7050	34.86	98.04
.240	5725	6250	21.79	94.12
.230	4975	5500	19.32	90.20
.220	4485	5025	19.33	86.27
.210	4100	4575	13.63	82.35
.200	3835	4285	12.64	78.43
.190	3615	4035	10.93	74.51
.180	3430	3825	9.84	70.59
.170	3280	3600	2.98	66.67
.160	3145	3415	0.68	62.74
.150	3060	3285		58.82
.140	2985	3195	0	54.90
.130	2930	3125	0	50.98
.120	2885	3060	0	47.06
.110	2845	3010	0	43.14
.100	2825	2965	0	39.22
.090	2790	2925	0	35.29
.080	2765	2895	0	31.37
.070	2750	2865	0	27.45
.060	2735	2840	0	23.53
.050	2720	2820	0	19.61
.040	2710	2805	0	15.69
.030	2705	2785	0	11.76
.020	2700	2770	0	7.84
.010	2700	2760	0	3.92
.000	2700	2750	0	1.46

TABLE XIV

Cavitation Conditions: Standard
Axial Position: Z = 0.000
R = 0.255 in.

r (in)	Reduced Data		Computed Values	
	N_2	N_1	F%	r%
.250	6550	7065	35.86	98.04
.240	5725	6300	24.27	94.12
.230	4975	5450	14.91	90.20
.220	4485	4875	9.48	86.27
.210	4100	4535	15.32	82.35
.200	3835	4230	11.00	78.43
.190	3615	3975	8.75	74.51
.180	3430	3770	8.29	70.59
.170	3280	3565	3.43	66.67
.160	3145	3400	2.69	62.74
.150	3060	3275	0	58.82
.140	2985	3175	0	54.90
.130	2930	3100	0	50.98
.120	2885	3035	0	47.06
.110	2845	2990	0	43.14
.100	2825	2940	0	39.22
.090	2790	2910	0	35.29
.080	2765	2875	0	31.37
.070	2750	2845	0	27.45
.060	2735	2820	0	23.53
.050	2720	2805	0	19.61
.040	2710	2790	0	15.69
.030	2705	2780	0	11.76
.020	2700	2775	0	7.84
.010	2700	2775	0	3.92
.000	2700	2775	0	1.46

TABLE XV

Cavitation Conditions: 1st. mark
Axial Position: Z = 0.000
R = 0.255 in.

r (in)	Reduced Data		Computed Values	
	N_2	N_1	F%	r%
.250	6550	6875	22.95	98.04
.240	5725	6325	28.60	94.12
.230	4975	5650	27.85	90.20
.220	4485	5050	16.92	86.27
.210	4100	4540	8.58	82.35
.200	3835	4200	5.33	78.43
.190	3615	3985	9.19	74.51
.180	3430	3800	10.30	70.59
.170	3280	3635	9.18	66.67
.160	3145	3510	11.42	62.74
.150	3060	3405	8.53	58.82
.140	2985	3315	7.42	54.90
.130	2930	3245	6.22	50.98
.120	2885	3175	3.57	47.06
.110	2845	3120	3.06	43.14
.100	2825	3070	0	39.22
.090	2790	3025	0.41	35.29
.080	2765	2990	0.22	31.37
.070	2750	2960	0	27.45
.060	2735	2930	0	23.53
.050	2720	2900	0	19.61
.040	2710	2880	0	15.69
.030	2705	2865	0	11.76
.020	2700	2850	0	7.84
.010	2700	2835	0	3.92
.000	2700	2835	0	1.46

TABLE XVI

Cavitation Conditions: Nose
Axial Position: Z = 0.250
R = 0.268 in.

r (in)	Reduced Data		Computed Values	
	N_2	N_1	F%	r%
.263	5800	6225	32.68	98.13
.253	5325	5925	27.85	94.40
.243	4850	5600	30.91	90.67
.233	4450	5275	31.05	86.94
.223	4175	4975	25.29	83.21
.213	3965	4640	14.43	79.48
.203	3800	4325	4.37	75.75
.193	3665	4075	0	72.01
.183	3225	3860	0	68.28
.173	3415	3710	0	64.55
.163	3310	3575	0	60.82
.153	3215	3465	0	57.09
.143	3125	3385	3.01	53.36
.133	3040	3305	4.44	49.63
.123	2965	3235	5.53	45.90
.113	2905	3170	4.80	42.16
.103	2850	3115	5.33	38.43
.093	2810	3065	3.76	34.70
.083	2770	3015	2.81	30.97
.073	2740	2980	2.85	27.24
.063	2710	2935	0.49	23.51
.053	2690	2900	0	19.78
.043	2675	2870	0	16.04
.033	2655	2850	0	12.31
.023	2645	2835	0	8.58
.013	2640	2820	0	4.85
.003	2640	2815	0	1.12

TABLE XVII

Cavitation Conditions: Standard
Axial Position: Z = 0.250
R = 0.268 in.

r (in)	Reduced Data		Computed Values	
	N_2	N_1	F%	r%
.263	5800	7175	98.31	98.13
.253	5325	6860	61.28	94.40
.243	4850	6050	31.14	90.67
.233	4450	5275	9.69	86.94
.223	4175	4800	2.94	83.21
.213	3965	4465	0.09	79.48
.203	3800	4175	0	75.75
.193	3665	3950	0	72.01
.183	3525	3770	0	68.28
.173	3415	3615	0	64.55
.163	3310	3485	0	60.82
.153	3215	3270	0	57.09
.143	3125	3245	0	53.36
.133	3040	3125	0	49.63
.123	2965	3025	0	45.90
.113	2905	2960	0	42.16
.103	2850	2900	0	38.43
.093	2810	2850	0	34.70
.083	2770	2815	0	30.97
.073	2740	2780	0	27.24
.063	2710	2755	0	23.51
.053	2690	2735	0	19.78
.043	2675	2715	0	16.04
.033	2655	2705	0	12.31
.023	2645	2700	0	8.58
.013	2640	2690	0	4.85
.003	2640	2690	0	1.12

TABLE XVIII

Cavitation Conditions: Visible
Axial Position: Z = 0.625
R = 0.289 in.

r (in)	Reduced Data		Computed Values	
	N_2	N_1	F%	r%
.284	4250	4225	0	98.27
.274	3800	3850	4.77	94.81
.264	3540	3600	3.88	91.35
.254	3370	3450	4.89	87.89
.244	3240	3350	6.82	84.43
.234	3100	3250	9.61	80.97
.224	2990	3160	9.66	77.51
.214	2885	3070	9.80	74.05
.204	2795	3000	10.90	70.59
.194	2715	2925	10.00	67.13
.184	2635	2860	11.22	63.67
.174	2575	2800	9.90	60.21
.164	2515	2745	10.14	56.75
.154	2465	2695	9.50	53.29
.144	2415	2650	10.08	49.83
.134	2375	2610	9.52	46.37
.124	2340	2570	8.32	42.91
.114	2305	2540	9.54	39.45
.104	2270	2510	10.30	35.97
.094	2245	2490	10.76	32.53
.084	2225	2470	10.04	29.07
.074	2205	2455	11.02	25.61
.064	2185	2440	11.81	22.15
.054	2180	2425	7.84	18.69
.044	2170	2415	8.66	15.22
.034	2165	2410	8.74	11.76
.024	2160	2405	8.81	8.30
.014	2155	2400	8.92	4.84
.004	2155	2400	8.77	1.38

TABLE XIX

Cavitation Conditions: Nose
Axial Position: Z = 0.625
R = 0.289 in.

r (in)	Reduced Data		Computed Values	
	N_2	N_1	F%	r%
.284	4250	4800	54.13	98.27
.274	3800	4425	36.07	94.81
.264	3540	4125	24.72	91.35
.254	3370	3875	15.31	87.89
.244	3240	3675	9.70	84.43
.234	3100	3505	9.29	80.97
.224	2900	3365	7.79	77.51
.214	2885	3225	5.75	74.05
.204	2795	3110	4.94	70.59
.194	2715	300	3.14	67.13
.184	2635	2915	4.87	63.67
.174	2575	2830	2.48	60.21
.164	2515	2765	3.76	56.75
.154	2465	2705	3.31	53.29
.144	2415	2650	3.77	49.83
.134	2375	2610	4.63	46.37
.124	2340	2570	4.18	42.91
.114	2305	2540	5.87	39.45
.104	2270	2515	7.99	35.97
.094	2245	2490	7.24	32.53
.084	2225	2470	7.01	29.07
.074	2205	2455	8.22	25.61
.064	2185	2440	9.16	22.15
.054	2180	2430	6.75	18.69
.044	2170	2420	7.11	15.22
.034	2165	2415	7.06	11.76
.024	2160	2410	7.09	8.30
.014	2155	2405	7.20	4.84
.004	2155	2405	7.04	1.38

TABLE XX

Cavitation Conditions: Standard
Axial Position: Z = 0.625
R = 0.289 in.

r (in)	Reduced Data		Computed Values	
	N_2	N_1	F%	r%
.284	4250	5225	91.87	98.27
.274	3800	4625	41.47	94.81
.264	3540	4200	21.63	91.35
.254	3370	3915	12.54	87.89
.244	3240	3705	7.99	84.43
.234	3100	3520	7.17	80.97
.224	2990	3370	5.64	77.51
.214	2885	3235	4.98	74.05
.204	2795	3125	4.92	70.59
.194	2715	3030	4.94	67.13
.184	2635	2945	6.00	63.67
.174	2575	2865	4.13	60.21
.164	2515	2800	5.07	56.75
.154	2465	2740	4.50	53.29
.144	2415	2695	6.52	49.83
.134	2375	2655	6.72	46.37
.124	2340	2620	6.93	42.91
.114	2305	2595	9.08	39.45
.104	2270	2570	10.63	35.97
.094	2245	2550	10.70	32.53
.084	2225	2530	9.92	29.07
.074	2205	2520	12.08	25.61
.065	2185	2505	12.44	22.15
.054	2180	2495	9.76	18.69
.044	2170	2485	10.00	15.22
.034	2165	2480	9.85	11.76
.024	1260	2475	9.82	8.30
.014	2155	2470	9.92	4.84
.004	2155	2470	9.70	1.38

TABLE XXI

Cavitation Conditions: Visible and Nose
Axial Position: Z = 0.786
R = 0.297 in.

r (in)	Reduced Data		Computed Values	
	N_2	N_1	F%	r%
.282	4050	4050	0	94.95
.252	3370	3370	0	84.85
.222	3010	3010	0	74.75
.192	2760	2760	0	64.65
.162	2590	2590	0	54.55
.132	2490	2490	0	44.44
.102	2415	2415	0	34.34
.072	2370	2370	0	24.24
.042	2335	2335	0	14.14
.012	2325	2324	0	4.04

TABLE XXII

Cavitation Conditions: Standard
Axial Position: Z = 0.786
R = 0.297 in.

r (in)	Reduced Data		Computed Values	
	N_2	N_1	F%	r%
.292	4600	4880	25.92	98.32
.282	4050	4750	44.14	94.95
.272	3750	4160	9.80	91.58
.262	3540	3910	9.45	88.22
.252	3370	3725	9.52	84.85
.242	3215	3540	7.54	81.48
.232	3105	3385	4.05	78.11
.222	3010	3245	1.22	74.75
.212	2915	3120	0.41	71.38
.202	2835	3010	0	68.01
.192	2760	2910	0	64.65
.182	2690	2810	0	61.28
.172	2640	2730	0	57.91
.162	2590	2675	0	54.55
.152	2550	2620	0	51.18
.142	2515	2565	0	47.81
.132	2490	2535	0	44.44
.122	2460	2495	0	41.08
.112	2435	2465	0	37.71
.102	2415	2440	0	34.34
.092	2395	2420	0	30.98
.082	2380	2400	0	27.61
.072	2370	2380	0	24.24
.062	2355	2365	0	20.86
.052	2340	2350	0	17.51
.042	2335	2335	0	14.14
.032	2330	2330	0	10.77
.022	2325	2320	0	7.41
.012	2325	2315	0	4.04
.002	2320	2310	0	0.67

TABLE XXIII

Cavitation Conditions: 1st. mark
Axial Position: Z = 0.786
R = 0.297 in.

r (in)	Reduced Data		Computed Values	
	N_2	N_1	F%	r%
.292	4600			98.32
.282	4050			94.95
.272	3750			91.58
.262	3540	6900		88.22
.252	3370	6480	75.72	84.85
.242	3215	5855	48.37	81.48
.232	3105	5275	25.53	78.11
.222	3010	4655	0.12	74.75
.212	2915	4230	0	71.38
.202	2835	3990	0	68.01
.192	2760	3795	0	64.65
.182	2690	3650	0	61.28
.172	2640	3550	0	57.91
.162	2590	3465	1.50	54.55
.152	2550	3385	1.10	51.18
.142	2515	3320	1.55	57.81
.132	2490	3265	0.94	44.44
.122	2460	3215	1.87	41.08
.112	2435	3165	1.04	37.71
.102	2415	3125	0.82	34.34
.092	2395	3085	0.29	30.98
.082	2380	3050	0	27.61
.072	2370	3020	0	24.24
.062	2355	2995	0	20.86
.052	2340	2975	0.41	17.51
.042	2335	2955	0	14.14
.032	2330	2940	0	10.77
.022	2325	2930	0	7.41
.012	2325	2920	0	4.04
.002	2320	2915	0	0.67

TABLE XXIV

Cavitation Conditions: Visible
Axial Position: Z = 1.163
R = 0.317 in.

r (in)	Reduced Data		Computed Values	
	N_2	N_1	F%	r%
.312	3050	3300	33.45	98.42
.302	2900	3025	5.14	95.27
.292	2790	2840	0	92.11
.282	2710	2720	0	88.96
.272	2640	2645	0	85.80
.262	2585	2585	0	82.65
.252	2530	2530	0	79.50
.242	2485	2485	0	76.34
.232	2440	2440	0	73.19
.222	2400	2400	0	70.03
.212	2370	2370	0	66.88
.202	2330	2330	0	63.72
.192	2305	2305	0	60.57
.182	2275	2275	0	57.41
.172	2250	2250	0	54.26
.162	2225	2225	0	51.10
.152	2205	2205	0	47.95
.142	2185	2185	0	44.79
.132	2165	2165	0	41.64
.122	2150	2150	0	38.49
.112	2140	2140	0	35.33
.102	2130	2130	0	32.18
.092	2120	2120	0	29.02
.082	2110	2110	0	25.87
.072	2100	2100	0	22.71
.062	2095	2095	0	19.56
.052	2090	2090	0	16.40
.042	2085	2085	0	13.25
.032	2085	2085	0	10.09
.022	2085	2085	0	6.94

TABLE XXV

Cavitation Conditions: Nose
Axial Position: Z = 1.163
R = 0.317 in.

r (in)	Reduced Data		Computed Values	
	N_2	N_1	F%	r%
.312	3050	3525	61.45	98.42
.302	2900	3320	26.98	95.27
.292	2790	3150	15.25	92.11
.282	2710	3035	10.87	88.96
.272	2640	2955	10.23	85.80
.262	2585	2885	8.60	82.65
.252	2530	2825	8.53	79.50
.242	2485	2780	8.72	76.34
.232	2440	2730	8.12	73.19
.222	2400	2680	6.98	70.03
.212	2370	2645	6.72	66.88
.202	2330	2610	8.00	63.72
.192	2305	2575	6.26	60.57
.182	2275	2545	6.86	57.41
.172	2250	2520	7.02	54.26
.162	2225	2495	7.13	51.10
.152	2205	2470	6.26	47.95
.142	2185	2450	6.64	44.79
.132	2165	2430	6.81	41.64
.122	2150	2415	6.83	38.49
.112	2140	2400	5.73	35.33
.102	2130	2390	6.12	32.18
.092	2120	2380	6.27	29.02
.082	2110	2375	7.58	25.87
.072	2100	2365	7.21	22.71
.062	2095	2360	6.98	19.56
.052	2090	2355	6.90	16.40
.042	2085	2350	6.89	13.25
.032	2085	2350	6.69	10.09
.022	2085	2350	6.60	6.94

TABLE XXVI

Cavitation Conditions: Standard
Axial Position: Z = 1.163
R = 0.317 in.

r (in)	Reduced Data		Computed Values	
	N_2	N_1	F%	r%
.312	3050	3225	25.00	98.42
.302	2900	3075	12.06	95.27
.292	2790	2965	9.28	92.11
.292	2710	2885	7.93	88.96
.272	2640	2820	7.74	85.80
.262	2585	2755	5.80	82.65
.252	2530	2700	5.87	79.50
.242	2485	2655	5.71	76.34
.232	2440	2610	5.60	73.19
.222	2400	2570	5.48	70.03
.212	2370	2535	4.61	66.88
.202	2330	2500	5.64	63.72
.192	2305	2465	3.76	60.57
.182	2275	2440	5.10	57.41
.172	2250	2410	4.08	54.26
.162	2225	2385	4.37	51.10
.152	2205	2365	4.42	47.95
.142	2185	2345	4.47	44.79
.132	2165	2330	5.49	41.64
.122	2150	2310	4.05	38.49
.112	2140	2295	3.18	35.33
.102	2130	2285	3.65	32.18
.092	2120	2275	3.82	29.02
.082	2110	2265	3.93	25.87
.072	2100	2255	4.01	22.71
.062	2095	2250	3.98	19.56
.052	2090	2245	3.98	16.40
.042	2085	2240	4.01	13.25
.032	2085	2235	1.96	10.09
.022	2085	2230	3.35	6.94

TABLE XXVII

Cavitation Conditions: 1st. mark
Axial Position: Z = 1.163
R = 0.317 in.

r (in)	Reduced Data		Computed Values	
	N_2	N_1	F%	r%
.312	3050			98.42
.302	2900			95.27
.292	2790	5975		92.11
.282	2710	5925		88.96
.272	2640	5780	84.57	85.80
.262	2585	5675	75.53	82.65
.252	2530	5485	64.23	79.50
.242	2485	5175	47.16	76.34
.232	2440	4775	27.87	73.19
.222	2400	4375	10.66	70.03
.212	2370	4000	0	66.88
.202	2330	3640	0	63.72
.192	2305	3515	0	60.57
.182	2275	3420	0	57.41
.172	2250	3360	0	54.26
.162	2225	3300	0.24	51.10
.152	2205	3255	1.93	47.95
.142	2185	3215	3.37	44.79
.132	2165	3175	4.07	41.64
.122	2150	3145	4.77	38.49
.112	2140	3125	5.51	35.33
.102	1230	3100	5.05	32.18
.092	2120	3075	4.66	29.02
.082	2110	3065	7.00	25.87
.072	2100	3045	6.34	22.71
.062	2095	3025	4.41	19.56
.052	2090	3015	5.27	16.40
.042	2085	3005	5.45	13.25
.032	2085	2995	3.27	10.09
.022	2085	2990	3.00	6.94